Abstract

Improving regional-scale greenhouse gas inventories in an agriculture-dominated landscape using a multi-scale approach

Xin Zhang

2013

Quantifying greenhouse gas (GHG) fluxes on a regional scale are critical for both national and global climate mitigation strategies. However, over the past decade, regional fluxes of the three prominent greenhouse gases, carbon dioxide (CO_2), methane (CH_4), and nitrous oxide (N_2O), have been poorly constrained due to inadequate GHG reporting and quantification, and the inherent spatial heterogeneity of GHG fluxes. To improve greenhouse gas inventories on a regional scale, this dissertation evaluates the role of crops in regional CH_4 and N_2O fluxes, and constrains regional GHG fluxes for an agriculture-dominated landscape in the upper Midwest United States based on tall tower observations.

To address the large uncertainties in quantifying GHG fluxes from cropland, this research established an observation system that targets GHG fluxes on three contrasting scales. At the plant scale, we redesigned a steady-state flow-through chamber and conducted the first direct measurement of CO_2, CH_4, and N_2O fluxes from corn and soybean, two prominent Midwestern crops. At the ecosystem scale, we used eddy covariance and flux-gradient measures in soybean and corn fields to determine GHG fluxes from the plant-soil ecosystem. At the regional scale, we made the first high frequency and high precision measurements of all three greenhouse gases from a 244 m tall tower observatory to evaluate the regional GHG fluxes from bottom-up inventories. To facilitate this

evaluation, our research examined multiple methods for determining regional fluxes based on tall tower observations, including eddy covariance, equilibrium boundary layer, modified Bowen ratio, and modified nocturnal boundary layer methods. The results from these approaches were compared with state-of-the-art emissions inventories and Carbon Tracker modeling products.

Research results demonstrate substantial CH_4 and N_2O fluxes from both soybean and corn plants, but the fluxes were typically one magnitude lower than the regional flux. We found that both corn and soybean plants emitted CH_4 during the day (0.4 ± 0.1 nmol m^{-2} s^{-1}) and absorbed CH_4 at night (-0.8 ± 0.8 nmol m^{-2} s^{-1}). Throughout the growing season, soybean was a small source of N_2O (0.03 ± 0.05 nmol m^{-2} s^{-1}), and the corn flux was slightly negative (-0.01 ± 0.04 nmol m^{-2} s^{-1}). In contrast, as observed using the tall tower, the regional CH_4 and N_2O fluxes during the late growing season were 16.0 nmol m^{-2} s^{-1} and 0.19 nmol m^{-2} s^{-1}, respectively. Fertilization significantly increased N_2O emissions from soybean and CO_2 uptake from both corn and soybean, but it did not have a significant impact on CH_4 flux.

At the regional scale (10^4–10^6 km^2), equilibrium boundary layer method produced the same seasonality of regional CO_2 flux as determined using the eddy covariance method, flux aggregation method, and the Carbon Tracker. However, the equilibrium method underestimated the growing season CO_2 flux by about 60%, mainly due to neglecting the advection term in the context of a large spatial gradient. Assuming a minimum impact of advection on regional CH_4 and N_2O fluxes in the late growing season, we applied the equilibrium method to estimate regional CH_4 and N_2O fluxes, and the result was in agreement with other planetary boundary layer methods, but was six and two times

higher than the Emission Database for Global Atmospheric Research, a frequently used bottom-up inventory. The disparity indicated a large underestimation of current emission inventory, and urged further investigation on underestimated or missing sources in the agriculture-dominated landscape around the tall tower.

Improving regional-scale greenhouse gas inventories in an agriculture-dominated landscape using a multi-scale approach

A Dissertation

Presented to the Faculty of the Graduate School

of

Yale University

in Candidacy for the Degree of

Doctor of Philosophy

by

Xin Zhang

Dissertation Director: Xuhui Lee

May 2013

Table of Contents

List of Figures

List of Tables

Acknowledgements

I would like to first thank my advisor for being extremely inspiring and supportive during my doctoral research. He provided me with both direction and flexibility, which kept me on track while also allowing me to explore my own path. I especially appreciate his very great patience in helping me with my papers. He has always been my role model in the academic world.

My sincere appreciation also goes to all of my committee members: Prof. Tim Griffis, Prof. Mark Ashton, and Prof. Peter Raymond. Prof. Griffis provided me with unlimited support throughout my doctoral study with his knowledge, experience, resources, passion, and encouragement. I cannot thank him enough for still being an encouragement to me even after two rejections. Prof. Ashton and Prof. Raymond opened the door of ecology for me, and enabled me to think of my research in the context of ecosystem management. Their questions have always been thought-provoking, and they have been very considerate and supportive. I cannot imagine publishing a book chapter without Prof. Ashton's advice and instruction.

My field work would be impossible without my two invaluable fieldwork assistants—and good friends—Wei Xiao and Ning Hu. They both will run into a storm with me to save a chamber with no hesitation, and will even go to a field in the middle of the night to do samples work.

In addition, I would like to send my special thanks to all of my lovely colleagues in Minnesota: Prof. John Baker, Prof. Dylan Millet, Matt Erickson, Joe Fassbinder, Ming

Chen, Natalie Schultz, Bill Breiter, and Jeremy Smith. They have been always ready to help during my field work, and they are extremely patient with all of my questions.

I also want to thank all of my lab mates: Lei Zhao, Jianping Huang, Kyounhee Kim, Lisa Welp, and Hui-ju Wu. I find myself very lucky to be part of a group of people who are always ready to share and help.

I also want to express my sincere thanks to my long-term mentor, Prof. C.S. Kiang. It is because of his full support that I had a chance to study at Yale. Over the last five years he also provided me with lots of suggestions, guidance, and encouragement, which helped me to get through this exercise.

I want to send my thanks to all the friends I met in the last five years. All of you enriched the color of my life during my doctoral studies. My specially thanks go to Alan Brewster, Felicia Zimmerman, Minh Dung Hoang, Yier Jin, Shaoyu Hou, Nanxin Li, Wei Zhang, Xiaoting Hou, Yu Liu, Jie Wei, and many more. I am not even able to finish this list.

I would like to thank the University of Minnesota's UMore Park for the use of its facilities, and the Rice Family Foundation, the Yale Institute for Biospheric Studies, and the Yale Center for Environmental Law & Policy for providing the research funds for this dissertation work.

Last but not least, I want to thank my parents, Aixiang Zhang and Xuehua Sun, for providing endless love and unconditional support. Notably, they both worked with me for a field experiment in 2009, contributing their engineering expertise, patience, and happiness. I cannot imagine better parents than them.

Finally, I would like express how honored and fortunate I am to have been able to spend the last five years at Yale, a place for seeking light and truth. Yale's open and diversified community and its abundant intellectual resources broadened my vision, enabling me to pursue the truths in my beliefs.

Chapter 1: Introduction

"You cannot manage what you cannot measure" is a truism for the realm of management and industry, but it is also applicable to climate change science and policy (Marquis and Tans, 2008). In order to predict the future trends of global warming and determine climate change mitigation strategies, we must be able to measure and understand the characteristics, such as the sizes and distributions, of the sources and sinks of greenhouse gas (GHG). The current GHG fluxes have been determined primarily on three different scales: the plot/sectoral scale, the regional scale, and the global scale. The plot/sectoral scale's GHG fluxes have been the major focus of the science and policy community. Direct measurements have been carried out to determine the characteristics of emissions, while reporting guidelines have been introduced (IPCC, 2006) to collect emissions data in order to upscale plot/sectoral GHG fluxes. However, large discrepancies still exist in certain sources and sinks, especially in biological sources and sinks. For example, Keppler *et al.* (2006) reported that strong CH_4 flux from terrestrial plants had been neglected in the global CH_4 budget (Keppler *et al.*, 2006), but many other researchers reported that CH_4 flux from terrestrial plants are either not observable or are negligible (Nisbet *et al.*, 2009).

On a global scale, GHG fluxes have also been frequently studied, mainly through two approaches: 1) a bottom-up approach, which aggregates plot/sectoral scale GHG fluxes to the global scale based on land cover information and voluntary reports from different countries or industrial sectors, and 2) a top-down approach, which estimated the GHG fluxes based on atmospheric observation and inverse modeling (Nisbet and Weiss, 2010). The bottom-up approach provides an estimation of aggregated GHG fluxes from different sectors, but large uncertainties exist in certain sectors. For example, agriculture is one of

the most uncertain sectors for estimating the three major GHG fluxes (CO_2, CH_4, and N_2O). Cropland was mostly considered carbon neutral or a carbon source in the IPCC inventory guideline. However, carbon uptake by certain crop types is substantial, while post-harvest emissions vary largely in different regions. CH_4 emissions from rice agriculture and ruminant animals are about half of anthropogenic emissions levels, but the higher estimation boundary could be four times greater than the lower estimation (IPCC, 2001). In addition, the recently claimed emissions from terrestrial plants could account for another 10% to 45% of global emissions. The estimation of N_2O emissions from the agriculture sector has been improved on a global scale, but large uncertainties still exist on plots to regional scales (Reay *et al.,* 2012). The chamber measurements of soil N_2O flux within the same plot can vary by a factor of two or more (Denmead, 2008), and the current N_2O inventory in the U.S. is based on IPCC methods that may have underestimated N_2O emissions by a factor of three or more (Kort *et al.*, 2008). Moreover, it is also unclear how much N_2O soil absorbs as a sink. In addition to the large uncertainties in different sectors, bottom-up methods might under-report the emissions estimated by top-down approach by more than 50% (Mühle *et al.*, 2010; Stohl *et al.*, 2009). The large uncertainties in certain sectors and the major discrepancy between the bottom-up and top-down approaches indicate that the current GHG inventory, mostly based on the bottom-up approach, needs to be improved by a better understanding of GHG fluxes on plot/sector scales, and must be constrained by the top-down approach on regional scale.

Determining and monitoring GHG fluxes on regional scale (10^2 km^2 to 10^6 km^2) is critical for a comprehensive national GHG mitigation strategy, but is still very

challenging to carry out. A review of the current capacity for estimating national GHG anthropogenic emissions suggests that, in developed countries, the bottom-up anthropogenic emissions of all GHG, except for CO_2, suffers from major uncertainties, ranging from 10% to more than 100% (Table 1.1) (National Research Council, 2010). The uncertainties are even larger in developing countries that have not widely adopted accurate estimation methods. On the other hand, limited by available GHG observations and the performance of atmospheric models (such as resolution and accuracy), estimating regional scale GHG fluxes with a top-down approach still suffers from large uncertainties (>50%) (National Research Council, 2010). Due to the limitations in both approaches, little research has been conducted at the regional level. It is critical to fill this knowledge gap, because monitoring the regional GHG fluxes with both top-down and bottom-up approaches can be used to 1) evaluate and monitor the plot/sectoral scale estimation, 2) identify and quantify missing sources and sinks, and 3) refine the global GHG budget. Consequently, this dissertation is dedicated to tackling the challenges in plot and regional scale GHG fluxes (including CO_2, CH_4, and N_2O) with multiple observations and models in an agriculture-dominated landscape. The research will especially focus on the CH_4 and N_2O flux from croplands, one of the biggest uncertainties in the current GHG budget.

In this chapter, I will first review the current status of GHG fluxes quantification, highlight the knowledge gaps, especially in the agricultural sector, and then discuss the impact of fertilization on the GHG fluxes. Consequently, I determine the major research questions and research methods, and give an outline for this dissertation.

Table 1.1. The level of current uncertainty in estimating national anthropogenic GHG budgets in developed countries (adapted from Table S.1 in NRC 2010 report).

	Bottom-up approach (UNFCCC inventory)	**Top-down approach**
CO_2	1	4-5
CH_4	2-3	3-5
N_2O	2-5	4-5
CFCs, PFCs, HFCs, and SF6	1-4	4-5

Note: 1 means that the uncertainty smaller than 10%; 2, 3, and 4 mean that uncertainty levels are between 10% and 25%, between 25% and 50%, and between 50% and 100%, respectively; and 5 means that the uncertainty is bigger than 100%—in other words, it is not certain whether it is a sink or a source.

1.1. Regional CO_2 flux

Accounting for about 60% of the GHG radiative forcing, globally CO_2 has mainly been researched for its sources and sinks. Supported by the evidences, such as decreasing O_2 concentrations and increasing $^{13}C/^{12}C$ ratios (Keeling *et al.*, 2005), the dramatic CO_2 increase since the Industrial Revolution is mainly attributed to fossil fuel emissions.

Current fossil fuel emissions are mainly estimated with a bottom-up approach based on economic statistics and voluntary reports, which tends to underestimate total emissions due to the incomplete nature of the reporting, especially in developing countries. Even though the direct human-induced emissions from agriculture and forestry land use changes are only about 30% of fossil fuel emissions globally (Forster *et al.*, 2007), agricultural and forestry lands play an important role in regional carbon budgets. However, the estimation of biogenic CO_2 flux (flux from cropland and other natural sources/sinks) suffers from large uncertainties because of the heterogeneous land cover type and the inherent heterogeneity of CO_2 fluxes from different land cover types (Chen *et al.*, 2009). As a result, a top-down constraint at the regional level is essential for monitoring CO_2 emissions.

1.1.1. Observation network on atmospheric CO_2

So far, a global network for monitoring CO_2 exchange between the land surface and atmosphere has been established. This network includes four main types of observation, each of which could be applied to estimate regional CO_2 budgets:

1) ***Ground-based CO_2 concentration measurement.*** The National Oceanic and Atmospheric Administration of the United States (NOAA) runs the largest

monitoring network in the world, including six sites with continuous on-site measurement and approximately 50 sites with weekly flask samples (http://www.esrl.noaa.gov/gmd/ccgg/flask.html). These observation sites, located in remote areas such as the South Pole, have been providing basic information on background CO_2 concentration changes. Observation from other organizations and countries is also shared at the World Data Centre for Greenhouse Gases (WDCGG, http://ds.data.jma.go.jp/gmd/wdcgg/wdcgg.html). The WDCGG has better coverage in Europe and Japan, but both the NOAA and the WDCGG have poor coverage in Africa, the Middle East, and northern Asia. By assimilating 28,000 CO_2 concentration observations worldwide, CarbonTracker provides an estimation of CO_2 flux on a $1° \times 1°$ resolution (Peters *et al.*, 2007), but the uncertainty of the CO_2 flux product is significant at the regional level, especially for regions lacking the constraints of ground CO_2 concentration measurements.

2) ***Flux tower measurement.*** In recent years, the network of flux towers, called FLUXNET (Baldocchi *et al.*, 2001), has expanded dramatically from fewer than 10 in 1991 to more than 500 worldwide in 2010 (http://fluxnet.ornl.gov/). Flux towers, depending on location and height, can provide direct measurements of CO_2 flux over certain land cover types or an estimation of regional CO_2 fluxes.
3) ***Aircraft measurement.*** Aircraft can provide direct CO_2 concentration profiles and flux measurements at much higher altitudes, and can yield multiple samples over a large landscape within a short time period. They have been used to estimate the regional to continental GHG fluxes with the assistance of the atmospheric transportation model (Lin *et al.*, 2003; Lin *et al.*, 2004).

4) ***Remote sensing.*** This type of measurement provides two types of information depending on the satellite: land cover types or column-accumulated CO_2 concentrations. The first type of information has been mostly investigated and could be used in aggregating regional biological fluxes (Chen *et al.*, 2008). The second type of information has been extracted from several satellite observations, including the Greenhouse Gases Observing Satellite (GOSAT) launched by Japan (Hamazaki *et al.*, 2004) and the European Space Agency's environmental satellite (ENVISAT), with SCIAMACHY (SCanning Imaging Absorption spectroMeter for Atmospheric CHartographY) on board (Buchwitz *et al.*, 2005). The measurement accuracy of CO_2 concentrations has been improved to a 1.1–1.2 ppm monthly average in a 500-kilometer radius (Schneising *et al.*, 2012), and the Orbiting Carbon Observatory 2 (OCO-2), expected to be launched by NASA by the end of 2014, may further improve measurement precision (Hammerling *et al.*, 2012). However, satellite measurement is still limited by inherent problems such as data gaps due to cloud coverage and poor orbital configurations.

Even though different types of CO_2 observation have become increasingly available globally, the estimation of regional carbon budgets based on these data is still largely uncertain. For example, Desai *et al.* showed discrepancies among CarbonTracker products, equilibrium boundary layer estimations based on tall tower measurements, and bottom-up ecosystem model results (Desai *et al.*, 2010). Consequently, Chapter 4 assembled all available data from the four sources above in the upper Midwest in order to improve the quantification of regional GHG fluxes.

Table 1.2. A summary of current atmospheric CO_2 observations

Categories	**Observation scales**	**Advantage**	**Disadvantage**	**Examples of operating programs**
Ground concentration networks	Global	Provides the baseline CO_2 concentration	Small spatial coverage for each measurement, needs good calibration	CCGG Cooperative Air Sampling Network (operated by NOAA) WDCGG (operated by WMO) (Conway *et al.*, 1994)
Flux tower	Plot to regional	Continuous and direct	Spatial coverage, need good calibration	FLUXNET (Baldocchi *et al.*, 2001)
Aircraft	Regional to global	Direct measurements at higher altitudes, yield multiple samples over a large landscape within a short time period	High expense, limited by weather conditions, and are very indiscrete	HIAPER Pole-to-Pole Observations (HIPPO) (Wofsy *et al.*, 2011)
Remote sensing	Global	Global coverage	Temporal and spatial gaps; uncertainties in measurement	GOSAT, ENVISAT (Buchwitz *et al.*, 2005; Frankenberg *et al.*, 2008; Schneising *et al.*, 2012)

1.1.2. The role of cropland in regional CO_2 flux

Unlike the steady increases in CO_2 concentrations measured at remote background sites, CO_2 concentrations at continental sites could be sizably different in terms of both the annual mean and temporal variation. Strong CO_2 depletion has been observed in the Midwest's Corn Belt (Miles *et al.*, 2012), indicating another strong regional carbon signal related to human activities, in addition to fossil fuel emissions. Even though the crop carbon budget is usually neglected in the national GHG inventory, it worth more investigation, because:

1) The CO_2 uptake by cropland (net primary production) is substantial, equal to approximately 40% of the fossil fuel emissions in the U.S. (West *et al.*, 2011). Improving the management of crop carbon will also lead to GHG mitigation.
2) Even though the net impact of cropland on CO_2 flux is close to zero at the country level and even the global level, cropland can significantly change the regional carbon budget due to the spatial imbalance of production and consumption. Many crops have very different seasonal patterns of CO_2 flux from natural vegetation, such as forests and grasslands (Corbin *et al.*, 2010). For example, the CO_2 uptake by corn plots occurs over a shorter time period and is more intense. As a result, intensive agricultural activities will change regional environmental conditions such as CO_2 concentrations and land surface properties, which may further affect regional weather, climate, and ecosystem functions.
3) Some efforts have been made to examine the regional carbon budget, but large discrepancies still exist between bottom-up and top-down estimations (Desai *et al.*, 2010; Desai *et al.*, 2008; Lauvaux *et al.*, 2012). In regions such as the Midwest,

which has strong biological signals of CO_2 variation, it is very difficult to constrain bottom-up estimations of fossil fuel emissions.

To quantify regional CO_2 flux in a landscape dominated by cropland, and to re-evaluate the role of cropland in regional budgets, we carried out a tall tower measurement in Minnesota and two eddy covariance towers in soybean and cornfields for three years. We estimated regional carbon budgets with three top-down approaches and one bottom-up approach. The analysis of these measurements is presented in Chapter 4.

1.2. CH_4 flux from the global to the regional scale

Attributed to the increasing observation network for CH_4 worldwide and improvements in the global inverse model, the global CH_4 budget has been relatively well constrained (Dlugokencky *et al.*, 2011), but emissions from certain sectors, such as the agricultural sector, still suffers from great uncertainty and, as a result, the reasons for the reduced growth rate of CH_4 concentration from 1980s is still under debate. According to an IPCC report, the global annual CH_4 emissions from 1997 to 2006 were 503–610 Tg yr^{-1} (Forster *et al.*, 2007). The emissions from wetlands and rice agriculture were 100–231 Tg $yr^{-1}$and 31–112 Tg yr^{-1}, making these potentially the top two source categories among all anthropogenic and natural sources, and accounting for up to 60% of total emissions. Emissions from the energy sector were 74-106 Tg yr^{-1}, accounting for only about 15% of total emissions. In contrast, Bousquet *et al.* (2006) estimated similar global CH_4 emissions (525±8 Tg yr^{-1}), but only attributed 31±5 Tg yr^{-1} to CH_4 emissions from rice agriculture (Bousquet *et al.*, 2006). The major variation within and between studies suggests a poor constraint on the CH_4 flux from the rice agriculture and wetlands sectors, and allows for the possibility of unidentified sources/sinks.

In recent years, terrestrial plants have been reported as a new source of CH_4, contributing up to 45% of global CH_4 emissions (Keppler *et al.*, 2006). This new finding may lead to a significant increase in CH_4 flux from the whole agriculture sector (not only rice), and may indicate an uncharacterized mechanism for CH_4 production in aerobic environments. Consequently, it is very important to evaluate and quantify this new source. So far many studies have been conducted to measure plant CH_4 flux, either directly or indirectly, but major discrepancies still exist, even among the independent studies on the same plant species (Zhang *et al.*, in review). Some studies confirmed the emissions from terrestrial plants and proposed mechanisms for the observed emissions (Bruhn *et al.*, 2012). For example, Vigano *et al.* (2008; 2009) found that UV radiation induces CH_4 emissions from plant leaf tissues (Vigano *et al.*, 2009; Vigano *et al.*, 2008), Wang *et al.* reported that cutting injuries stimulate CH_4 emissions from plants (Wang *et al.*, 2009), and Mukhin *et al.* (2009) and Covey *et al.* (2012) both found that methanogenic activities in woody plants also generate significant amounts of methane. However, many other studies suggested that CH_4 flux from plants was either not as strong as reported by Keppler *et al.* or was not observable (Nisbet *et al.*, 2009), and that the up-scaling mechanism used in Keppler's study overestimated the impact of terrestrial plants on the global CH_4 budget (Beerling *et al.*, 2008; Dueck *et al.*, 2007; Kirschbaum and Walcroft, 2008). The discrepancy among studies may be caused in part by measurement artifacts, and no direct measurements of plant CH_4 flux in fields have been taken due to measurement challenges. To tackle these challenges and reduce measurement artifacts, we redesigned a steady-state flow-through chamber and conducted a direct field measurement of CH_4 flux from soybean and corn plants. The details of our methods and results are in Chapter 2.

Compared to a global scale, larger uncertainties exist in the CH_4 flux on regional scales, and constraining regional CH_4 flux based on atmospheric observations is urgently needed to provide an independent evaluation of bottom-up CH_4 inventories. Most regional CH_4 flux estimations are based on bottom-up approaches; for example, the Emission Database for Global Atmospheric Research (EDGAR) was developed by the European Commission, Joint Research Centre (JRC)/Netherlands Environmental Assessment Agency (PBL) based on IPCC guidelines. So far only a few studies have provided top-down estimation of regional CH_4 flux, and most have suggested a large underestimation by the bottom-up method. Kort *et al.* (2008) found that EDGAR underestimated the regional CH_4 flux by a factor of 1.08 with a summer aircraft measurement over northern America and an inverse modeling technique (Kort *et al.*, 2008). Similarly, Jeong *et al.* (2012) found that the California-specific emissions map underestimated CH_4 emissions by a factor of 1.55 to 1.84. The underestimation is smaller in northwest Europe, where Bergamaschi *et al.* (2010) found that the regional flux derived from a network of monitoring stations in Europe was only 21% higher than that of EDGAR v4.0. Invest modeling based on tower and/or aircraft measurements provided a reasonable estimation of regional fluxes, but the modeled results, especially the spatial distributions of emissions, were sensitive to the a priori emissions map and available observations (Bergamaschi *et al.*, 2010; Jeong *et al.*, 2012; Villani *et al.*, 2010). As a result, in Chapter 4 we examine and evaluate the performance of several boundary layer budget methods and an inverse modeling method on estimating regional CO_2 flux, and applied the boundary layer budget methods in estimating regional CH_4 fluxes.

1.3. N_2O flux from a global to a regional scale

As with CH_4, the exchange of N_2O between the land surface and the atmosphere has been well constrained on a global scale—approximately 16 Tg N_2O-N yr^{-1} in the 1990s (Mosier *et al.*, 1998; Reay *et al.*, 2012)—according to the atmospheric sink and the observed N_2O buildup in the atmosphere. Recent studies using bottom-up and top-down methods for estimating N_2O emissions from the agriculture sector produced relatively consistent results, ranging from 4.2 to 7.1 N_2O-N yr^{-1} (Crutzen *et al.*, 2008; Del Grosso *et al.* 2008; Syakila and Kroeze, 2011). In the top-down estimation, Crutzen *et al.* (2008) considered that the natural sources were in a similar state to that of the preindustrial era (10.2 Tg N_2O-N yr^{-1}), and that all anthropogenic emissions, from expected industrial sources, are caused by agriculture, either directly or indirectly; as a result, the agricultural emissions were 5.6-6.5 Tg N_2O-N yr^{-1}.

Two main types of bottom-up estimation of global N_2O emissions were carried out. One is based on IPCC guidelines (IPCC, 2006; Del Grosso *et al.* 2008; Syakila and Kroeze, 2011), which aggregate emissions from different source categories based on emission factors. Agricultural emissions were divided into several categories, including agriculture, biomass and biofuel burning, human excreta, rivers, estuaries, coastal zones, and atmospheric depositions (Denman *et al.*, 2007); each category had its own emission factors. The other bottom-up estimation assumed a universal emission factor of N_2O based only on newly added nitrogen to the land surface via chemical, biological, or atmospheric processes (Crutzen *et al.*, 2008). Similarly, Davidson (2009) assumed two different emission factors for manure and fertilizer input to estimate N_2O emissions from all direct and indirect agricultural emissions except biomass burning.

Even though these bottom-up estimations on a global scale have reached good agreement among themselves and with top-down estimation, it cannot be concluded that they also work well on regional scale flux estimations, because these bottom-up methods neglected the large heterogeneity of N_2O emissions from the plot to the regional scale. For example, due to limited information, many countries only use the universal emission factors provided by the IPCC guidelines (Tier 1), with some using country-specific emission factors (Tier 2), while estimation using direct measurements and modeling results (Tier 3) is very rare. 2) Direct and indirect emissions do not necessarily occur in the same region, and their rates are heterogeneous. Indirect emissions caused by nitrogen addition in the agricultural sector includes atmospheric deposition, nitrogen leaching and runoff, and human sewage, and accounts for roughly 2.2 Tg N_2O-N yr^{-1}, even greater than the direct N_2O emissions (2.6Tg N_2O-N yr^{-1}) (Syakila and Kroeze, 2011). However, it is difficult to track the locations of indirect emissions and distinguish them from emissions from natural sources.

To enable the bottom-up estimation of N_2O on a regional scale and parameterize the N_2O emissions from different land cover types, two main types of measurements were taken (Denmead, 2008). A soil chamber was widely applied to measure N_2O flux from soil. Even though the chamber provided a direct measurement of soil N_2O flux, it poorly addressed the spatial and temporal heterogeneity of the N_2O flux due to its limited coverage over space and time (Jones *et al.*, 2011; Fassbinder *et al.*, 2012). The variation coefficient of the chamber's measurement in the same plot could be over 100% (Denmead, 2008; Jones *et al.*, 2011). In addition, the chamber artifact may largely bias the result (see Chapter 2). The other type of measurement was based on instrumented

towers using micrometeorology techniques, such as eddy covariance and flux-gradient techniques. This type of measurement become available in recent years since N_2O measurement precision and frequency improved dramatically, but the results from the eddy covariance approach need to be further validated since it potentially suffers from 30%–1800% uncertainties (Kroon *et al.*, 2010). The flux-gradient technique has better performance produced results similar to those of the averaged chamber fluxes measured in the same fertilized plot (Denmead, 2008).

Because of the strong heterogeneity of soil N_2O flux suggested by the soil chamber measurement and the heterogeneous land cover on a regional level, the regional flux estimated with a bottom-up method, including both a simple emission factor approach and complex process-based or empirical models, suffered great uncertainty (Leip *et al.*, 2011). Consequently, a top-down constraint on a regional scale is necessary to provide independent constrains for regional flux estimation. Regional N_2O flux estimates based on tall tower or aircraft measurements have become available in recent years, mostly using an inverse modeling approach (Corazza *et al.*, 2011; Kort *et al.*, 2008; Miller *et al.*, 2012; Thompson *et al.*, 2011). Both Kort *et al.* (2008) and Miller *et al.* (2012) suggested a substantial underestimation of an EDGAR bottom-up inventory, indicating the importance of a top-down regional flux constraint. However, inverse modeling is still limited by available observation, and the uncertainties of inverse modeling need to be further evaluated. In contrast, boundary layer budget methods such as the equilibrium method can provide reasonable estimations of regional CO_2 flux based on limited observation data (Helliker *et al.*, 2004), so in Chapter 4 we examined the performance of

boundary layer budget methods in estimating regional N_2O flux and used the results to constrain the bottom-up estimation.

1.4. The impact of nitrogen enrichment on GHG fluxes

Reactive nitrogen (Nr) from anthropogenic sources has increased more than 10-fold since the 1860s (from 15 Tg N yr^{-1} in 1860 to 156 Tg N yr^{-1} in the 1990s), mainly due to increasing population and food demands, and is expected to keep increasing (Galloway *et al.*, 2004). In the early 1990s the total new Nr input from anthropogenic sources was at a rate of 114 Tg N yr^{-1}, of which 75% and 3% was from fertilization (about 86 Tg N yr^{-1}) and the expanded planting of nitrogen-fixing plants (about 3.5 Tg N yr^{-1}), respectively (Crutzen *et al.*, 2008; Galloway *et al.*, 2004).

This anthropogenic nitrogen input significantly improved cropland productivity and increased the carbon sequestration by terrestrial ecosystems; however, it also was accompanies by many environmental problems, and the carbon benefit might be offset by additional CH_4 and N_2O emissions induced by nitrogen enrichment (Zaehle *et al.*, 2011). A meta-analysis of the influence of nitrogen addition on CO_2, CH_4, and N_2O fluxes from both agricultural and natural ecosystems suggested that, even though nitrogen enrichment can enhance carbon uptake by forest and agricultural systems by 2%–6%, it also increases CH_4 emissions and/or suppresses CH_4 uptake, as well as increasing N_2O emissions by more than a factor of two (Liu and Greaver, 2009).

So far, the impact of nitrogen enrichment on global GHG budgets has not been well quantified (Dalal and Allen, 2008), and discrepancies exist in terms of how much the stimulated N_2O and CH_4 emissions can offset the carbon benefit. Liu and Greaver (2009)

concluded that the additional CH_4 and N_2O emissions led by nitrogen enrichment offset 53%–76% of the carbon benefits by additional carbon sequestration, while Zaehle *et al.* suggested that only N_2O emissions can offset the whole carbon benefit. Moreover, Hoben *et al.* (2011) reported that N_2O emissions increase exponentially with nitrogen enrichment rates, suggesting that the offset of the carbon benefit may increase as dramatically as the intensifying nitrogen enhancement. As a result, it is critical to quantify the response of GHG fluxes to nitrogen enhancement. Consequently, we examined the impact of fertilization on plant CO_2, plant CH_4, and N_2O fluxes from plant and soil-plant ecosystems in Chapters 2 and 3 and evaluated the impact of fertilization on regional GHG fluxes.

1.5. Research questions and methods

This work determined to address the following research questions:

1) Do crop plants emit or absorb CH_4 and N_2O? Is crop plant flux important to regional GHG flux from an agriculture-dominated landscape?

2) Does nitrogen fertilization affect GHG fluxes from plant and soil-plant ecosystems? How great is the impact of nitrogen enhancement on regional GHG fluxes?

3) How great are the uncertainties in using boundary layer budget methods to estimate regional CO_2 fluxes based on tall tower measurements? Are these methods applicable to estimating regional CH_4 and N_2O fluxes, and how great are these uncertainties in the context of limited regional observations?

4) How is the regional GHG flux estimated from a tower measurement (top-down method) compared with the bottom-up estimation based on IPCC guidelines? What is the implication for quantifying global GHG fluxes?

To address these questions, we established an observation system measuring GHG flux on three contrasting scales: a plant/soil scale, an ecosystem scale, and a regional scale. On the plant/soil scale, we redesigned a steady-state flow-through chamber to measure the CO_2, CH_4, and N_2O fluxes from the aboveground sections of crop plants (soybean and corn) in 2008 and 2009 in a soybean-corn rotation field at the University of Minnesota's Outreach, Research and Education Park. Six soil chambers were installed to measure soil N_2O flux from the same plot (Fassbinder *et al.*, 2012). The CO_2 and N_2O flux from a soil-plant ecosystem was measured by an eddy covariance method and flux-gradient method, respectively, in the middle of the same field. Another CO_2 eddy covariance measurement was conducted simultaneously in another field with the opposite rotation schedule. The regional flux was measured at a 244 m tall tower facility three kilometers southeast of the soybean-corn rotation field (Griffis *et al.*, 2010). The experiment site, located 20 kilometers south of Minneapolis, is surrounded by an agriculture-dominated landscape (Figure 1.1.).

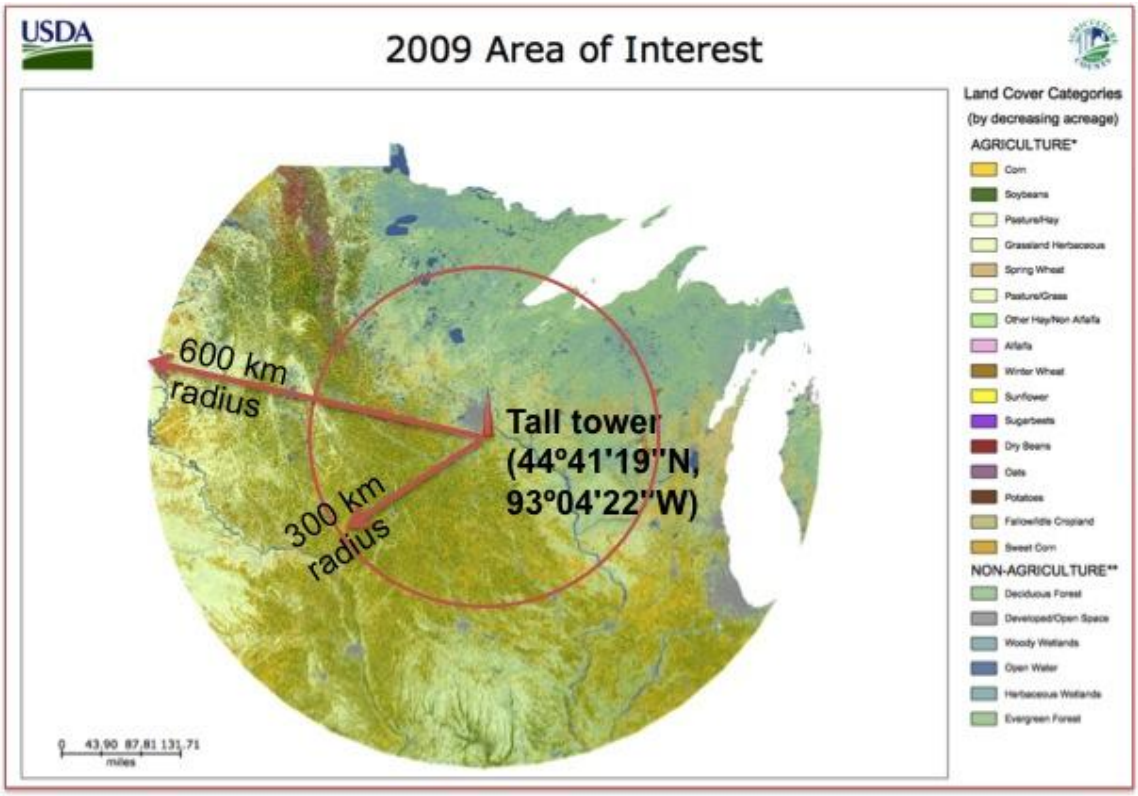

Figure 1.1. Land cover types around the tall tower (USDA Crop Data Layer data in 2009). This graph was produced by CropScape (http://nassgeodata.gmu.edu/CropScape). In the legend, only the top 16 agriculture categories and the top six non-agriculture categories are listed.

1.6. Dissertation outline

This dissertation is composed of five chapters. The first chapter provides an overview of current GHG fluxes quantification on a regional to a global scale, emphasizes the importance of constraining regional GHG fluxes with top-down methods, and points out the knowledge gap in determining a plant's GHG fluxes. It further summarizes the major research questions and methods and provides an outline of this dissertation.

Chapters 2 to 4 present in detail the research conducted for addressing the research questions concluded in Chapter 1. Chapter 2 examines the CH_4 flux from corn and soybean plants and determined the role of plant flux in the agriculture-dominated landscape. Chapter 3 quantifies the N_2O flux from plant, soil, and soil-plant ecosystems, as well as the agriculture-dominated landscape during the growing season, and evaluates the impact of fertilization on N_2O flux from different scales. Chapter 4 mainly focuses on examining the methodologies for quantifying regional GHG flux. In this chapter we tested multiple bottom-up and top-down methods for estimating regional CO_2 flux and evaluated the performance and uncertainties of the equilibrium method. Further, we applied the equilibrium method to estimating regional N_2O and CH_4 fluxes and evaluated the uncertainties of the estimation.

Finally, Chapter 5 summarizes the major results from the whole dissertation research and provides insights into the research and policy implications on GHG regulation.

1.7. References

Baldocchi, D. et al., 2001. FLUXNET: A new tool to study the temporal and spatial variability of ecosystem-scale carbon dioxide, water vapor, and energy flux densities. Bulletin of the American Meteorological Society, 82(11): 2415-2434.

Beerling, D.J., Gardiner, T., Leggett, G., McLeod, A. and Quick, W.P., 2008. Missing methane emissions from leaves of terrestrial plants. Global Change Biology, 14(8): 1821-1826.

Bergamaschi, P. et al., 2010. Inverse modeling of European CH_4 emissions 2001–2006. Journal of Geophysical Research-Atmospheres, 115.

Bousquet, P. et al., 2006. Contribution of anthropogenic and natural sources to atmospheric methane variability. Nature, 443(7110): 439-443.

Bruhn, D., Møller, I.M., Mikkelsen, T.N. and Ambus, P., 2012. Terrestrial plant methane production and emission. Physiologia Plantarum, 144(3): 201-209.

Buchwitz, M. et al., 2005. Atmospheric methane and carbon dioxide from SCIAMACHY satellite data: initial comparison with chemistry and transport models. Atmospheric Chemistry and Physics, 5: 941-962.

Chen, B., Chen, J.M., Mo, G., Black, A. and Worthy, D.E.J., 2008. Comparison of regional carbon flux estimates from CO_2 concentration measurements and remote sensing based footprint integration. Global Biogeochemical Cycles, 22(GB2012).

Chen, B.Z. et al., 2009. Assessing tower flux footprint climatology and scaling between remotely sensed and eddy covariance measurements. Boundary-Layer Meteorology, 130(2): 137-167.

Conway, T.J., Tans, P.P., Waterman, L.S. and Thoning, K.W., 1994. Evidence for interannual variability of the carbon cycle from the National Oceanic and Atmospheric Administration/Climate Monitoring and Diagnostics Laboratory Global Air Sampling Network. Journal of Geophysical Research-Atmospheres, 99(D11): 22831-22855.

Corazza, M. et al., 2011. Inverse modelling of European N_2O emissions: assimilating observations from different networks. Atmospheric Chemistry and Physics, 11(5): 2381-2398.

Corbin, K.D. et al., 2010. Assessing the impact of crops on regional CO_2 fluxes and atmospheric concentrations. Tellus Series B-Chemical and Physical Meteorology, 62(5): 521-532.

Covey, K.R., Wood, S.A., Warren, R.J., Lee, X. and Bradford, M.A., 2012. Elevated methane concentrations in trees of an upland forest. Geophysical Research Letters, 39.

Crutzen, P.J., Mosier, A.R., Smith, K.A. and Winiwarter, W., 2008. N_2O release from agro-biofuel production negates global warming reduction by replacing fossil fuels. Atmospheric Chemistry and Physics Discussions, 8(2): 389-395.

Dalal, R.C. and Allen, D.E., 2008. Greenhouse gas fluxes from natural ecosystems. Australian Journal of Botany, 56(5): 369-407.

Davidson, E.A., 2009. The contribution of manure and fertilizer nitrogen to atmospheric nitrous oxide since 1860. Nature Geoscience, 2(9): 659-662.

Del Grosso, S.J., Wirth, T., Ogle, S.M. and Parton, W.J., 2008. Estimating agricultural nitrous oxide emissions. Eos, Transactions, American Geophysical Union, 89(51), 529, doi:10.1029/2008EO510001.

Denmead, O.T., 2008. Approaches to measuring fluxes of methane and nitrous oxide between landscapes and the atmosphere. Plant and Soil, 309(1-2): 5-24.

Desai, A.R. et al., 2008. Influence of vegetation and seasonal forcing on carbon dioxide fluxes across the Upper Midwest, USA: Implications for regional scaling. Agricultural and Forest Meteorology, 148(2): 288-308.

Desai, A.R., Helliker, B.R., Moorcroft, P.R., Andrews, A.E. and Berry, J.A., 2010. Climatic controls of interannual variability in regional carbon fluxes from top-down and bottom-up perspectives. Journal of Geophysical Research-Biogeosciences, 115.

Dlugokencky, E.J., Nisbet, E.G., Fisher, R. and Lowry, D., 2011. Global atmospheric methane: budget, changes and dangers. Philosophical Transactions of the Royal Society-A. Mathematical, Physical, and Engineering Sciences, 369(1943): 2058-2072.

Dueck, T.A. et al., 2007. No evidence for substantial aerobic methane emission by terrestrial plants: A ^{13}C-labelling approach. New Phytologist, 175(1): 29-35.

Eggleston, H.S., Buendia, L., Miwa, K., Ngara, T. and Tanabe, K. (Editors), 2006. IPCC guidelines for national greenhouse gas inventories, Volume 4: Agriculture, forestry and other land use. IGES.

Fassbinder, J.J., Schultz, N.M., Baker, J.M. and Griffis T.J., 2012. Automatic, low-power chamber system for measuring N_2O emissions. Journal of Environmental Quality, accepted with revisions.

Forster, P. et al., 2007. Changes in atmospheric constituents and in radiative forcing. In: Climate Change 2007: The physical science basis. Contribution of Working Group I to the Fourth Assessment Report of the Intergovernmental Panel on Climate Change (Solomon, D. Qin, M. Manning, Z. Chen, M. Marquis, K. Averyt, M. Tignor and H. Miller, Editors). Cambridge, UK: Cambridge University Press.

Frankenberg, C. et al., 2008. Tropical methane emissions: A revised view from SCIAMACHY onboard ENVISAT. Geophysical Research Letters, 35(15).

Galloway, J.N. et al., 2004. Nitrogen cycles: Past, present, and future. Biogeochemistry, 70(2): 153-226.

Griffis, T.J. et al., 2010. Influence of C_4 vegetation on $^{13}CO_2$ discrimination and isoforcing in the upper Midwest, United States. Global Biogeochemical Cycles, 24: 16.

Griffis, T.J., Lee, X., Baker, J.M., Russelle, M., Zhang, X., Venterea, R. and Millet D., 2012. Large nitrous oxide emission factors for the United States Corn Belt revealed by atmospheric concentration measurements. Submitted to Nature October 1, 2012, currently in review.

Hamazaki, T., Kuze, A. and Kondo, K., 2004. Sensor system for greenhouse gas observing satellite (GOSAT). Infrared Spaceborne Remote Sensing XII, 5543: 275-282.

Hammerling, D.M., Michalak, A.M. and Kawa, S.R., 2012. Mapping of CO_2 at high spatiotemporal resolution using satellite observations: Global distributions from OCO-2. Journal of Geophysical Research-Atmospheres, 117.

Helliker, B.R. et al., 2004. Estimates of net CO_2 flux by application of equilibrium boundary layer concepts to CO_2 and water vapor measurements from a tall tower. Journal of Geophysical Research-Atmospheres, 109(D20).

Hoben, J.P., Gehl, R.J., Millar, N., Grace, P.R. and Robertson, G.P., 2011. Nonlinear nitrous oxide (N_2O) response to nitrogen fertilizer in on-farm corn crops of the US Midwest. Global Change Biology, 17(2): 1140-1152.

IPCC, 2006. IPCC Guidelines for National Greenhouse Gas Inventories, 5 volumes, Institute for Global Environmental Strategies, Hayama, Kanagawa, Japan.

Jeong, S. et al., 2012. Seasonal variation of CH_4 emissions from central California. Journal of Geophysical Research-Atmospheres, 117.

Jones, S.K. et al., 2011. Nitrous oxide emissions from managed grassland: a comparison of eddy covariance and static chamber measurements. Atmospheric Measurement Techniques, 4(10): 2179-2194.

Keeling, C.D. and Whorf, T.P., 2005. Atmospheric CO_2 records from sites in the SIO air sampling network. In: Trends: A Compendium of Data on Global Change. Carbon Dioxide Information Analysis Center, Oak Ridge National Laboratory, U.S. Department of Energy, Oak Ridge, TN, http://cdiac.esd.ornl.gov/trends/co2/sio-keel-flask/sio-keel-flask.html.

Keeling, C.D., Bollenbacher, A.F. and Whorf, T.P., 2005. Monthly atmospheric $^{13}C/^{12}C$ isotopic ratios for 10 SIO stations. In: Trends: A Compendium of Data on Global Change. Carbon Dioxide Information Analysis Center, Oak Ridge National Laboratory, U.S. Department of Energy, Oak Ridge, TN, http://cdiac.ornl.gov/trends/co2/iso-sio/iso-sio.html.

Keppler, F., Hamilton, J.T.G., Braß, M. and Röckmann, T., 2006. Methane emissions from terrestrial plants under aerobic conditions. Nature, 439(7073): 187-191.

Kirschbaum, M.U.F. and Walcroft, A., 2008. No detectable aerobic methane efflux from plant material, nor from adsorption/desorption processes. Biogeosciences, 5(6): 1551-1558.

Kort, E.A., Eluszkiewicz, J., Stephens, B.B., Miller, J.B., Gerbig, C., Nehrkorn, T., Daube, B.C., Kaplan, J.O., Houweling, S. and Wofsy, S.C., 2008. Emissions of CH_4 and N_2O over the United States and Canada based on a receptor-oriented modeling framework and COBRA-NA atmospheric observations. Geophysical Research Letters, 35(18).

Kroon, P.S., Hensen, A., Jonker, H.J.J., Ouwersloot, H.G., Vermeulen, A.T. and Bosveld, F.C., 2010. Uncertainties in eddy covariance flux measurements assessed from CH_4 and N_2O observations. Agricultural and Forest Meteorology, 150(6): 806-816.

Lauvaux, T. et al., 2012. Constraining the CO_2 budget of the corn belt: exploring uncertainties from the assumptions in a mesoscale inverse system. Atmospheric Chemistry and Physics, 12(1): 337-354.

Leip, A. et al., 2011. Estimation of N_2O fluxes at the regional scale: data, models, challenges. Current Opinion in Environmental Sustainability, 3(5): 328-338.

Lin, J.C. et al., 2003. A near-field tool for simulating the upstream influence of atmospheric observations: The Stochastic Time-Inverted Lagrangian Transport (STILT) model. Journal of Geophysical Research-Atmospheres, 108(D16).

Lin, J.C. et al., 2004. Measuring fluxes of trace gases at regional scales by Lagrangian observations: Application to the CO_2 Budget and Rectification Airborne (COBRA) study. Journal of Geophysical Research-Atmospheres, 109(D15).

Liu, L.L. and Greaver, T.L., 2009. A review of nitrogen enrichment effects on three biogenic GHGs: the CO_2 sink may be largely offset by stimulated N_2O and CH_4 emission. Ecology Letters, 12(10): 1103-1117.

Marquis, M. and Tans, P., 2008. Climate change - Carbon crucible. Science, 320(5875): 460-461.

Miles, N.L. et al., 2012. Large amplitude spatial and temporal gradients in atmospheric boundary layer CO_2 mole fractions detected with a tower-based network in the U.S. upper Midwest. Journal of Geophysical Research-Biogeosciences, 117.

Miller, S.M. et al., 2012. Regional sources of nitrous oxide over the United States: Seasonal variation and spatial distribution. Journal of Geophysical Research-Atmospheres, 117.

Mosier, A. et al., 1998. Closing the global N_2O budget: nitrous oxide emissions through the agricultural nitrogen cycle: OECD/IPCC/IEA phase II development of IPCC guidelines for national greenhouse gas inventory methodology. Nutrient Cycling in Agroecosystems, 52(2-3): 225-248.

Mühle, J. et al., 2010. Perfluorocarbons in the global atmosphere: tetrafluoromethane, hexafluoroethane, and octafluoropropane. Atmospheric Chemistry and Physics, 10(11): 5145-5164.

Mukhin, V.A. and Voronin, P.Y., 2009. Methanogenic activity of woody plants. Russian Journal of Plant Physiology, 56(1): 138-140.

Nisbet, E. and Weiss, R., 2010. Top-down versus bottom-up. Science, 328(5983): 1241-1243.

Nisbet, R.E.R. et al., 2009. Emission of methane from plants. Proceedings of the Royal Society-B. Biological Sciences, 276(1660): 1347-1354.

Peters, W. et al., 2007. An atmospheric perspective on North American carbon dioxide exchange: CarbonTracker. Proceedings of the National Academy of Sciences of the United States of America, 104(48): 18925-18930.

Reay, D.S. et al., 2012. Global agriculture and nitrous oxide emissions. Nature Climate Change, 2(6): 410-416.

Schneising, O. et al., 2012. Atmospheric greenhouse gases retrieved from SCIAMACHY: comparison to ground-based FTS measurements and model results. Atmospheric Chemistry and Physics, 12(3): 1527-1540.

Stohl, A. et al., 2009. An analytical inversion method for determining regional and global emissions of greenhouse gases: Sensitivity studies and application to halocarbons. Atmospheric Chemistry and Physics, 9(5): 1597-1620.

Syakila, A. and Kroeze, C., 2011. The global nitrous oxide budget revisited. Greenhouse Gas Measurement and Management, 1(1), 17-26.

Thompson, R.L., Gerbig, C. and Rodenbeck, C., 2011. A Bayesian inversion estimate of N_2O emissions for western and central Europe and the assessment of aggregation errors. Atmospheric Chemistry and Physics, 11(7): 3443-3458.

Vigano, I. et al., 2008. Effect of UV radiation and temperature on the emission of methane from plant biomass and structural components. Biogeosciences, 5(3): 937-947.

Vigano, I. et al., 2009. UV light induces methane emission from plant biomass: Mechanism and isotope studies. Geochimica Et Cosmochimica Acta, 73(13): A1382.

Villani, M.G., Bergamaschi, P., Krol, M., Meirink, J.F. and Dentener, F., 2010. Inverse modeling of European CH_4 emissions: sensitivity to the observational network. Atmospheric Chemistry and Physics, 10(3): 1249-1267.

Wang, Z.-P. et al., 2009. Physical injury stimulates aerobic methane emissions from terrestrial plants. Biogeosciences, 6(4): 615-621.

West, T.O., Bandaru, V., Brandt, C.C., Schuh, A.E. and Ogle, S.M., 2011. Regional uptake and release of crop carbon in the United States. Biogeosciences, 8(8): 2037-2046.

Wofsy, S.C., Team, H.S., Team, C.M. and Team, S., 2011. HIAPER Pole-to-Pole Observations (HIPPO): fine-grained, global-scale measurements of climatically important atmospheric gases and aerosols. Philosophical Transactions of the Royal Society a-Mathematical Physical and Engineering Sciences, 369(1943): 2073-2086.

Zaehle, S., Ciais, P., Friend, A.D. and Prieur, V., 2011. Carbon benefits of anthropogenic reactive nitrogen offset by nitrous oxide emissions. Nature Geoscience, 4(9): 601-605.

Zhang, X., Lee, X.H., Griffis, T.J., Baker, J.M., Erickson, M.D., Hu, N. and Xiao, W., 2012). The influence of plants on atmospheric methane in an agriculture-dominated landscape. In review.

Chapter 2: The influence of plants on atmospheric methane in an agriculture-dominated landscape

Abstract

The primary objective of this study is to clarify the influence of crop plants on atmospheric methane (CH_4) in an agriculture-dominated landscape in the Upper Midwest of the United States. Measurements were carried out at two contrasting scales. At the plant scale, CH_4 fluxes from soybean and corn plants were measured with a laser-based plant chamber system. At the landscape scale, the land surface flux was estimated with a modified Bowen ratio technique using measurements made on a tall tower. The chamber data revealed a diurnal pattern for the plant CH_4 flux: it was positive (an emission rate of 0.4 ± 0.1 nmol m^{-2} s^{-1}, average of soybean and corn, in reference to the unit ground area) during the day and negative (an uptake rate of -0.8 ± 0.8 nmol m^{-2} s^{-1}) during the night. At the landscape scale, the flux was estimated to be 14.8 nmol m^{-2} s^{-1} at night and highly uncertain during the day, but the available references and the flux estimates from the equilibrium methods suggested that the CH_4 flux during the entire observation period was similar to the estimated nighttime flux. Thus, soybean and corn plants have a negligible role in the landscape-scale CH_4 budget.

Keywords: methane; corn; soybean; agriculture; land surface flux; footprint analysis.

2.1. Introduction

Methane (CH_4) represents one of the primary greenhouse gases, and estimates of its terrestrial sinks and sources are subject to large uncertainties. To date, most studies have focused on CH_4 emissions from wetlands/peatlands, agricultural feed lots/lagoons, and municipal waste sites (Le Mer and Roger 2001; Mosher *et al.*, 1999; Shurpali *et al.*, 1993; Shurpali and Verma 1998). Recently, Keppler *et al.* (2006) suggested that the CH_4 flux of terrestrial vegetation may be up to 236 Tg yr^{-1}, accounting for about 45% of the global terrestrial emissions. The plant pathway of aerobic CH_4 generation suggested by Keppler *et al.* (2006) has led to a reevaluation of CH_4 sources and stimulated a new debate regarding the role of plants in greenhouse gas mitigation strategies (Butenhoff and Khalil 2007; Dueck and Van Der Werf 2008; Nisbet *et al.*, 2009; Parsons *et al.*, 2006). In this study, we examine the influence of agricultural crops (corn and soybean) on the plant-scale and landscape-scale CH_4 budget. Given the large spatial extent of corn and soybeans grown in the United States (U.S.), their high net primary productivity, and the large nutrient inputs used to support these systems (U.S. Department of Agriculture [USDA] 2009), we hypothesize that their influence on atmospheric CH_4 is important during the growing season and aim to better understand the underlying mechanisms.

At the plant scale, researchers have reported that CH_4 emissions are often below detection limits (Beerling *et al.*, 2008; Dueck *et al.*, 2007; Kirschbaum and Walcroft 2008), while others have demonstrated significant emissions for many plant species (Keppler *et al.*, 2006; Vigano *et al.*, 2008; Wang *et al.*, 2008). Even for the same species, the findings are not consistent. For example, in previous studies, the CH_4 flux for corn (*Zea mays*) ranged from -0.43 nmol m^{-2} s^{-1} to 11 nmol m^{-2} s^{-1} (Table 2.1). The discrepancy among the

published studies on plant-scale CH_4 flux can be partly attributed to experimental artifacts. Measurements of plant-scale CH_4 fluxes are challenging because plant-induced variations in CH_4 concentration are very small compared to ambient variations, and the measurements can be influenced by many experimental conditions. Evidence suggests that CH_4 flux is lower in the dark than if the plant is exposed to ultraviolet (UV) radiation (McLeod *et al.*, 2008; Vigano *et al.*, 2008, 2009), indicating that measurements made in artificial light environments may not represent field conditions. In some experiments, the plants are immersed in a CH_4-free gas or a gas with a low CH_4 concentration to improve the sensitivity of the CH_4 flux detection (Beerling *et al.*, 2008; Keppler *et al.*, 2006; Kirschbaum and Walcroft 2008; Vigano *et al.*, 2008). This experimental design excludes the possibility of plant uptake and may lead to additional CH_4 flux through the adsorption/desorption processes and through diffusion via the plant tissue driven by an enhanced concentration gradient between the leaf and the soil. Several experiments have involved detached plant tissues (Wang *et al.*, 2008; Vigano *et al.*, 2008), and the detected CH_4 emission may be caused by the physical damage associated with extracting tissue (Wang *et al.*, 2009). Furthermore, most plant chambers are characterized by increased temperature and humidity compared to ambient conditions (Keppler *et al.*, 2006; Kirschbaum and Walcroft 2008; Nisbet *et al.*, 2009). The effect of elevated temperature, humidity, and other altered abiotic conditions on plant CH_4 flux is not well-known.

Table 2.1. A summary of observed CH_4 flux from corn (*Zea mays*). For unit conversion, we assume a biomass value of 1652 g m^{-2}.

Reference	**Light type**	**Light Intensity (W m^{-2})**	**CH_4 background concentration (ppb)**	**Intact/detached**	**CH_4 Flux (nmol m^{-2} s^{-1})**
Beerling *et al*., 2008	Lamp	152	59	Intact	0.06 ± 0.57
	Dark	0	59	Intact	0.14 ± 1.15
Dueck *et al*., 2007	Lamp	65/130	2100	Intact	0.80 ±1.03
Kirschbaum and Walcroft 2008	Lamp	1	0	Intact	-0.007 ± 0.032
Nisbet *et al*., 2009	Lamp	39	1984±6	Detached leaves	-0.43 ± 0.49
	Lamp	39	2021±5	Detached leaves	0.74 ± 2.45
Keppler *et al*., 2006	Sunlight	-	0	Intact	11 (6-17)
	Dark	0	0	Intact	3 (1-6)
Vigano *et al*., 2008	UV lamp	49	Ambient or 0	Detached (fresh)	1.4
	UV lamp	49	Ambient or 0	Detached (dry)	0.7
This paper	Sunlight (with 10% UV reduction)	Ambient	Ambient	Intact	0.11 ± 0.06 (DOY 201–218)
	Dark	0	Ambient	Intact	-0.13 ± 0.12 (DOY 201–218)

Agricultural ecosystems are heavily managed and corn-soybean rotations require significant nutrient input (Karlen *et al.*, 1995). However, the impact of nitrogen enrichment on plant flux has not been addressed in the literature, while soil nitrogen has been extensively studied as a regulatory factor involved in soil CH_4 flux. Nitrogen enrichment affects the production and consumption pathways of CH_4 by increasing the redox potential and competing against CH_4 to react with methane monooxygenase. For soils emitting CH_4, nitrogen enrichment can increase the net emission by up to 97%, while for soils absorbing CH_4, nitrogen enrichment can suppress the uptake by 38% (Liu and Greaver 2009). We hypothesize that nitrogen enrichment should increase CH_4 emission or suppress CH_4 uptake from plants.

To date, most CH_4 studies have been based on chamber techniques that have relatively poor temporal and spatial resolution. However, methane fluxes are known to be episodic (ebullition events can be triggered by changes in atmospheric pressure) and have been shown to vary significantly within similar field conditions (Hendriks *et al.*, 2010; Kroon *et al.*, 2007; Pattey *et al.*, 2006; Smeets *et al.*, 2009). The heterogeneity of CH_4 flux implies that upscaling plot-scale measurements (the bottom-up method) to estimate the regional CH_4 budget will carry large uncertainties.

The tall tower top-down method can help constrain these uncertainties at regional scales. Few studies have attempted to measure the landscape-scale CH_4 budget based on near-continuous monitoring of atmospheric mixing ratios. Using the Weather Research and Forecast (WRF) and the Stochastic Time-inverted Lagrangian Transport (STILT) model to interpret the CH_4 concentration measured at a tall tower, Zhao *et al.* (2009) found that the CH_4 emission was 37 ± 21% higher than the bottom-up emission estimates. Another

successful application of this approach was reported by Werner *et al.* (2003), who measured CH_4 gradients at a 447-m tall tower in Wisconsin, which is about 300 km from our Minnesota research site, in a landscape of wetland and upland forests. They found that the emission flux of the wetlands exceeded the uptake flux of the forests, resulting in a net regional CH_4 flux of 17 ± 10 nmol m^{-2} s^{-1}.

Consequently, the objectives of this study are to:

1) Use a new dynamic chamber design to reduce measurement artifacts to clarify the influence of crop plants on atmospheric CH_4.

2) Explore whether nitrogen fertilization changes the magnitude or direction of CH_4 plant flux.

3) Examine the regional CH_4 budget using a top-down approach involving CH_4 concentration and gradient measurements on a tall tower and examine the relative role of agricultural plants in the regional budget.

2.2. Materials and methods

2.2.1. Research site

The field experiment was conducted at the University of Minnesota Outreach, Research and Education Park. The research site is located 20 km south of Minneapolis. The plant flux measurement was made in a field of a soybean (*Glycine max*)-corn (*Zea mays*) rotation management that is characteristic of the Upper Midwest (Griffis *et al.*, 2005). The soil is a Waukegan silt loam about 0.5–1.8 m thick, which is underlain by sand and gravel. This field was converted from a prairie to agriculture 130 years ago (Griffis *et al.*, 2005). The land management techniques applied at this site are typical for the region. In the 2008 soybean phase, no fertilizer was applied, except in a small area that was

reserved for the fertilizer treatment/experiment. In the 2009 corn phase, fertilizer in the form of anhydrous ammonia was applied at a rate of 112 kg N ha^{-1} on April 15 (Day of Year or DOY 106) except for the zone reserved for non-fertilization treatment.

In the 2008 soybean phase, three soybean plants were selected from three random plots for flux measurements. In the middle of the growing season (July 10, DOY 192), three additional plots of 1 m radius were treated with fertilizer (24-8-16, NPK; Scotts Miracle-Gro, Marysville, OH) at a rate of 500 kg N ha^{-1}. The fertilizer intensity was the upper limit of the growing season total N application rate found in the literature. The flux measurement was carried out on one plant in the center of each fertilization plot. The chamber measurements started on DOY 160 and ended on DOY 225. The plant density was 30 plants m^{-2}.

In the 2009 corn phase, measurements were made on three corn plants in three random plots. To test the effect of fertilization, a buffer strip (8 m × 30 m) was excluded from fertilization. Three unfertilized corn plants chosen from three random plots within the strip were also measured. The chamber measurement started on DOY 147 and ended on DOY 218. The plant density was 8.1 plants m^{-2}.

The tall tower (244 m) facility is located 3 km southeast of the soybean/corn field (Griffis *et al.*, 2010). A footprint analysis using the STILT model (Lin *et al.*, 2003) during the tall tower observation period (DOY 243 - 269, 2009) revealed that 66% of the tower footprint was cropland.

2.2.2. Measurement with plant chambers

A steady-state flow-through chamber system was used to measure the plant CH_4 and CO_2 fluxes (Figure 2.1). It consisted of plant chambers of varying sizes, a cooling apparatus,

and gas analyzers. To accommodate plant growth, we used three chamber sizes: small (25 cm × 25 cm × 25 cm), medium (50 cm × 50 cm × 50 cm), and large (50 cm × 50 cm × 150 cm). Two fans positioned near the top of the chamber and pointed at downward-facing angles promoted mixing inside. The small and medium chambers were made of transparent plexiglass with minimum light attenuation (<8% in the photosynthetically active radiation [PAR] waveband, and <10% in the UV waveband). The chamber was seated on a metal base frame 5 cm above the soil surface. Two plexiglass plates were placed on the base, allowing one plant stem to pass through a hole at the center. The chamber base was not sealed; instead, ambient air entered the chamber from the perimeter of the base, and the CH_4 and CO_2 concentrations in the air were continuously sampled and measured. The large chamber was used when the corn plants were taller than 1.5 m. It consisted of the medium chamber with the base removed and a skirt made of transparent polyethylene. The plexiglass chamber rested on a metal frame whose height was adjustable from 1 m to 1.7 m. The polyethylene skirt was attached to the sides of the plexiglass chamber using strong bonding tape, and was sealed by water. The bottom of the skirt was loosely tied to the base of the plant allowing air to enter from the base of the plant.

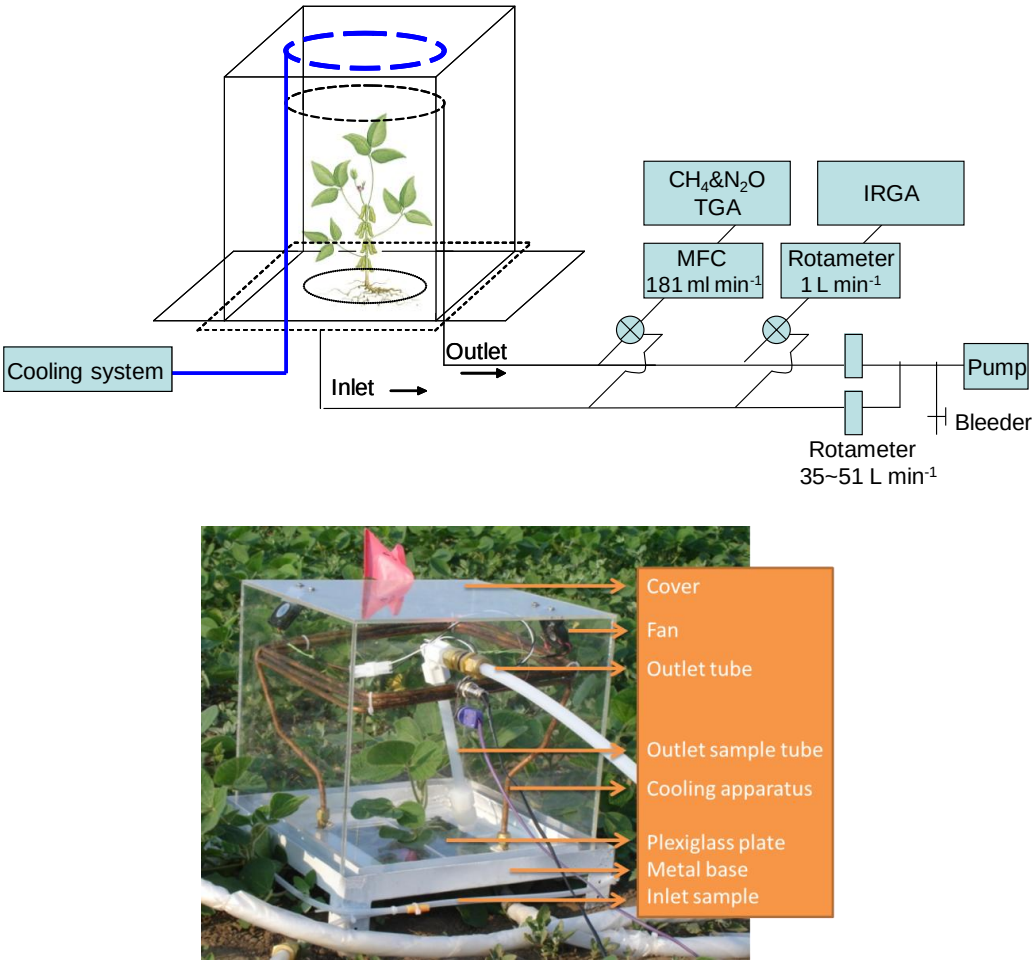

Figure 2.1. A schematic diagram and a picture of the plant chamber system.

A cooling system kept the chamber temperature consistent with ambient conditions by circulating chilled water through a heat exchanger inside the chamber. Control of the cooling was achieved by adjusting the water circulation rate. Temperature was monitored using thermocouples inside and outside the chamber. The difference between the chamber temperature and the ambient temperature was maintained to within ±3°C.

The chamber system could accommodate only one plant at a time. Therefore, we were limited to measuring one plant per day. The system was rotated sequentially among the replicated plots. One complete rotation took 6–7 days. The cooling system permitted continuous measurement throughout the daytime and nighttime without overheating in full sunlight. This arrangement was a compromise between capturing temporal variations at the diurnal and seasonal time scales and spatial variations among the replicates.

Two analyzers were used to measure the CO_2, N_2O, and CH_4 mixing ratios of the inlet and outlet air streams of the chamber. The base flow rate of the outlet was maintained at 35 L min^{-1}, 47 L min^{-1}, and 51 L min^{-1} for the small, medium, and large chambers, respectively. The flow rate was set relatively high to reduce the impact of the strong CO_2 depletion inside the chamber during the daytime. The inlet air was sampled with a tube with evenly distributed holes attached to the outside perimeter of the bottom of the chamber. Air entered from the unsealed bottom of the chamber as described and was pumped out (outlet air) at the base flow rates by a tube placed vertically inside the chamber (Figure 2.1). This tube had small sampling holes evenly distributed from the bottom to the top to avoid the artifact of the concentration gradient inside the chamber. All sampling tubes were made of high-density polyethylene material. Two subsamples were drawn from the inlet and outlet tubes for the CH_4/N_2O and CO_2/H_2O measurements,

at flow rates of 180 ml min^{-1} and 1.0 L min^{-1}, respectively. A tunable diode laser analyzer (TDL, model TGA 100A, Campbell Scientific Inc., Logan, Utah, USA) was used to measure the CH_4 and N_2O mixing ratios. The laser temperature was optimized and maintained at 90.80 K in 2008 and 91.30 K in 2009, while the temperature of the detectors was maintained at 135.5 K using liquid nitrogen. The sample cell pressure was maintained at 36 mb. The TDL was plumbed to a four-port manifold that used a switching sequence in the order of inlet, outlet, calibration zero, and calibration span, with 20 s spent on each port and the first 10 s after each switching omitted from the analysis. The CO_2 and H_2O mixing ratios were measured using an infrared gas analyzer (IRGA; LI-6262, LI-COR Inc., Lincoln, NE, USA). This analyzer was switched between the inlet and outlet air flows every 1 min, with the first 30 s after each switching excluded from the computation of the average concentrations. The analyzers were housed in an air-conditioned hut to minimize the impact of temperature fluctuations on the measurements. The CH_4 span calibration standard had a mixing ratio of 2.2 ppm (accuracy ±5%). The IRGA was manually calibrated with a standard CO_2 gas (391.03 ± 0.03 ppm) and a dew point generator (model LI-610, LI-COR, Lincoln, NE, USA) at the beginning of each field season.

The difference in mixing ratios between the chamber inlet and outlet was used to determine the plant flux as,

$$F_a = (C_o - C_i)\frac{P_a Q D}{R T} \quad (1)$$

where F_a is the flux expressed on the ground area basis (μmol m^{-2} s^{-1}), C_o and C_i are the gas mixing ratios of the outlet and inlet samples, respectively, P_a is the ambient air

pressure, *Q* is the air flow rate through the chamber, *D* is the plant density (plants m^{-2}), *R* is the ideal gas constant, and *T* is the temperature. This calculation was performed at half-hour intervals for three gases (CO_2, CH_4, and N_2O). The analysis of the N_2O data will be reported later.

2.2.3. Tall tower gradient measurement

From 30 August to 25 September 2009 (DOY 243–269), the TDL and IRGA analyzers were deployed at the tall tower to explore the behaviors of the CH_4 and CO_2 mixing ratios in the atmospheric boundary layer. Air was drawn from the 200 m and 3 m height at a flow rate of 1.3 L min^{-1} and 0.9 L min^{-1}, respectively, through two tubes (ID 0.96 cm) to the analyzers housed in a temperature-controlled building at the base of the tower (Griffis *et al.*, 2010). A portion of the flow (180 ml min^{-1} for TDL and 0.6 L min^{-1} for IRGA) was subsampled by the analyzers. The TDL air sampling sequence included 200 m, 3 m, calibration zero, and calibration span. Each sample lasted for 30 s. The data following the first 15 s of valve switching were excluded to avoid using residual air from the previous sample when calculating the mean concentrations. The IRGA was used to analyze the 200 m and 3 m concentrations sequentially with a sample interval of 1 min.

We calculated the landscape-scale CH_4 flux using the modified Bowen ratio method (MBR) (Meyers *et al.*, 1996; Werner *et al.*, 2003). This method is based on the assumption that the scalar quantities are transferred indiscriminately by turbulent eddies in the atmospheric boundary layer. Under this assumption, the CH_4 flux is given by

$$F_2 = F_1 \frac{\partial c_2 / \partial z}{\partial c_1 / \partial z} \quad (2)$$

where F_2 is the CH_4 flux, F_1 is the CO_2 flux, $\partial c_2/\partial z$ is the CH_4 gradient, and $\partial c_1/\partial z$ is the CO_2 gradient. The CO_2 flux was measured using the eddy covariance at 100 m at the tall tower (Griffis *et al.*, 2010).

2.2.4. Supporting measurements

At the chamber measurement site, standard micrometeorological and eddy flux variables were measured at half-hour intervals, including variables relevant to this study such as CO_2 flux, soil moisture, air temperature, solar radiation, and precipitation. The same set of measurements was made simultaneously in an adjacent field with a soybean-corn rotation schedule opposite that of the main field. Details of these measurements can be found in Baker and Griffis (2005) and Bavin *et al.* (2009).

2.3. Results

2.3.1. Leaf area index and biomass

In the literature, plant CH_4 flux is often expressed based on unit dry biomass weight and unit leaf area. To facilitate comparison with the published results, we measured the leaf area index (LAI) and the plant biomass. During the experimental period, we randomly sampled five plants in the fertilized zone and the unfertilized zone every week, measured the leaf area, dried the plant samples in an oven (temperature maintained at 60°C) for one week, and then measured the dry weight.

The unfertilized soybean plants had a maximum LAI of 3.3 $m^2\ m^{-2}$ on DOY 224 (11 August) and a dry weight of 14 gdw (grams of dry weight) $plant^{-1}$ on DOY 231 (18 August). The LAI and the dry weight for the fertilized soybean plants, measured at the end of the experiment on DOY 242, were 1.7 $m^2\ m^{-2}$ and 22.6 gdw $plant^{-1}$, respectively.

The maximum LAI of the unfertilized and fertilized corn plants during the 2009 season was 3.5 m^2 m^{-2} and 5.6 m^2 m^{-2}, respectively, and the maximum dry weight was 181 gdw $plant^{-1}$ and 231 gdw $plant^{-1}$, respectively. The unfertilized soybean plants grew to a maximum height of 0.40 ± 0.01 m while the fertilized ones reached 0.53 ± 0.13 m at the end of the experiment. The maximum height of the unfertilized and fertilized corn plants was 1.84 ± 0.30 m and 2.23 ± 0.04 m, respectively.

2.3.2. Zero gradient test and chamber blank tests

To quantify the precision of the CH_4 and N_2O concentration measurements and to determine the detection limits of the chamber system, we conducted a zero gradient test and three blank tests on each chamber.

The zero gradient test was carried out by co-locating two sample inlets at the same height (about 1 m above ground) to assess the difference between the two inlets resulting from potential sample artifacts. The results from this test indicate that the measurement precision for the half-hourly averaged CO_2 and CH_4 concentration was 0.15 ppm and 1.25 ppb (the standard deviation σ of the zero-gradient test result), respectively. The concentration difference between the two inlets was 0.04 ppm and -0.05 ppb and therefore not significantly different from 0 (Student's t-test at the 5% significance level for both gases).

Three blank tests were carried out on each chamber, with each test lasting 24 hours, by placing the chamber in the field without including any plants. The half-hour averaged concentration difference resulting from the blank test was not significantly different from 0 (Figure 2.2), indicating that there was no significant bias in the chamber flux measurement. The chamber flux detection limit was defined as three times the blank

standard deviation for each chamber size. The blank test flux was calculated with Equation 1 by assuming a plant density of 30 plants m^{-2} and 8.1 plants m^{-2} for soybean and corn, respectively. As a result, the detection limit of CH_4 flux for the small and medium chambers was 0.40 nmol m^{-2} s^{-1} and 0.21 nmol m^{-2} s^{-1} for soybean and 0.11 nmol m^{-2} s^{-1} and 0.06 nmol m^{-2} s^{-1} for corn, respectively. The different detection limits between corn and soybean were due to the different plant densities. The large chamber was used only for corn plants, and the CH_4 flux detection limit was 0.83 nmol m^{-2} s^{-1}. The small and the medium chambers had better precision than the large chamber.

Even though reducing the flow rate of the sampling system can improve the detection limit, reducing the flow will result in large CO_2 depletion inside the chamber during the daytime. Note that if we applied a flow rate that was used at the beginning of the growing season (35 L min^{-1}) to the middle of the growing season, the CO_2 concentration inside the chamber would be more than 100 ppm lower than the ambient value because of the plants' strong photosynthetic activity. Consequently, we adjusted the flow rate to reduce the artifact of CO_2 depletion. As a result, 35% of the measured CH_4 concentration difference, when plants were present in the chamber, was between -1.25 ppb and 1.25 ppb ($\pm 1\sigma$ of the zero gradient test), suggesting that the plant flux was too small to be resolved with this method (Figure 2.2). However, 65% of the flux data was detected with relatively high confidence, and the mean CH_4 flux of the three duplicates throughout the corn season was 0.085 ± 0.056 nmol m^{-2} s^{-1}, significantly higher than 0 (with a 5% significance level).

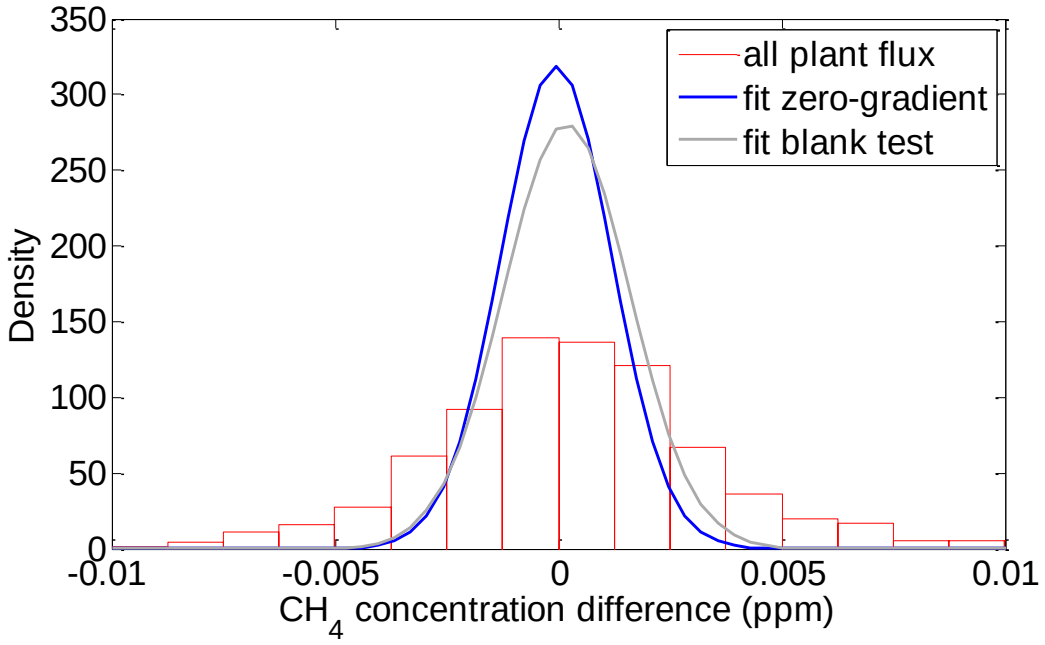

Figure 2.2. Distribution of the half-hour averaged CH_4 concentration difference between two sample points during a 24-hour chamber measurement period taken in 2009. The blue and grey lines are the normal distribution curves of the zero-gradient test and the blank test.

2.3.3. Plant CO_2 flux

To evaluate the validity of the chamber approach, the plant CO_2 flux measured with the chamber approach was compared with the plant flux estimated from the eddy covariance and soil chamber data. Here, we assume that the plant flux can be estimated as the difference between the net ecosystem CO_2 exchange (NEE) and soil respiration. In 2009, the NEE was measured in the middle of the G21 cornfield by an eddy covariance system (EC), and soil respiration was measured using three soil chambers located within the same field. The CO_2 flux measured from the plant chamber and that derived from the NEE showed that 1) the flux measured with the plant chambers captured the diurnal pattern of plant activity (Figure 2.3); 2) the flux measured with the plant chamber was linearly correlated with that estimated by the EC and soil flux ($p < 0.01$), and the fitted line was close to the 1:1 line (Figure 2.4).

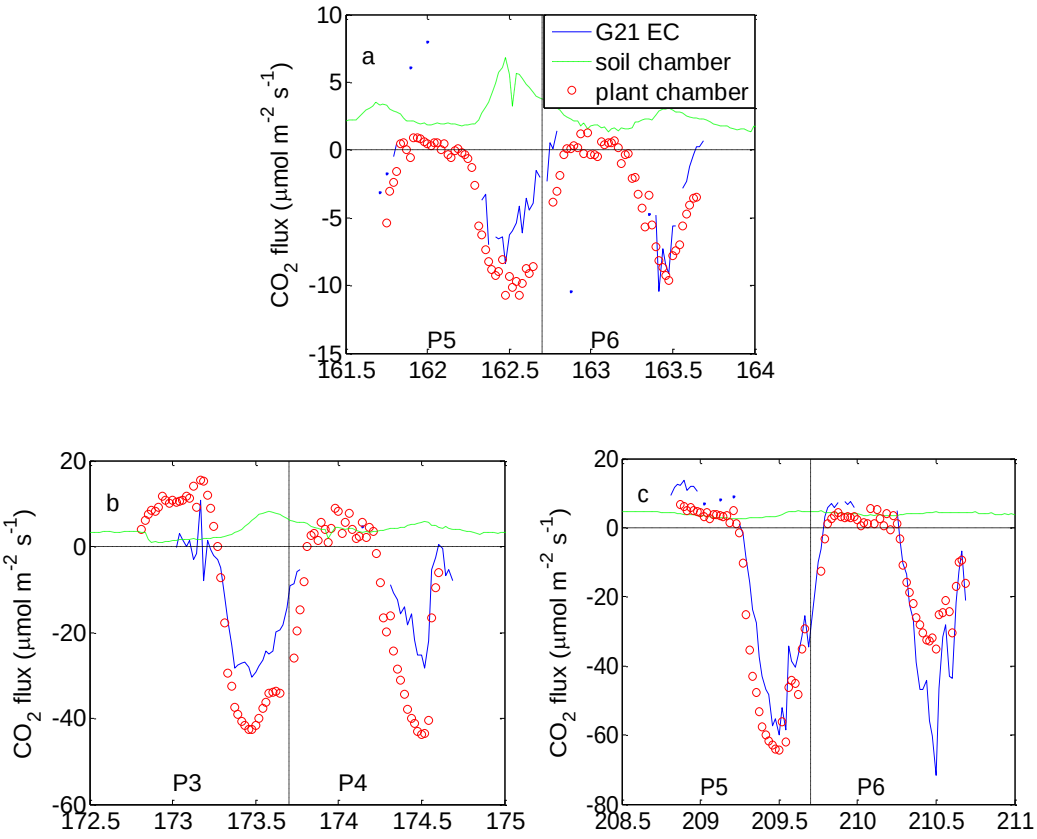

Figure 2.3. Half-hour averaged CO_2 flux measured with the eddy covariance system in the cornfields (blue line), soil chambers (green dash line), and plant chambers (red circle). a) small chamber, b) medium chamber, c) large chamber. P3-P6 means sampled corn plant 3-6. P3 and P5 were fertilized, while P4 and P6 were not fertilized. The measurement period was chosen according to the availability of the chamber measurement data and the G21 eddy covariance measurement data.

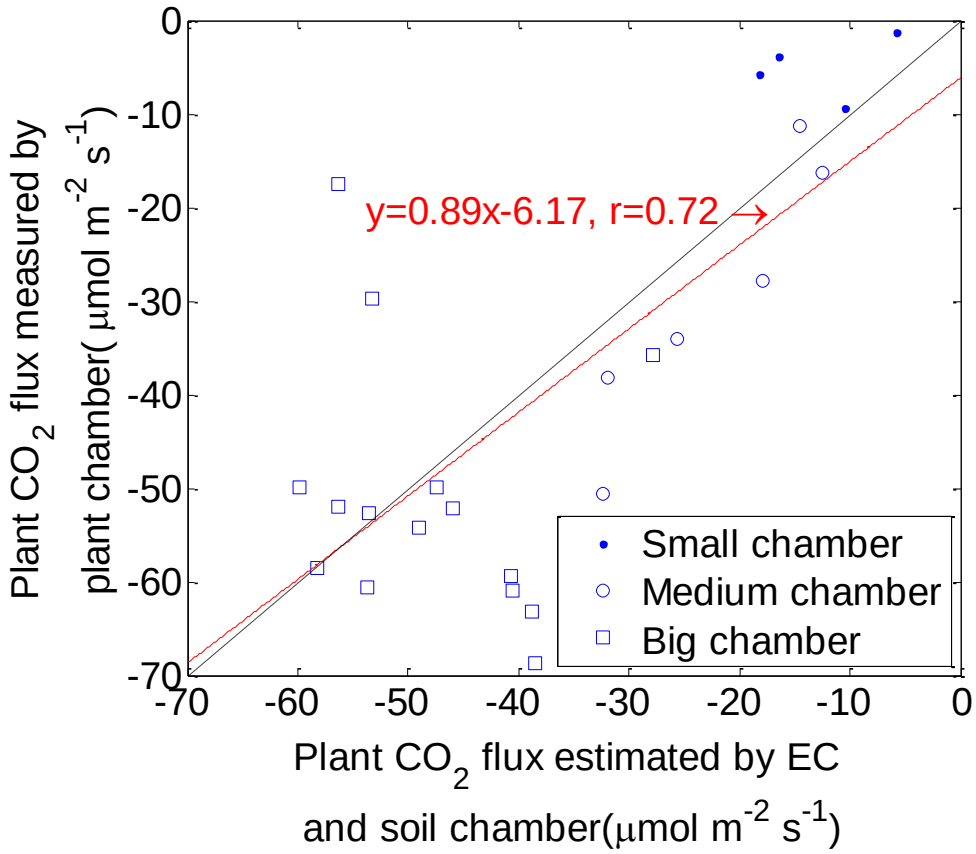

Figure 2.4. Comparison of the midday (10:00–16:00) averaged CO_2 flux estimated with the EC-Soil and measured with the plant chamber.

2.3.4. Plant CH_4 flux

Figure 2.5 shows the plant flux observed during the midday (10:00–16:00 LST) and midnight (22:00–04:00 LST) periods over the two growing seasons. The flux exhibited some diurnal variations, with slightly positive values during the day and negative values during the night. Throughout the soybean growing season, 91% of the midday average flux values were positive, with a maximum emission rate of 1.31 nmol m^{-2} s^{-1}. The flux did not simply increase as biomass accumulated. In comparison, 86% of the midnight flux values were negative, and the uptake signal appeared stronger later in the growing season with a maximum uptake rate of -4.38 nmol m^{-2} s^{-1}. During the corn season, 90% of the midday averages were positive, 76% of the midnight averages were negative, and the daytime fluxes peaked at the time when the biomass growth rate was the greatest. The maximum emission rate and the uptake rate for corn were 2.21 nmol m^{-2} s^{-1} and -2.55 nmol m^{-2} s^{-1}, respectively.

The flux values shown in Figure 2.5 are much lower than the values reported by Keppler *et al*. (2006), who estimated that intact plants emit CH_4 at a rate of 370 ng CH_4 gdw^{-1} h^{-1}, with a range of variations of 200–600 ng CH_4 gdw^{-1} h^{-1} under sunlight and 120 ng CH_4 gdw^{-1} h^{-1} (range 30 - 210 ng CH_4 gdw^{-1} h^{-1}) in the dark. We multiplied Keppler *et al.*'s rates with the dry plant weight and the density measured throughout the growing season to obtain the flux in units of nmol m^{-2} s^{-1}, and compared the results with our observations (Figure 2.5). Our results were below the lower limit of Keppler *et al*.'s estimate except at the beginning of the growing season when the plants were very small. The differences were as large as 100-fold. Furthermore, for nighttime periods, Keppler *et al*.'s values were positive while our observed flux was mostly negative.

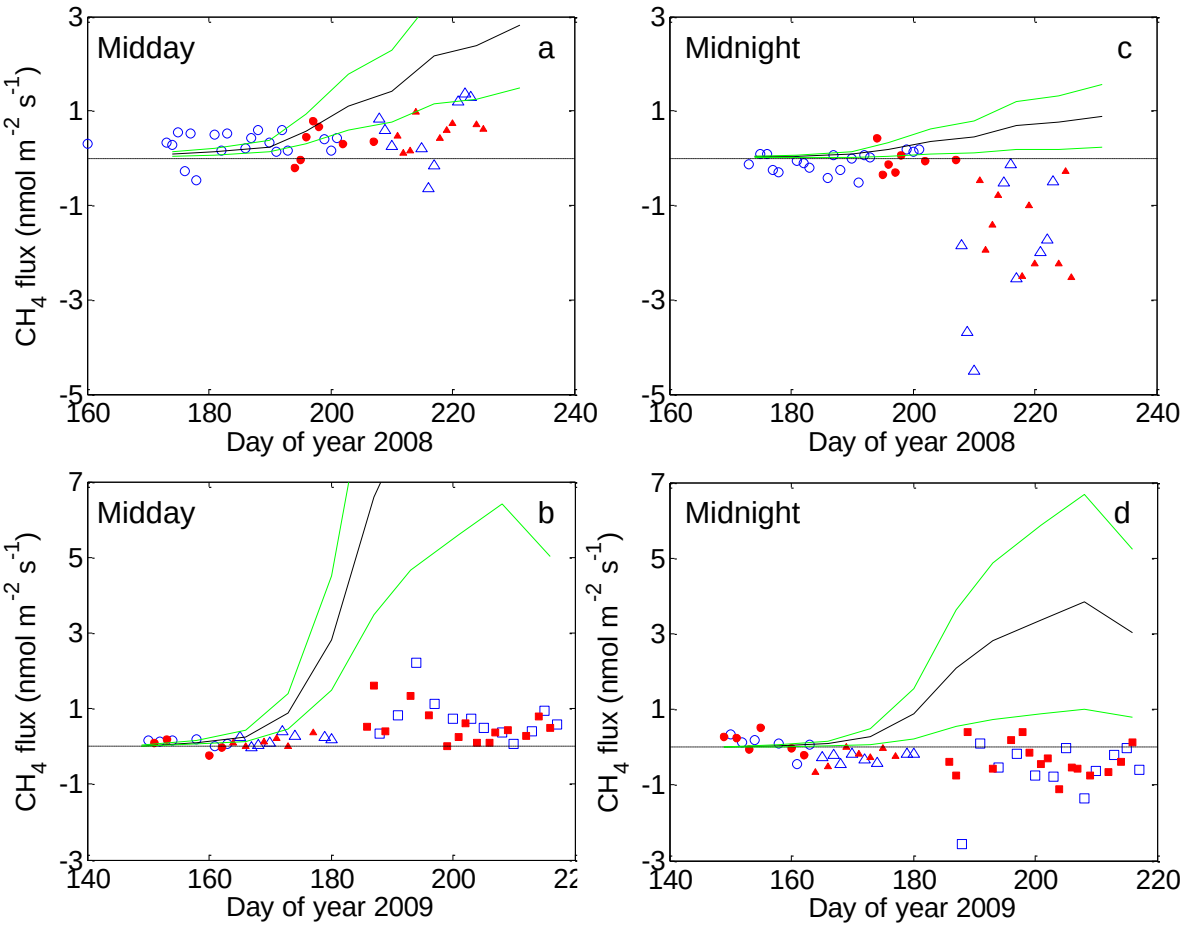

Figure 2.5. Midday (10:00–16:00 LST) and midnight (22:00–04:00 LST) plant fluxes in the soybean fields (a, c) and the cornfields (b, d) throughout the growing season: red filled symbols – fertilized plant flux; blue open symbols – unfertilized plant flux; circle, triangle, square – fluxes measured with the small chamber, the medium chamber, and the large chamber; black lines – CH_4 flux suggested by Keppler *et al.* (2006); green lines – the boundary of Keppler *et al.*'s estimates.

The daily mean (24-hour average) flux was small for both crops (Figure 2.6). During the soybean season, the daily flux ranged from -0.70 nmol m^{-2} s^{-1} to 0.47 nmol m^{-2} s^{-1} and was mostly positive during the first half (DOY 160–202) and negative during the second half of the growing season (DOY 207–225). During the corn season, the daily flux was slightly positive at the beginning, negative from DOY 160 to 175, and mostly positive over the last 42 days of the measurement period. Relatively large emissions (up to 1.08 nmol m^{-2} s^{-1}) were observed near the end of the measurement period in 2009. These daily values were much lower than those reported by Keppler *et al*. (2006).

In the discussion above, we did not distinguish fertilized and unfertilized plots. Figure 2.7 shows the fertilization effects on the daily, midday, and midnight CH_4 and CO_2 fluxes throughout the growing season. For each flux, we paired the data with and without fertilization treatment, and used a Student's t-test to examine the significance of the fertilization effect. The result shows that fertilization did not affect CH_4 fluxes in any of the three periods ($p > 0.05$). Fertilization increased the midday corn uptake of CO_2 ($p < 0.01$), and the daily corn CO_2 flux increased significantly as well ($p < 0.01$). However, the nighttime CO_2 emission from corn was not significantly affected. The fertilization effect on the daily and midday soybean CO_2 fluxes was not as significant as for corn (p=0.06 and 0.09, respectively), and the midnight flux was not significantly affected by fertilization.

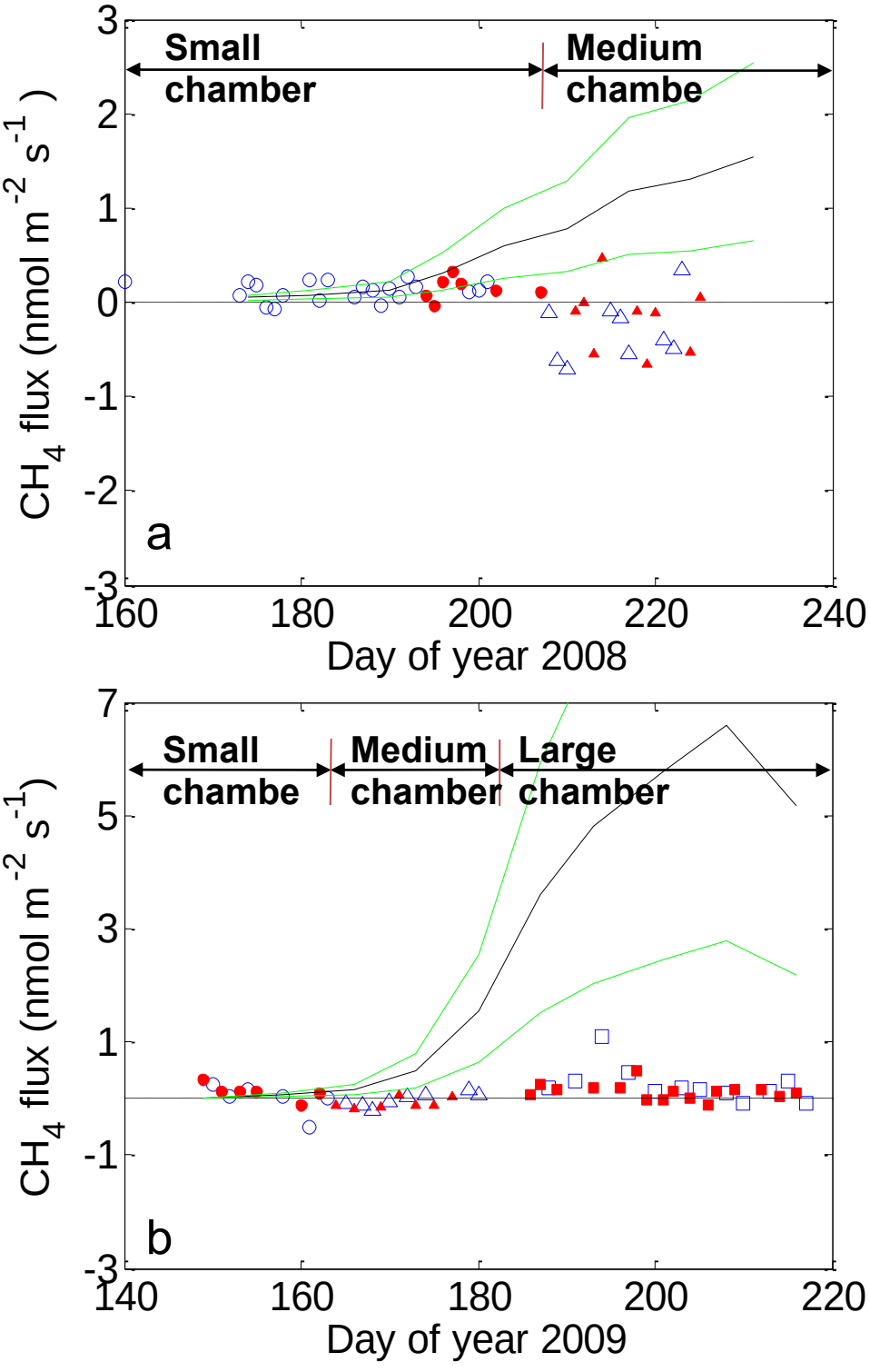

Figure 2.6. As in Figure 2.5 except for the daily average plant CH_4 flux in the soybean fields (a) and the cornfields (b).

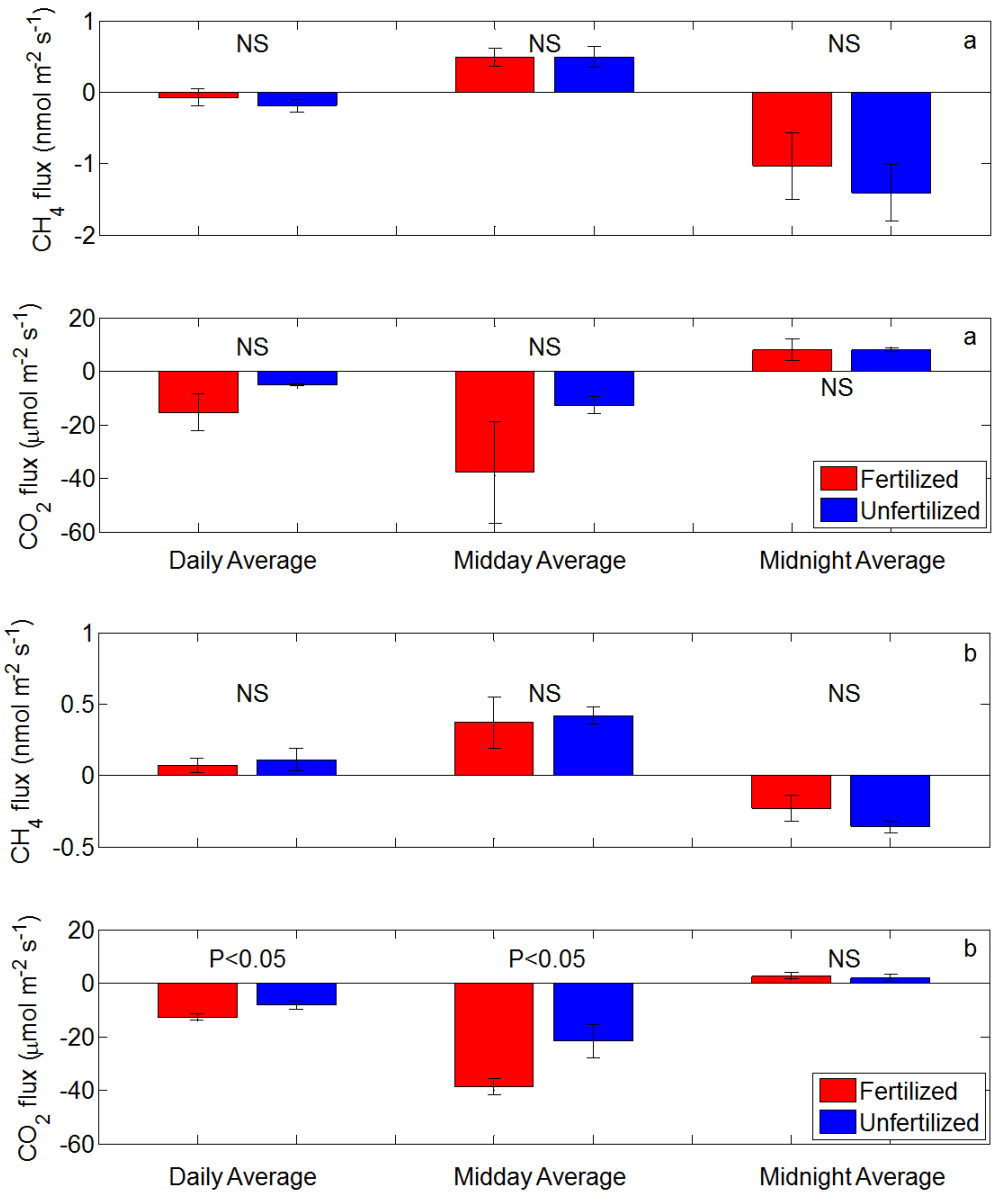

Figure 2.7. Daily, midday (10:00–16:00 LST), and midnight (22:00–04:00 LST) fluxes averaged over the soybean (a) and corn growing seasons (b). Error bars are standard deviations of the three replicate plots. NS denotes the difference between fertilized and unfertilized plant fluxes being insignificant ($p > 0.05$).

Table 2.2 summarizes the linear correlation between CH_4 fluxes and environmental variables, including incident solar radiation, air temperature, soil water content at 10 cm depth, and soil temperature at 10 cm. These variables were considered in previous studies on plant CH_4 emission and uptake (Keppler *et al.*, 2006; Nisbet *et al.*, 2009). These results show that the midday flux of corn and soybean was positively correlated with solar radiation, with *p*-values of 0.004 and 0.08, respectively. The correlation with other environmental variables was not consistent for soybean and corn. The midday corn CH_4 flux was moderately correlated with air temperature, soil water content, and soil temperature, but the soybean CH_4 flux was not. Regarding the midnight measurement, corn CH_4 flux was only negatively correlated with air temperature, while soybean CH_4 flux was only weakly correlated with soil moisture.

The correlation between the CH_4 and CO_2 fluxes was also tested to examine the potential relations between CH_4 flux and the process of photosynthesis and respiration. The analysis shows that CH_4 plant flux was negatively correlated with CO_2 flux throughout the day for corn and soybean, and that fertilization did not affect this correlation.

Table 2.2. Linear correlation of plant CH_4 flux with environmental variables and CO_2 flux

	n	Solar radiation	Air temperature	Soil moisture	Soil temperature	CO_2 flux
			Corn			
Midday flux	52	0.37****	0.25**	-0.36***	0.27**	-0.35***
Midnight flux	56	N/A	-0.30**	0.09	0.05	-0.15*
			Soybean			
Midday flux	46	0.21*	0.04	-0.07	0.08	-0.21*
Midnight flux	45	N/A	0.00	0.24*	-0.08	-0.72****

Note: n – sample size; Levels of significance are denoted by ns ($p > 0.1$), * ($0.05 < p < 0.1$), ** ($0.01 < p \leq 0.05$), *** ($0.001 < p \leq 0.01$), and **** ($p \leq 0.001$)

2.3.5. Tall tower CH_4 observation

The CH_4 concentration at 3 m and 200 m at the tall tower site exhibited diurnal variations, which suggests that this agriculture-dominated landscape released CH_4 at night, but the direction of the daytime flux was not clear (Figure 2.8). After 19:00 LST, with the formation of the stable nighttime boundary layer, CH_4 accumulated near the ground surface, and the 3 m concentration peaked around 07:00 LST. The peak value varied from day to day, and the average at 07:00 LST was 2.232 ± 0.291 ppm. After sunrise, turbulent motion in the surface layer diluted the CH_4-rich air near ground with air from higher altitudes and increased the CH_4 concentration at 200 m above the ground. The concentration at both heights decreased until 16:00 LST, when the concentration at both heights was approximately 1.996 ppm. These diurnal trends suggest that the surface was a source at night. However, these trends cannot indicate land surface uptake during daytime because the depletion could also be attributed to the entrainment at the top of the convective boundary layer.

The CH_4 and CO_2 concentration gradients at night also suggest nighttime release of CH_4 by the landscape. The CH_4 concentration gradient in the 3 to 200 m air layer was consistently negative (concentration at 200 m < concentration at 3 m) at night (-0.62 ± 0.60 ppb m^{-1}), similar to the CO_2 gradient (-0.23 ± 0.09 ppm m^{-1}). During the observation period, the midnight (22:00–04:00 LST) average CH_4 gradient (G_{CH4}) was positively correlated to the midnight CO_2 gradient (G_{CO2}) (Figure 2.9a). The relation between the two gradients was $G_{CH4}= 3.8\times10^{-3} G_{CO2}+2.6\times10^{-4}$ (linear correlation r = 0.54, number of observations n = 25). Due to the strong daytime mixing in the boundary layer, the CH_4 and CO_2 gradients during midday (10:00–16:00) were very small: the CH_4 gradient was -

$6.2\times10^{-3} \pm 3.0\times10^{-2}$ ppb m^{-1} (not significantly different from 0 according to a Student's t-test with a significance level of 5%), and the CO_2 gradient was $9.12\times10^{-3} \pm 9.97\times10^{-3}$ ppm m^{-1}.

The CH_4 fluxes calculated with the MBR method also indicated a nighttime emission, similar to the pattern observed from the concentration gradient. During the observation period, the CH_4 flux at night was 14.8 ± 10.3 nmol m^{-2} s^{-1}. The numbers in the parentheses represent 95% confidence intervals. Unfortunately, the CH_4 fluxes from the MBR method during the daytime were not reliable due to the small CH_4 and CO_2 gradients.

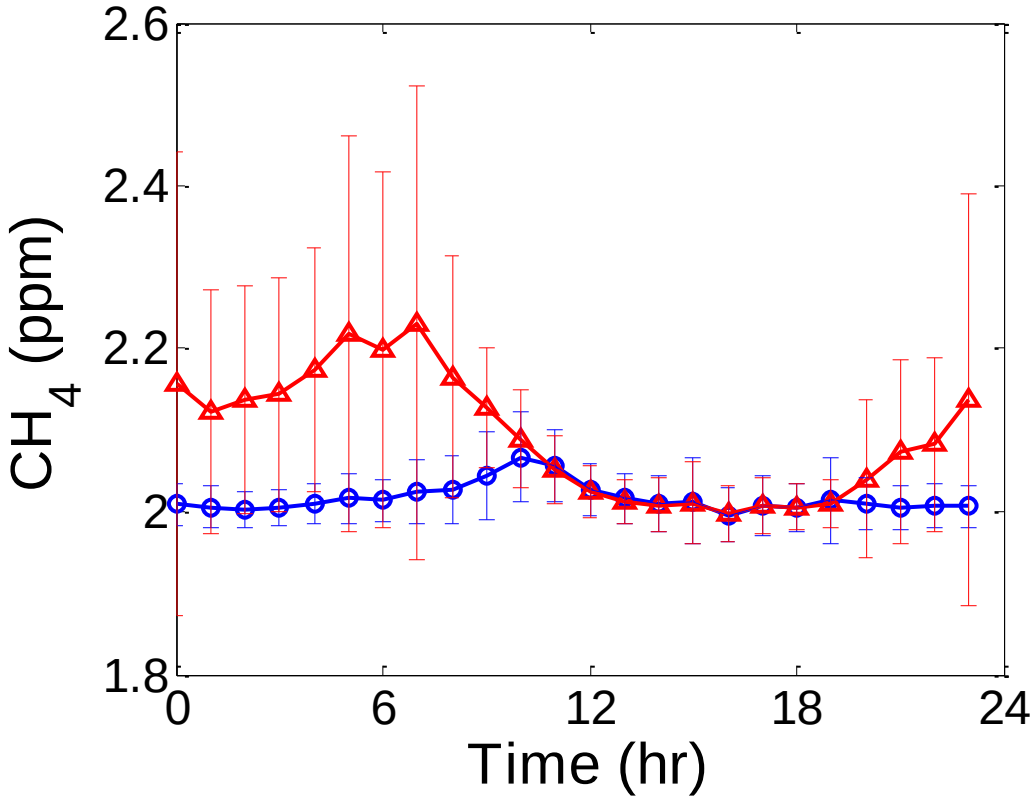

Figure 2.8. Diurnal composite of the CH_4 concentration at 3 m and 200 m above the ground during DOY 243–269, 2009. Red triangles and blue circles are the hourly mean values of the concentration at 3 m and 200 m, respectively, and the error bars are the standard deviations of 30-min observations.

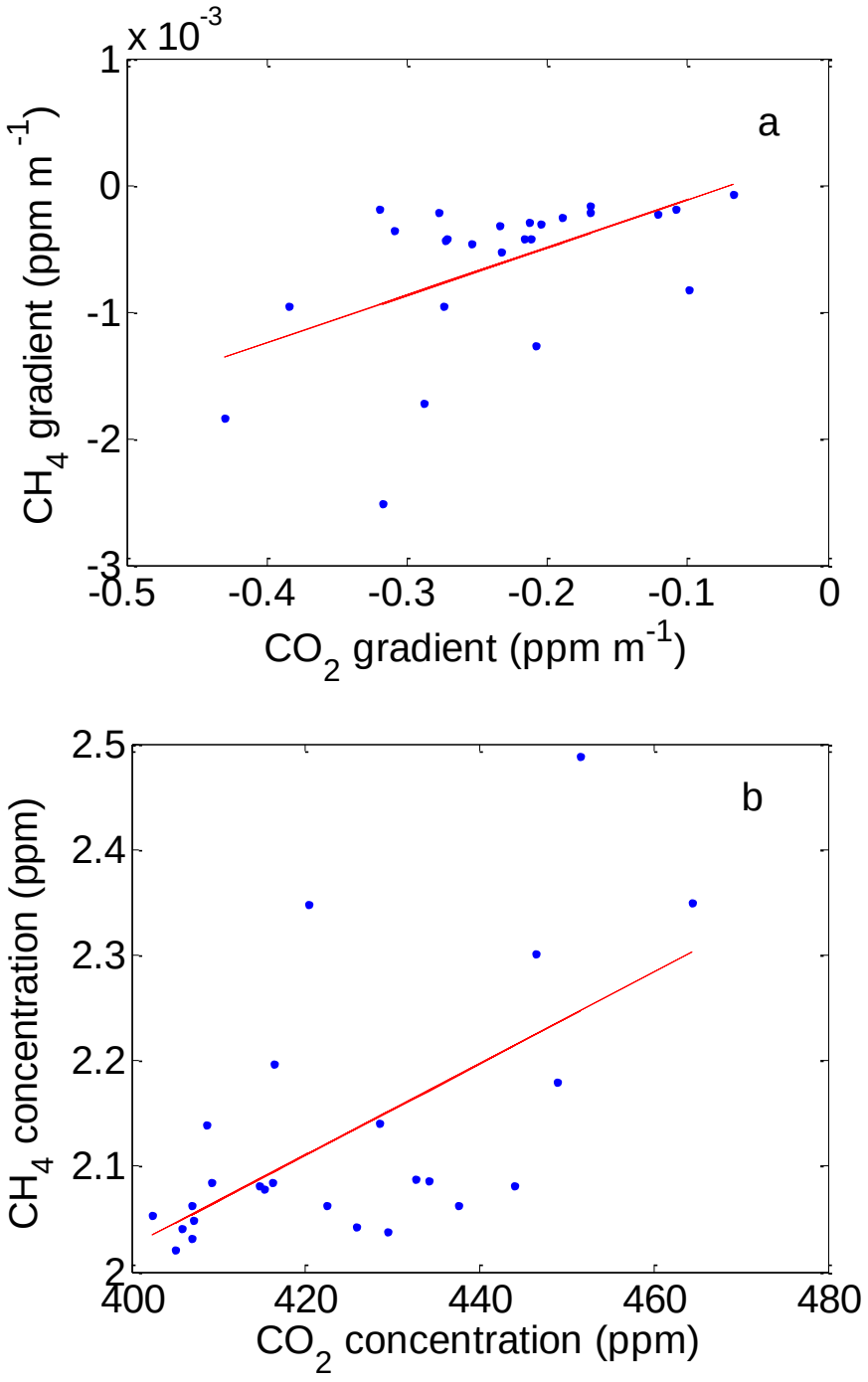

Figure 2.9. Linear relationship between the night CH_4 and CO_2 gradients (a) and the CH_4 and CO_2 mixing ratios (b) at the 3 m height, DOY 243–269, 2009. The results of the linear regression are shown as red lines. Each data point represents a block average between 22:00 and 04:00 LST.

2.4. Discussion

2.4.1. Plant-scale CH_4 exchange

2.4.1.1. Comparison with published results

Corn is one of the most studied plant species regarding CH_4 source/sink behavior. Table 2.1 presents a comprehensive summary of all known results. Our results are presented for the period between DOY 201 and 218 when LAI exceeded 5.1 m^2 m^{-2} and the plant biomass density exceeded 202 gdw plant $^{-1}$. To facilitate the comparison, we multiplied the published values in units of ng CH_4 gdw^{-1} h^{-1} by the mean dry biomass density over this period (1652 gdw m^{-2}) to obtain flux values in units of nmol m^{-2} s^{-1}. During this period, the midday flux was 0.11±0.06 nmol m^{-2} s^{-1}. Beerling *et al*. (2008), Dueck *et al*. (2008), Kirschbaum and Walcroft (2008), and Nisbet *et al*. (2009) all showed that the flux of the intact shoot and detached leaves was not significantly different from zero. Vigano *et al*. (2008) reported that when UV radiation reaches 49 W m^{-2}, fresh corn plant tissues emit CH_4 at a rate of 50 ng CH_4 gdw^{-1} h^{-1}, which is equivalent to 1.4 nmol m^{-2} s^{-1} or about ten times higher than our midday value. This difference could result from the difference in UV exposure. For instance, Vigano *et al*.'s UV flux intensity was twice as high as the average value in our experiment.

Some of the variations among these studies may have been a consequence of using different measurement methods and experimental conditions. To minimize measurement artifacts, we constructed the chamber system without impacting major physiological processes such as photosynthesis and respiration. In this design, special attention was given to temperature, radiation, and CH_4 and CO_2 background concentrations. The temperature inside the chamber was kept consistent with that of ambient air. The

plexiglass chamber material had a transmissivity of 92% for visible light and 90% for UV radiation. The CH_4 concentration inside the chamber was within 0.02 ppm of the ambient value. On average, the CO_2 concentration inside the chamber was 9 and 66 ppm lower than ambient in the daytime and 4 and 11 ppm higher than ambient at night during the soybean and corn growing seasons, respectively. The altered CO_2 levels did not have an appreciable effect on the plant function, at least from the perspective of CO_2 exchange. For example, the midday CO_2 uptake of unfertilized soybean and fertilized corn (from 10:00 to 16:00 LST) was -12 ± 3 μmol m^{-2} s^{-1} and -39 ± 3 μmol m^{-2} s^{-1}, respectively (Figure 2.7). These values were comparable to the plant flux derived from NEE and soil respiration measurements.

Keppler *et al*.'s (2006) results contrast sharply with ours and other studies. The mean flux of the four studies conducted in normal light levels (Berling *et al*., 2008; Dueck *et al*., 2007; Nisbet *et al*., 2009; this study) is 0.26 ± 0.51 nmol m^{-2} s^{-1} and is one order of magnitude smaller than Keppler *et al*.'s flux value. Although this is not a new conclusion, the fact that our measurements were made in the field under near-ambient conditions further supports the view that extrapolation of Keppler *et al*.'s results to the global scale will severely overestimate the role of plants in the atmospheric CH_4 budget (Ferretti *et al*., 2007; Houweling *et al*., 2006).

2.4.1.2 The role of radiation

That both corn and soybean emitted CH_4 during the day and absorbed CH_4 at night (Figure 2.7) suggests a role of radiation in regulating the plant CH_4 exchange with the atmosphere. The day-to-day variations in CH_4 production were positively correlated with solar radiation (Table 2.2). McLeod *et al*. (2008) and Vigano *et al*. (2008, 2009) found

that the CH_4 flux in dark conditions appears lower than if the plant is exposed to UV radiation, implying a photochemical production mechanism. Our results also reveal a negative correlation with the CO_2 flux (Figure 2.10, Table 2.2), raising another possibility that the daytime emission was linked to photosynthesis. The fact that Kirschbaum and Walcroft (2008) did not observe a significant CH_4 flux may be related to the very low light intensity of their experiments (Table 2.1).

In the absence of solar radiation, the fertilized and unfertilized corn and soybean plants were small sinks of CH_4 (Figure 2.7). In soils, methanotrophy is a known pathway of CH_4 oxidation removing CH_4 from the air (Le Mer and Roger 2001). Our results show that plants can also remove CH_4. The mechanism for the uptake phenomenon is not known, but an association with plant dark respiration was suggested by the correlation shown in Figure 2.10. A negative CH_4 flux was undetected in some previous studies because the plant was immersed in a CH_4-free gas or a gas with a very low CH_4 concentration during the experiment (Beerling *et al*., 2008; Keppler *et al*., 2006; Kirschbaum and Walcroft 2008).

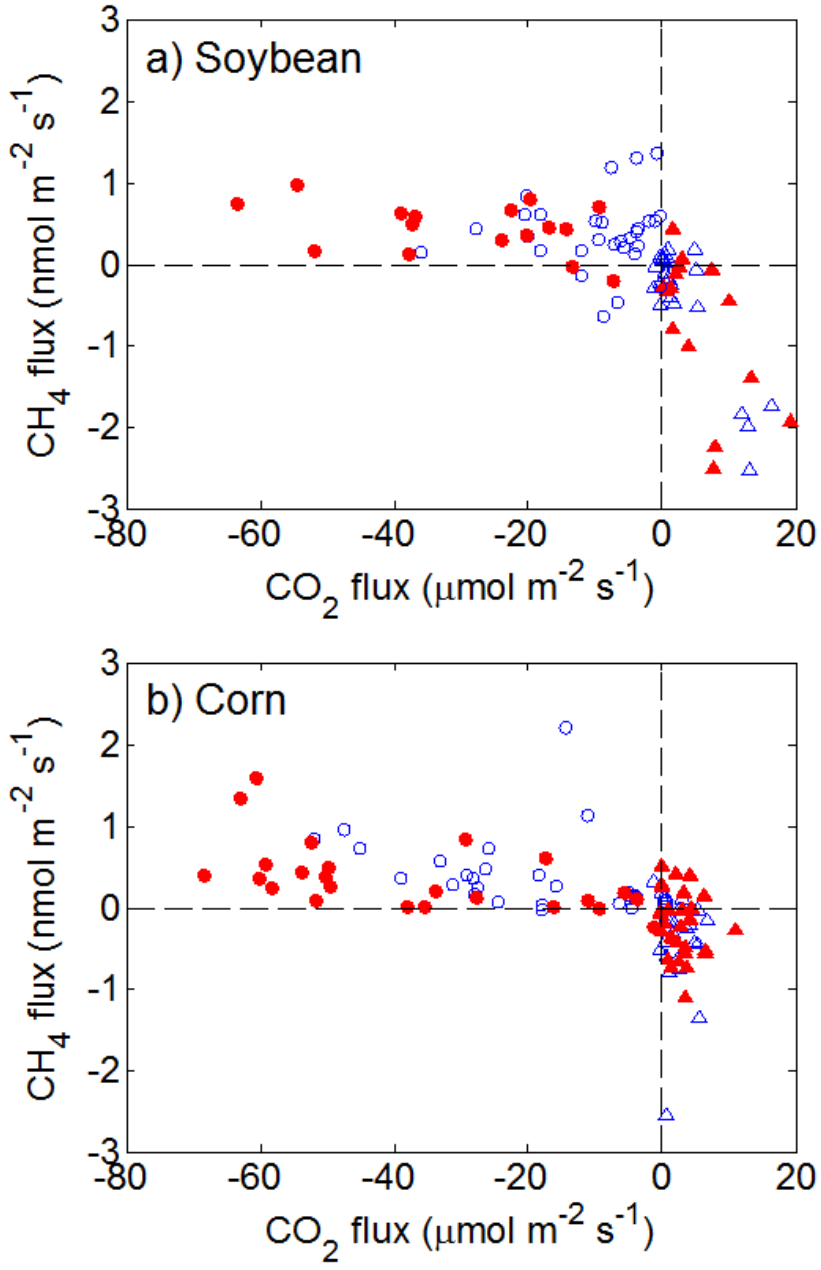

Figure 2.10. Relationships between the plant CO_2 and CH_4 fluxes (a: soybean; b: corn): red filled circles – midday fluxes from fertilized plants; blue open circles – midday fluxes from unfertilized plants; red filled triangle – midnight fluxes from fertilized plants; blue open triangle – midnight fluxes from unfertilized plants.

2.4.1.3 Impact of fertilization

Fertilization did not significantly affect the plant CH_4 fluxes averaged over daily (24-hour), midday, or midnight periods. However, even though not statistically significant, the seasonal mean of CH_4 uptake during the midnight periods was smaller in fertilized plots than in unfertilized plots for corn and soybean, and this was consistent with the impact of fertilization on agricultural soil reported in the literature (Jacinthe and Lal 2003; Mosier *et al*., 2006; Suwanwaree and Robertson 2005). A meta-analysis suggests that CH_4 uptake by soil is inhibited by fertilization at a rate of 0.012 ± 0.006 kg CH_4-C ha^{-1} $year^{-1}$ per 1 kg N ha^{-1} $year^{-1}$. By multiplying the fertilization rate for corn and soybean, respectively, soil CH_4 uptake should have been reduced by 0.36 ± 0.18 nmol m^{-2} s^{-1} and 1.6 ± 0.8 nmol m^{-2} s^{-1}. In comparison, the reduction in plant CH_4 uptake during the midnight periods in our study was 0.13 nmol m^{-2} s^{-1} and 0.28 nmol m^{-2} s^{-1} for corn and soybean, respectively. Another recent study in the Midwest US suggests that fertilization reduces soil uptake of CH_4 by 0.19± 0.25 nmol m^{-2} s^{-1} and 0.11 ± 0.08 nmol m^{-2} s^{-1} in fields cultivated with corn and soybean (Johnson *et al*., 2010). The difference between the reduction in the soil CH_4 uptake reported in the literature and our study suggests that applying the soil inhibition factor to plant CH_4 flux may lead to an overestimation of the fertilization impact of as much as six times.

2.4.2. Landscape-scale flux and uncertainties

2.4.2.1. Sources and sinks within the tower footprint

To examine the contributions of other sources and sinks in the tower footprint, we conducted a source footprint analysis with the STILT model (Lin *et al*., 2003). At each time point, 100 air parcels were released at the receptor (44º41'19"N, 93º04'22"W, 200 m)

and were transported backward for two days. The aggregated distribution of the air parcels defines the footprint of the tall tower. Overlaying this footprint map on the data on the type of land cover from the US Geological Survey, we estimated that 66% of the footprint during the observation period was cropland, 11% was grassland, 11% was forest, 2% was wetland, 4% was water, and 6% was developed land.

Even though the landscape is dominated by cropland, the flux from crop plants was negligible in the landscape-scale CH_4 budget, since the plant flux was one to two orders of magnitude smaller than the landscape-scale CH_4 flux. In midday, the (unfertilized) soybean and (fertilized) corn flux was 0.49 ± 0.15 nmol m^{-2} s^{-1} and 0.37 ± 0.18 nmol m^{-2} s^{-1}, respectively, while at midnight, the soybean and corn flux was -1.41 ± 0.40 nmol m^{-2} s^{-1} and -0.23 ± 0.09 nmol m^{-2} s^{-1}. In comparison, the landscape flux observed at the tall tower during the later growing season was 14.8 nmol m^{-2} s^{-1} at midnight.

Cropland soils in the Midwest US have been investigated intensively for CH_4 flux (Alluvione *et al*., 2009; Adviento-Borbe *et al*., 2007; Mosier *et al*., 2006; Omonode *et al*., 2007; Ussiri *et al*., 2009). Divergence exists in the published results due to the complex production and consumption mechanisms of CH_4 by methanogenesis and methanotropic bacteria. These studies show that the soil CH_4 flux in corn or corn-soybean rotation croplands ranges from -0.94 to 0.73 nmol m^{-2} s^{-1}. Adviento-Borbe *et al*. (2007) reported that the CH_4 soil flux in a soybean-corn rotation field in eastern Nebraska was -0.94 nmol m^{-2} s^{-1}. Ussiri *et al*. (2009) suggested that tillage may have a significant impact on flux. In a comparative study in Ohio, the soil CH_4 flux ranged from -0.08 nmol m^{-2} s^{-1} under no-till to 0.73 nmol m^{-2} s^{-1} in a field subject to moldboard plowing. Omonode *et al*. (2007) reported that no-till fields emitted CH_4 at a rate of 0.25 nmol m^{-2} s^{-1} and tilled fields were

a net sink of CH_4 at a rate of -0.28 nmol m^{-2} s^{-1} in Indiana. Alluvione *et al*. (2009) and Moiser *et al*. (2006), however, found tillage had a negligible impact on the CH_4 soil flux in cornfields in Colorado, and Bavin *et al*. (2009) found it extremely difficult to even measure a significant CH_4 flux from bare soils in strip till or conventional managed fields. The difference among these studies may be related to soil properties and to how many years the field has been in no-till or till practice (Mosier *et al*., 2006). However, all observed fluxes, either positive or negative, were about one magnitude lower than the regional flux.

Native grassland and forest soils seem to have higher CH_4 oxidation rates than cropland soils. In Inner Mongolia, the semi-arid grasslands consume CH_4 at a rate of 0.48 to 0.61 nmol m^{-2} s^{-1} (Wang *et al*., 2005), while in the southern Rocky Mountains, forest soils take up CH_4 at a rate of 1.2 nmol m^{-2} s^{-1} (Bowling *et al*., 2009). These findings are consistent with a comprehensive literature review by Le Mer and Roger (2001), which suggested that the CH_4 consumption by upland soils ranges between 0 and 1.74 nmol m^{-2} s^{-1}, depending on the disturbance regime such as tillage and fertilization (Le Mer and Roger 2001). As a result, grassland and forest may mainly contribute to the uptake of CH_4 from the atmosphere, which was very likely offset by the emission from another type of land cover.

Wetland and developed land, two minor land use categories in the tower footprint, are strong sources of CH_4. In one study, wetland CH_4 emissions were estimated to be 61–87 nmol m^{-2} s^{-1} in Minnesota in September (Shurpali and Verma 1998). A recent field experiment showed that the CH_4 emission is about 20 nmol m^{-2} s^{-1} in a boreal fen in western Canada (Long *et al*., 2010). In developed areas, CH_4 can be emitted by fossil fuel

combustion, landfills, and natural gas leakage (Mosher *et al*., 1999; Nakagawa *et al*., 2005; Zimnoch *et al.*, 2010). Nakagawa *et al.* (2005) reported that automobile exhaust contributed up to 30% of CH_4 sources in an urban area in Japan. An investigation by Mosher *et al.* (1999) at nine landfill sites in the northeastern US showed the emission rate of the landfills ranged from 6.6×10^3 to 9.4×10^4 nmol m^{-2} s^{-1}. Regarding natural gas leakage, a study conducted in the urban area of Krakow, Poland, suggests that natural gas led to an emission flux of 14 nmol m^{-2} s^{-1}(Zimnoch *et al.*, 2010). Consequently, even though wetland and developed land account for only 8% of the tall tower footprint, they may dominate the CH_4 budget.

2.4.2.2. Uncertainties in the MBR measurement

The MBR method provided a more robust estimate of the CH_4 flux under stable nighttime conditions than under unstable daytime conditions. The high CH_4 concentration near the ground at night indicated that the ground surface was a source of CH_4. Furthermore, the CO_2 and CH_4 vertical gradients were large at night and correlated with each other (Figure 2.9a). The nighttime CH_4 flux was 14.8 nmol m^{-2} s^{-1} according to the MBR method. For comparison, the midnight CH_4 flux, obtained by multiplying the slope of the regression shown in Figure 2.9b with the nighttime CO_2 flux, was 17.1 ± 9.4nmol m^{-2} s^{-1}. This latter estimate is independent of the assumption of equal eddy diffusivity between the two gases. Instead, this estimate assumes that the buildup of CO_2 and CH_4 in the stable air layer near the ground resulted from their respective land surface sources so that CO_2 can be used as a tracer to constrain the CH_4 surface flux. The same method was used by Kelliher *et al.* (2002) to determine the N_2O flux in a grassland landscape affected by animal grazing.

It is not clear whether the regional daytime flux is positive or negative because the small daytime gradients are difficult to resolve. However, it is clear that the daytime CH_4 flux is not large enough to decrease the daily averaged CH_4 flux to the magnitude of the plant flux or even switch the sign of the flux. Zhang *et al.* (in preparation) estimated the regional CH_4 flux from the entire observation period with the equilibrium boundary layer method, and the result suggested the landscape around the tall tower emits CH_4 at a rate of 16.0 ± 3.1nmol m^{-2} s^{-1}, on the same magnitude as our MBR estimation at midnight. As a result, the nighttime CH_4 flux estimated with the MBR method can provide a reasonable constraint on the CH_4 budget during our observation period. Longer-term measurements and analyses are required to better understand the seasonal variability, annual budget, and source contributions of CH_4 emissions in the Upper Midwest.

2.5. Conclusions

We observed that soybean and corn plants emitted CH_4 during the daytime (mean midday values 0.49 ± 0.15 nmol m^{-2} s^{-1} and 0.37 ± 0.18 nmol m^{-2} s^{-1}, respectively) and absorbed CH_4 during the nighttime (mean midnight values -1.41 ± 0.40 nmol m^{-2} s^{-1} and -0.23 ± 0.09 nmol m^{-2} s^{-1}). The strength of the plant flux was at least one order of magnitude smaller than that suggested by Keppler *et al.* (2006). Fertilization did not have a significant impact on the plant CH_4 flux. The plant CH_4 flux was one to two orders of magnitude smaller than the landscape-scale CH_4 flux measured at the tall tower.

The CH_4 flux estimated with the MBR method at the tall tower was 14.8 nmol m^{-2} s^{-1} during the midnight periods and was highly uncertain during the midday periods. Because of the small vertical CH_4 and CO_2 gradients, the nighttime flux was robust and in

agreement with an independent tracer estimate. The potential diurnal variation in the flux direction underscores the importance of improving the daytime regional flux estimate.

2.6. References

Adviento-Borbe, M.A.A., Haddix, M.L., Binder, D.L., Walters, D.T. and Dobermann, A., 2007. Soil greenhouse gas fluxes and global warming potential in four high-yielding maize systems. Global Change Biology, 13(9): 1972-1988.

Alluvione, F., Halvorson, A.D. and Del Grosso, S.J., 2009. Nitrogen, tillage, and crop rotation effects on carbon dioxide and methane fluxes from irrigated cropping systems. Journal of Environmental Quality, 38(5): 2023-2033.

Baker, J.M. and Griffis, T.J., 2005. Examining strategies to improve the carbon balance of corn/soybean agriculture using eddy covariance and mass balance techniques. Agricultural and Forest Meteorology, 128(3-4): 163-177.

Beerling, D.J., Gardiner, T., Leggett, G., McLeod, A. and Quick, W.P., 2008. Missing methane emissions from leaves of terrestrial plants. Global Change Biology, 14(8): 1821-1826.

Bowling, D.R., Miller, J.B., Rhodes, M.E., Burns, S.P., Monson, R.K. and Baer, D., 2009. Soil, plant, and transport influences on methane in a subalpine forest under high ultraviolet irradiance. Biogeosciences, 6(7): 1311-1324.

Butenhoff, C.L. and Khalil, M.A.K., 2007. Global methane emissions from terrestrial plants. Environmental Science & Technology, 41(11): 4032-4037.

Dueck, T. and van der Werf, A., 2008. Are plants precursors for methane? New Phytologist, 178(4): 693-695.

Dueck, T.A., de Visser, R., Poorter, H., Persijn, S., Gorissen, A., de Visser, W., Schapendonk, A., Verhagen, J., Snel, J., Harren, F.J.M., Ngai, A.K.Y., Verstappen, F., Bouwmeester, H., Voesenek, L. and van der Werf, A., 2007. No evidence for substantial aerobic methane emission by terrestrial plants: a C-13-labelling approach. New Phytologist, 175(1): 29-35.

Ferretti, D.F., Miller, J.B., White, J.W.C., Lassey, K.R., Lowe, D.C. and Etheridge, D.M., 2007. Stable isotopes provide revised global limits of aerobic methane emissions from plants. Atmospheric Chemistry and Physics, 7: 237-241.

Griffis, T.J., Baker, J.M., Sargent, S.D., Erickson, M., Corcoran, J., Chen, M. and Billmark, K., 2010. Influence of C-4 vegetation on (CO_2)-C-13 discrimination and isoforcing in the upper Midwest, United States. Global Biogeochemical Cycles, 24: 16.

Griffis, T.J., Lee, X., Baker, J.M., Sargent, S.D. and King, J.Y., 2005. Feasibility of quantifying ecosystem-atmosphere (COO)-O-18-O-16 exchange using laser spectroscopy and the flux-gradient method. Agricultural and Forest Meteorology, 135(1-4): 44-60.

Hendriks, D.M.D., van Huissteden, J. and Dolman, A.J., 2010. Multi-technique assessment of spatial and temporal variability of methane fluxes in a peat meadow. Agricultural and Forest Meteorology, 150(6): 757-774.

Houweling, S., Rockmann, T., Aben, I., Keppler, F., Krol, M., Meirink, J.F., Dlugokencky, E.J. and Frankenberg, C., 2006. Atmospheric constraints on global emissions of methane from plants. Geophysical Research Letters, 33(15).

Jacinthe, P.A. and Lal, R., 2003. Nitrogen fertilization of wheat residue affecting nitrous oxide and methane emission from a central Ohio Luvisol. Biology and Fertility of Soils, 37(6): 338-347.

Johnson, J.M.F., Archer, D. and Barbour, N., 2010. Greenhouse gas emission from contrasting management scenarios in the northern corn belt. Soil Science Society of America Journal, 74(2): 396-406.
Karlen, D.L., Duffy, M.D. and Colvin, T.S., 1995. Nutrient, labor, energy, and economic evaluations of two farming systems in Iowa. Journal of Production Agriculture, 8(4): 540-546.
Kelliher, F.M., Reisinger, A.R., Martin, R.J., Harvey, M.J., Price, S.J. and Sherlock, R.R., 2002. Measuring nitrous oxide emission rate from grazed pasture using Fourier-transform infrared spectroscopy in the nocturnal boundary layer. Agricultural and Forest Meteorology, 111(1): 29-38.
Keppler, F., G., H.J.T., M., B. and Rockmann, T., 2006. Methane emissions from terrestrial plants under aerobic conditions. Nature, 439: 187-191.
Kroon, P.S., Hensen, A., Jonker, H.J.J., Zahniser, M.S., van 't Veen, W.H. and Vermeulen, A.T., 2007. Suitability of quantum cascade laser spectroscopy for CH_4 and N_2O eddy covariance flux measurements. Biogeosciences, 4(5): 715-728.
Le Mer, J. and Roger, P., 2001. Production, oxidation, emission and consumption of methane by soils: A review. European Journal of Soil Biology, 37(1): 25-50.
Lin, J.C., Gerbig, C., Wofsy, S.C., Andrews, A.E., Daube, B.C., Davis, K.J. and Grainger, C.A., 2003. A near-field tool for simulating the upstream influence of atmospheric observations: The Stochastic Time-Inverted Lagrangian Transport (STILT) model. Journal of Geophysical Research-Atmospheres, 108(D16).
Liu, L.L. and Greaver, T.L., 2009. A review of nitrogen enrichment effects on three biogenic GHGs: the CO_2 sink may be largely offset by stimulated N_2O and CH_4 emission. Ecology Letters, 12(10): 1103-1117.
Long, K.D., Flanagan, L.B. and Cai, T., 2010. Diurnal and seasonal variation in methane emission in a northern Canadian peatland measured by eddy covariance. Glob Change Biol, 16: 2420-2435
McLeod, A.R., Fry, S.C., Loake, G.J., Messenger, D.J., Reay, D.S., Smith, K.A. and Yun, B.W., 2008. Ultraviolet radiation drives methane emissions from terrestrial plant pectins. New Phytologist, 180(1): 124-132.
Meyers, T.P., Hall, M.E., Lindberg, S.E. and Kim, K., 1996. Use of the modified Bowen-ratio technique to measure fluxes of trace gases. Atmospheric Environment, 30(19): 3321-3329.
Mosher, B.W., Czepiel, P.M., Harriss, R.C., Shorter, J.H., Kolb, C.E., McManus, J.B., Allwine, E. and Lamb, B.K., 1999. Methane emissions at nine landfill sites in the northeastern United States. Environmental Science & Technology, 33(12): 2088-2094.
Mosier, A.R., Halvorson, A.D., Reule, C.A. and Liu, X.J.J., 2006. Net global warming potential and greenhouse gas intensity in irrigated cropping systems in northeastern Colorado. Journal of Environmental Quality, 35(4): 1584-1598.
Nakagawa, F., Tsunogai, U., Komatsu, D.D., Yamada, K., Yoshida, N., Moriizumi, J., Nagamine, K., Iida, T. and Ikebe, Y., 2005. Automobile exhaust as a source of C-13- and D-enriched atmospheric methane in urban areas. Organic Geochemistry, 36(5): 727-738.
Nisbet, R.E.R., Fisher, R., Nimmo, R.H., Bendall, D.S., Crill, P.M., Gallego-Sala, A.V., Hornibrook, E.R.C., Lopez-Juez, E., Lowry, D., Nisbet, P.B.R., Shuckburgh, E.F.,

Sriskantharajah, S., Howe, C.J. and Nisbet, E.G., 2009. Emission of methane from plants. Proceedings of the Royal Society B-Biological Sciences, 276(1660): 1347-1354.

Omonode, R.A., Vyn, T.J., Smith, D.R., Hegymegi, P. and Gal, A., 2007. Soil carbon dioxide and methane fluxes from long-term tillage systems in continuous corn and corn-soybean rotations. Soil & Tillage Research, 95(1-2): 182-195.

Parsons, A.J., Newton, P.C.D., Clark, H. and Kelliher, F.M., 2006. Scaling methane emissions from vegetation. Trends in Ecology & Evolution, 21(8): 423-424.

Pattey, E., Strachan, I.B., Desjardins, R.L., Edwards, G.C., Dow, D. and MacPherson, J.I., 2006. Application of a tunable diode laser to the measurement of CH_4 and N_2O fluxes from field to landscape scale using several micrometeorological techniques. Agricultural and Forest Meteorology, 136(3-4): 222-236.

Shurpali, N.J. and Verma, S.B., 1998. Micrometeorological measurements of methane flux in a Minnesota peatland during two growing seasons. Biogeochemistry, 40(1): 1-15.

Shurpali, N.J., Verma, S.B., Clement, R.J. and Billesbach, D.P., 1993. Seasonal distribution of methane flux in a Minnesota peatland measured by eddy correlation. Journal of Geophysical Research-Atmospheres, 98(D11): 20649-20655.

Smeets, C., Holzinger, R., Vigano, I., Goldstein, A.H. and Rockmann, T., 2009. Eddy covariance methane measurements at a Ponderosa pine plantation in California. Atmospheric Chemistry and Physics, 9(21): 8365-8375.

Suwanwaree, P. and Robertson, G.P., 2005. Methane oxidation in forest, successional, and no-till agricultural ecosystems: Effects of nitrogen and soil disturbance. Soil Science Society of America Journal, 69(6): 1722-1729.

United States Department of Argriculture, 2009. U.S. Summary and State Data. 2007. Census Rep Agric 1: 7-16.

Ussiri, D.A.N., Lal, R. and Jarecki, M.K., 2009. Nitrous oxide and methane emissions from long-term tillage under a continuous corn cropping system in Ohio. Soil & Tillage Research, 104(2): 247-255.

Vigano, I., Holzinger, R., Rockmann, T., van Dijk, A., Keppler, F., Greule, M., Brand, W.A., van Weelden, H. and van Dongen, J., 2009. UV light induces methane emission from plant biomass: Mechanism and isotope studies. Geochimica Et Cosmochimica Acta, 73(13): A1382-A1382.

Vigano, I., van Weelden, H., Holzinger, R., Keppler, F., McLeod, A. and Rockmann, T., 2008. Effect of UV radiation and temperature on the emission of methane from plant biomass and structural components. Biogeosciences, 5(3): 937-947.

Wang, Y.S., Xue, M., Zheng, X.H., Ji, B.M., Du, R. and Wang, Y.F., 2005. Effects of environmental factors on N_2O emission from and CH_4 uptake by the typical grasslands in the Inner Mongolia. Chemosphere, 58(2): 205-215.

Wang, Z.P., Gulledge, J., Zheng, J.Q., Liu, W., Li, L.H. and Han, X.G., 2009. Physical injury stimulates aerobic methane emissions from terrestrial plants. Biogeosciences, 6(4): 615-621.

Wang, Z.P., Han, X.G., Wang, G.G., Song, Y. and Gulledge, J., 2008. Aerobic methane emission from plants in the Inner Mongolia steppe. Environmental Science & Technology, 42(1): 62-68.

Werner, C., Davis, K., Bakwin, P., Yi, C.X., Hurst, D. and Lock, L., 2003. Regional-scale measurements of CH_4 exchange from a tall tower over a mixed temperate/boreal lowland and wetland forest. Global Change Biology, 9(9): 1251-1261.

Zhao, C.F., Andrews, A.E., Bianco, L., Eluszkiewicz, J., Hirsch, A., MacDonald, C., Nehrkorn, T. and Fischer, M.L., 2009. Atmospheric inverse estimates of methane emissions from Central California. Journal of Geophysical Research-Atmospheres, 114: D16302.

Zimnoch, M., Godlowska, J., Necki, J.M. and Rozanski, K., 2010. Assessing surface fluxes of CO_2 and CH_4 in urban environment: a reconnaissance study in Krakow, Southern Poland. Tellus Series B-Chemical and Physical Meteorology, 62(5): 573-580.

Chapter 3: Quantifying nitrous oxide flux from agriculture sources on multiply scales and its implication on current IPCC greenhouse gas guidelines

Abstract

As the third primary greenhouse gas and the greatest ozone-depleting substance, nitrous oxide (N_2O) has been researched extensively to determine its global budget. However, large uncertainties still exist in estimating the strength of the sources and sinks of this trace gas in relation to agricultural activities. These uncertainties were addressed in the present study by measuring and cross-comparing the N_2O fluxes from multiply scales, namely the soil and the individual plant, the soil-plant ecosystem, and the agricultural landscape. Observations made on three contrasting scales indicated that: 1) N_2O flux from unfertilized soybean (0.03 ± 0.05 nmol m^{-2} s^{-1}) and corn plants (-0.01 ± 0.04 nmol m^{-2} s^{-1}) was more than one magnitude lower than N_2O emission from the soil-plant ecosystem, indicating that the emission is largely from the soil; 2) Fertilization only increased the corn plant flux for a short period (about 20 days), and it had no significant impact on the flux averaged across the growing season. However, late-season fertilization dramatically increased soybean plant emission. 3) Both corn and soybean plants serve as a conduit of N_2O emission from soil, but they can also absorb or produce N_2O. 4) IPCC guidelines underestimated regional N_2O emission from an agriculture-dominated landscape by neglecting the nitrogen enhancement through Biological Nitrogen Fixation and underestimating the indirect emission factor of N_2O.

.

3.1. Introduction

Nitrous oxide (N_2O), one of the three major greenhouse gases, has a Global Warming Potential that is 298 times that of CO_2, and it is a critical substance with respect to stratospheric ozone depletion (Ravishankara *et al.*, 2009). Since the industrial revolution, atmospheric N_2O has increased dramatically, from 270 ppb to 319 ppb (Forster *et al.*, 2007), mainly due to enhanced anthropogenic emissions. Mitigation of N_2O emission will require a complete inventory of all N_2O sources and sinks. Major sources and sinks have been identified, but large uncertainties still exist for estimating their effective sizes on both regional and global scale. For example, global N_2O emission from agricultural activities (not including cattle and feedlots), accounts for about a quarter of the total anthropogenic emission, but varies in a wide range from 0.6 to 14.8 Tg N yr^{-1} (Mosier *et al.*, 1998).

One of the greatest uncertainties in N_2O inventory from agriculture ecosystems is the N_2O flux that occurs from plants (Misselbrook *et al.,* 2011). Some studies have been conducted to determine this N_2O flux and have suggested that plants should not be neglected as a source of N_2O (Chen *et al.*, 1999; Marinho *et al.*, 2004; Pihlatie *et al.*, 2005; Smart and Bloom, 2001; Zou *et al.*, 2005). For example, Chen *et al.* (1999) found that N_2O emission from rye grass (*Lolium perenne* L.) could reach 1.16 nmol m^{-2} s^{-1}, while the emission from the grass-soil ecosystem ranged from 0.33 to 5.50 nmol m^{-2} s^{-1}. Marinho *et al.* (2004) reported that the averaged N_2O emission from a soybean (*Glycine max*) plant during its growing season is 0.22±0.40 nmol m^{-2} s^{-1}, which is similar to the soil emission (0.21±0.45 nmol m^{-2} s^{-1}). In addition, the maximum N_2O emission from soybean plants after rainfall (1.14±0.21 nmol m^{-2} s^{-1}) is comparable to the emission from

soils (1.50±0.54 nmol m^{-2} s^{-1}). Zou *et al.* (2005) suggested that N_2O emission from wheat plants (*Triticum aestivum* L. cv. Veery 10) accounts for 25% of the total emission for the whole growing season, ranging from 10% to 62% at different growing stages.

In contrast, Lensi and Chalamet (1981) and Grundmann *et al.* (1993) observed that corn (*Zea mays* L.) could absorb N_2O at a rate of up to 15 µg N-N_2O $plant^{-1}$ h^{-1} (1.19 nmol m^{-2} s^{-1}, assuming a plant density of 8 plants m^{-2}). Using the same method as Chen *et al.* (1999) and Zou *et al.* (2005), Müller (2003) indicated the possibility that grass can emit or absorb N_2O during the photoperiod. Consequently, no consensus has been reached regarding the role of plants in the exchange of N_2O in the biosphere-atmosphere.

The divergence observed in N_2O fluxes from plants could be partly attributed to different plant species and fertilization patterns; however, measurement artifacts could also have significantly affected the previous observations. Three major artifacts have been examined in the literature: 1) Discrepancies due to the carrier gas used in gas chromatography (GC) measurements. A significant relationship was found between the N_2O concentrations and CO_2 concentrations when nitrogen (N_2) was used as the carrier gas during a GC measurement (Zheng *et al.*, 2008). This artifact leads to significant overestimation of N_2O emission from plants. 2) Discrepancies due to light conditions. Two pathways have been proposed to explain N_2O emission from plants: N_2O diffusion from roots and nitrate assimilation by the plants (Chang *et al.*, 1998; Smart and Bloom, 2001). Use of an opaque chamber or taking measurements in the dark will affect both of these potential pathways for N_2O emission by reducing photosynthesis and transpiration (Muller, 2003). 3) Discrepancies due to the use of controlled environments and indirect measurement methods. Typically, measurements of N_2O flux are conducted in

laboratories under well controlled environments; however, in the field, N_2O flux is affected by many factors, such as precipitation and soil conditions. This complicates the extrapolation of lab results to estimate the actual emission in the field. Only a few studies have been conducted under field conditions and these have compared the N_2O emissions from the soil-plant ecosystem before and after harvesting the plants (Chen *et al.,* 1999; Muller, 2003; Zou *et al.,* 2005). This indirect method is built on the assumption that N_2O emission from soil would not be affected by harvesting the plants.

However, most observations of the N_2O flux from croplands have been determined using soil chamber measurements, which neglect the plant flux and have inherent disadvantages in addressing the spatial and temporal heterogeneity of N_2O soil emissions. As the high-frequency measurement of N_2O concentrations has become available in recent years, micrometeorological methods (such as eddy covariance and flux-gradient) have been applied successfully for determining N_2O flux at the ecosystem scale (Wagner-Riddle *et al.*, 1997; Phillips *et al.*, 2007; Denmead, 2008; Kroon *et al.*, 2010; Molodovskaya *et al.*, 2011). Both eddy covariance and flux-gradient methods allow ecosystem-scale, real-time, and continuous flux measurement and have limited disturbance to the ecosystem. Each of these methods has its advantages/disadvantages. For example, eddy covariance systems provide a direct measurement of the N_2O exchange with limited assumptions but require fast response systems, while the flux-gradient method has lower requirement on frequency response of the concentration measurement, estimating the eddy diffusivity for N_2O can be challenging. Some studies used the flux-gradient method to continuously measure N_2O flux from agricultural field with different cover crops and management methods, and identified the impact of manure application, fallow, and tillage on the

timing and the amount of N_2O emission (Wagner-Riddle *et al.*, 1997; Phillips *et al.*, 2007), but few have evaluate the flux-gradient method with the soil chamber observation, and compare the result with the estimates based on IPCC guidelines. Large uncertainties also exist in determining regional N_2O emissions. IPCC guidelines for national greenhouse gas inventories (De Klein et al., 2006) have been widely adopted because of its relatively easy parameterization, but recent studies based on tall tower or aircraft observations reported that the IPCC method might underestimate regional N_2O emissions by a factor of two or more (Kort *et al*., 2008; Miller *et al*., 2012). Here, we estimated the regional N_2O flux based on near-continuous measurements from a tall tower located within the US Corn Belt to help understand the influence of agricultural plants and soils on the regional budget and to reassess the IPCC approach for this region.

Therefore the objectives of the present study are to:

1) Quantify N_2O flux from soybean and corn plants growing in the field using a new chamber designed to limit artifacts;

2) Explore whether nitrogen fertilizer enhances the N_2O flux from the plants;

3) Evaluate the influence of N_2O flux from soybean and corn plants on the soil-plant flux and the regional flux from a landscape dominated by agriculture;

4) Evaluate the IPCC approach in estimating regional N_2O flux for the Midwest US.

3.2. Materials and Methods

3.2.1. Research site and the observation system

This research was conducted at the University of Minnesota Outreach, Research, and Education Park, in Rosemount, Minnesota, in parallel with the CH_4 research described in Chapter 2. In addition to the plant chamber measurement and the tall tower measurement for determining the N_2O flux from the plant and from the landscape around the tall tower, respectively (Chapter 4), a closed-path eddy covariance system was installed at the G21 site in the middle of a soybean-corn rotation field to measure the N_2O flux from the soil-plant ecosystem. The measurement system on three different scales (plant scale, ecosystem scale, and regional scale) enabled the evaluation of the role of the plants in the soil-plant ecosystem and in an agriculture-dominated landscape (Figure 3.1). The date of each measurement is recorded in supplementary materials Table 3.4. N_2O concentrations in the three-scale experiments were measured by a tunable diode laser analyzer (TDL) (model TGA 100A, Campbell Scientific Inc., Logan, UT, USA).

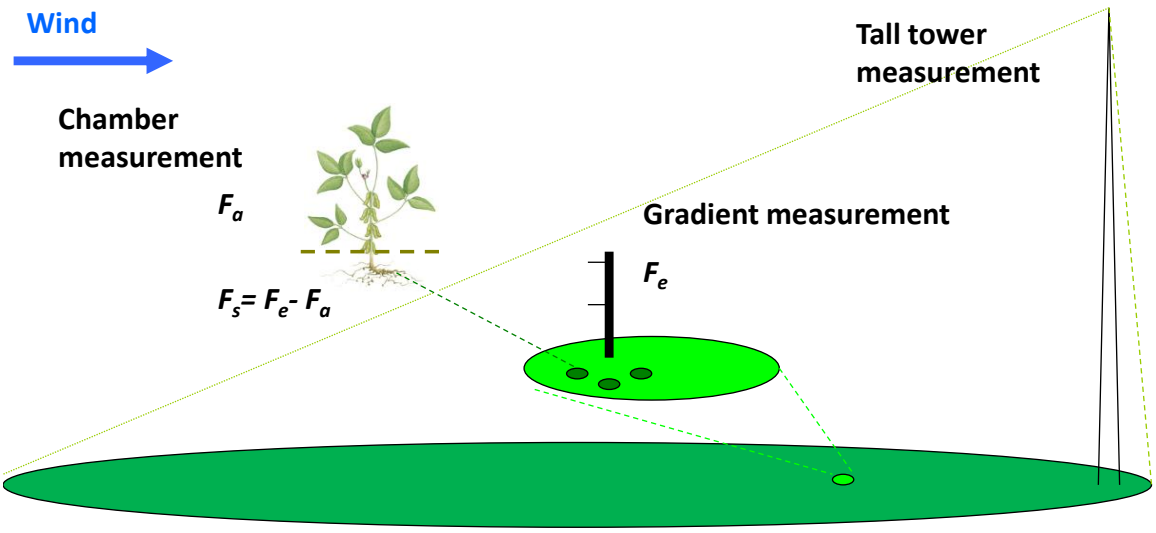

Figure 3.1. Schematic diagram of the three-scale observation system. The observation system includes a chamber measurement targeting on plant scale flux, a flux-gradient measurement targeting on soil-plant ecosystem scale flux, and a tall tower measurement targeting on regional scale flux.

3.2.2. Plant chamber measurement

Determining N_2O plant fluxes without disturbing the living environment of the plant is very challenging. The plant chamber was designed to minimize chamber artifacts and disturbance of plant activities to avoid affecting the N_2O flux from plant (Chang *et al.*, 1998; Smart and Bloom, 2001).We used a transparent cover that allowed 92% of the visible light and 90% of the UV radiation to reach the plant. The difference between the chamber temperature and the ambient temperature was maintained within ±3°C by a cooling system. The airflow through the chamber was kept higher than 20 L min^{-1} and was increased in the middle of growing season due to a strong CO_2 depletion inside the chamber. As a result, the CO_2 concentration difference was kept within 9 and 66 ppm during the day and between 4 and 11 ppm at night for corn and soybean, respectively. The newly designed plant chamber did not appear to have any dramatic effect on plant activities because the leaf area index (LAI), dry weights, and heights of the measured plants were not significantly different from those of the other plants in field, and the midday (10:00 – 16:00 LST) CO_2 uptake rates by the plants (-12±3 μmol m^{-2} s^{-1} by unfertilized soybean and -39±3 μmol m^{-2} s^{-1} by fertilized corn) were comparable to the CO_2 flux measured by an eddy covariance system at G21.

Due to the relatively high flow rate through the plant chamber, the concentration difference between the inlet and outlet of the chamber was very small; consequently, the precision and the accuracy of the TDL measurement were critical. We conducted a blank chamber test for each chamber type (small, medium, and large chambers) to determine the accuracy and precision of the chamber measurement. In addition, two types of sampling strategy were examined: 1) sampling the air from the chamber inlet and outlet

sequentially (2 site switching) for 20 s each; and 2) sampling the air from the inlet, outlet, zero tank, and calibration tank sequentially (4 site switching) for 20 s each. The blank chamber test was conducted by running the chamber system for 24 hour without enclosing a plant (Table 3.1).

The chamber test results indicated that the concentration difference between the inlet and outlet sample points was not significantly different from zero, but was consistently negative, indicating a measurement bias towards a more negative flux (supplementary materials Table 3.5). Therefore, we corrected this bias according to the blank test for each chamber during the plant measurement. In addition, even though incorporation of the measurement taken at the zero tank and the calibration tank would improve the accuracy of the concentration measurement, doing so reduced the frequency of the measurements by half, so that the measurement precision of the concentration difference at the inlet and outlet sample points was reduced by about 50%.

Table 3.1. The precision of the plant chamber measurement for plant N_2O flux.

Chamber	Calibration	N_2O (nmol m^{-2} s^{-1})
Small (soybean)	no	0.03
Medium (soybean)	no	0.04
Small (corn)	no	0.01
Medium (corn)	no	0.01
Medium (corn)	yes	0.06
Large (corn)	yes	0.09

Note: Calibration of the N_2O concentration measurement was added during the later corn season by measuring zero gas and span gas along with the air samples from the chamber inlet and outlet. A blank test with the calibration method applied was carried out for medium and large chambers in the corn year.

3.2.3. Flux-gradient measurement

A N_2O gradient measurement was conducted on a 10 m tower in the middle of a soybean-corn rotation field (with a fetch of more than 180 m in every direction) in order to monitor the N_2O flux from the soil-plant ecosystem (Baker and Griffis, 2005). The N_2O mixing ratios were typically measured at 1 m and 2 m; but in the corn season, due to the taller corn canopy, the measurement height was adjusted appropriately during the later growing season (supplementary materials Table 3.6).

The flux of the soil-plant ecosystem (F_{sp}) was derived from the gradient measurement, with the vertical profile of concentration ($\partial c/\partial z$) and diffusivity (K) (Kaimal and Finnigan, 1994).

$$\mathrm{F_{sp}} = -\mathrm{K}\frac{\partial \mathrm{c}}{\partial \mathrm{z}} \tag{3.1}$$

The diffusivity was calculated by

$$\mathrm{K} = \frac{\mathrm{k u_*(z-d)}}{\emptyset_\mathrm{h}} \tag{3.2}$$

where k is von Karman constant (k=0.41), u_* is friction velocity measured at the tower, z is the geometric mean of z_1 and z_2 ($z = (z_1 z_2)^{1/2}$), zero-plane displacement (d) is approximately 2/3 of the canopy height, and φ_h is the dimensionless vertical temperature gradient calculated by Equation 3.3.

$$\emptyset_\mathrm{h} = \begin{cases} (1+16|\mathrm{z/L}|)^{-1/2}, & -2 \le \mathrm{z/L} \le 0 \\ (1+5\mathrm{z/L}), & 0 \le \mathrm{z/L} \le 1 \end{cases} \tag{3.3}$$

In this equation, the Monin-Obukhov length (L) was calculated as follows:

$$\frac{z}{L} = -\frac{\left(\frac{g}{\bar{\theta}}\right)(\overline{w'\theta'})_0}{\frac{u_*^3}{kz}} \tag{3.4}$$

where g is gravitational acceleration, $\bar{\theta}$ is the mean potential temperature, and $(\overline{w'\theta'})_0$ is the potential temperature flux at the land surface.

3.2.4. Regional flux from the tall tower measurement

The N_2O mixing ratio was measured at the 3 m and 200 m levels during a tall tower intensive campaign period (DOY243-269) in 2009. The regional flux from the tall tower measurement was determined by the equilibrium method (Betts *et al.*, 2004; Helliker *et al.*, 2004), which assumes the land surface flux will reach equilibrium with the trace gas exchange at the top of the boundary layer over a period of time longer than half-month. As a result, the land surface flux can be estimated from the subsidence rate at the top of the boundary layer and the difference between the trace gas concentration within and above the boundary layer. Detailed analysis on determining regional N_2O flux based on the tall tower measurement and the equilibrium method is presented in Chapter 4.

To estimate the annual N_2O flux from the landscape around the tall tower, we assume the seasonal pattern of N_2O concentration at the tall tower was the same as that on WBI tower and SGP tower measured by NOAA (Table 4.5). This assumption is reasonable considering that both towers are located in the Midwest US and in an agriculture-dominated landscape. As a result, the N_2O concentration within the boundary layer at the tall tower could be extrapolated based on N_2O concentration at the tall tower measured in September, and the seasonal pattern observed at the two towers.

3.2.5 Supporting measurements

Some of the N_2O emission data are expressed on leaf area basis or dry weight basis. Therefore, we measured LAI and dry weight of the above ground section of plants every week (supplementary materials Table 3.7). Plants were sampled separately from the fertilized and unfertilized zone (five plants per sample), and the dry weight was measured after drying the plant in an oven (60°C) for one week.

Total Nitrogen and NO_3-N in soil were measured on 4 August and 26 August 2008 for both the fertilized and unfertilized soybean plots. The same measurement was conducted at the beginning (2 June) and at the end of the 2009 growing season (12 August) for the fertilized and unfertilized corn plots (Table 3.2).

Standard micrometeorological and eddy flux variables were measured at half-hourly intervals at the G21 field and at an adjacent field with an opposite soybean-corn rotation schedule (G19). In addition, environmental parameters, such as soil moisture and air temperature, were recorded in field throughout the observation period (Bavin *et al.*, 2009; Griffis *et al.*, 2005).

Table 3.2. Total soil nitrogen and nitrate-N for the 2008 and 2009 growing seasons at chamber measurement plots. (Fertilizer was applied on July 10 for soybean and on April 15 for corn.)

Sample Time	Total Soil N (%)	Nitrate-N (mg kg^{-1})	Total Soil N (%)	Nitrate-N (mg kg^{-1})
Soybean phase 2008				
	Unfertilized Soil		**Fertilized Soil**	
04 August	0.078	8	0.094	38
26 August	0.077	6	0.095	73
Corn phase 2009				
	Unfertilized Soil		**Fertilized Soil**	
June	0.10	83	0.12	137
August	0.10	50	0.11	41

3.3. Results

3.3.1. Soybean plant flux

Through the 2008 observation period, the soybean plants emitted N_2O at the rate of 0.03 ± 0.05 nmol m^{-2} s^{-1}. Figure 3.2a summarizes the daily fluxes observed for soybean plants: 69% of the daily fluxes were positive, and among these, 80% were higher than the measurement precision of the chamber system. Emission of N_2O was observed consistently in the later growing season (DOY 205-225), and the highest emission rate was 0.23 nmol m^{-2} s^{-1}, or about five times higher than the measurement precision. Several negative daily fluxes were observed during the growing season, but the absolute value of these negative fluxes was very small: half of them were smaller than the measurement precision for small chamber (0.03 nmol m^{-2} s^{-1}), and the rest were less than two times larger than the measurement precision. The N_2O flux from the soybean plants was mostly positive at midnight (20:00-4:00) throughout the growing season (0.06 ± 0.06nmol m^{-2} s^{-1}), while the midday flux (10:00-16:00) had a large variation, from -0.21 to 0.41 nmol m^{-2} s^{-1}.

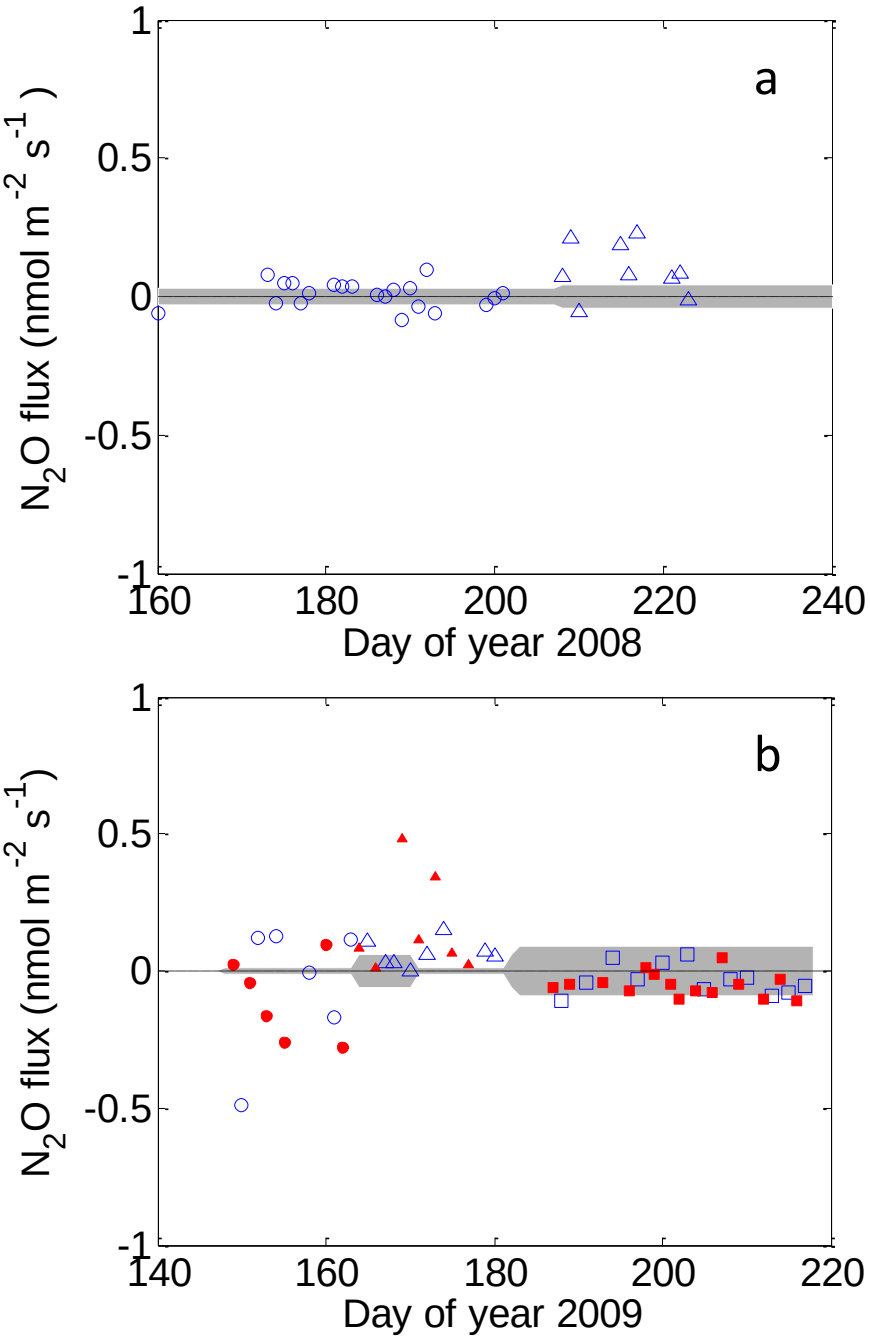

Figure 3.2. Daily plant N_2O flux from soybean (a) and corn (b) fields throughout the growing season: red filled symbols– fluxes from fertilized plants; blue open symbols – fluxes from unfertilized plants; circles, triangles, squares – fluxes measured using a small chamber, a medium chamber, and a large chamber, respectively; grey area – measurement precision of each type of chamber measurement.

3.3.2. Corn plant flux

Both N_2O emission and uptake were observed from corn plants at different growth stages (Figure 3.2b). During the early growth stage (DOY 149-180), corn plants were a strong source of N_2O in both the fertilized and unfertilized treatment. From DOY 163 to 180, all of the sampled plant fluxes were consistently positive, the mean N_2O emission from fertilized plants was 0.16 nmol m^{-2} s^{-1}, and was higher than the emission from unfertilized plants (0.06 nmol m^{-2} s^{-1}). Some strong negative daily fluxes were observed before DOY 163, and largest uptake rate reached -0.49 nmol m^{-2} s^{-1}. This does not likely represent a measurement bias because: 1) the TDL diagnostics were of high quality throughout the observation period; 2) the concentration measurement bias was removed through calibration; 3) the absolute values of these negative fluxes were larger than the measurement precision; and 4) these fluxes were not correlated with the background concentration change and the negative fluxes happened when the background concentration change rate was near zero (Figure 3.3).

During the later growing season, the N_2O flux from corn plants was very small but mostly negative. Even though only four out of 27 daily fluxes were above the measurement precision, all four of these daily fluxes were negative; in addition, among the rest of the fluxes, only 18% were positive. The N_2O fluxes for fertilized and unfertilized corn in this period were -0.05 and -0.03 nmol m^{-2} s^{-1}. These values suggested that the corn plant was a small N_2O sink during the late growing season.

Throughout the whole growing season, both fertilized and unfertilized corn plants were small N_2O sinks (-0.01±0.04 and -0.01±0.06 nmol m^{-2} s^{-1}), and N_2O uptake usually happened at night.

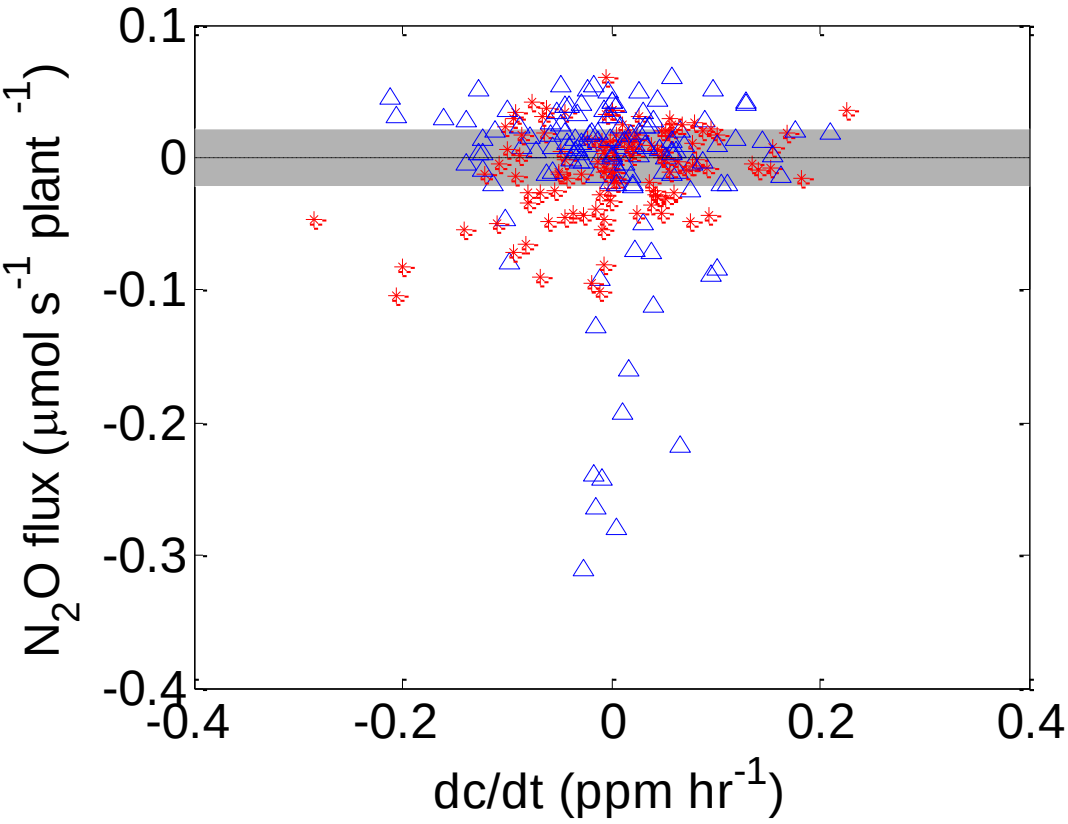

Figure 3.3. The impact of background N_2O concentration changes on N_2O flux. Blue triangles– flux from unfertilized plants; red stars– fluxes from fertilized plants; black dashed line– mean value of the blank test; grey area– standard deviation of the blank test.

3.3.3. N_2O emission from the soil-plant ecosystem

A zero-gradient test, conducted from DOY 118 to 128 (2009), suggested that no significant bias existed in the flux-gradient measurement from the 10 m tower. The zero-gradient test was carried out by co-locating the two sample inlets at the same height. The measured concentration difference between the two inlets was 0.01 ± 0.03 ppb for the daily average and the corresponding N_2O flux was -0.00 ± 0.11 nmol m^{-2} s^{-1}. Therefore, the background noise level for measuring N_2O daily flux by this flux-gradient method was 0.11 nmol m^{-2} s^{-1}.

During the soybean growing season (2008), 72% of the N_2O daily fluxes were above the background noise level and most were positive (Figure 3.4). The averaged N_2O emission from the soil-soybean ecosystem was 0.22 nmol m^{-2} s^{-1}.

In 2009, N_2O fluxes from the soil-corn ecosystem could be divided into three time periods (Figure 3.4): 1) from the beginning of the year to the first strong rain event after fertilization (DOY 0- 116). Here, N_2O fluxes were generally small, only 44% higher than the background noise level. The averaged N_2O flux in this period was -0.10 nmol m^{-2} s^{-1}; 2) After fertilization (DOY 117-200), N_2O emissions from the soil-plant ecosystem were very largeand averaged 1.32 nmol m^{-2} s^{-1}. The daily emission ranged up to 5.48 nmol m^{-2} s^{-1}. The first large emission event was observed beginning at DOY 138, but due to the data gap from DOY119 to 130, the emission may possibly have started as early as DOY 119; 3) In the later days of the growing season (DOY 201-220), the soil-plant ecosystem no longer maintained a N_2O emission rate, and uptake was observed for several days. During this time period, the averaged N_2O flux was -0.30 nmol m^{-2} s^{-1}, and the uptake rate reached a maximum of -2.6 nmol m^{-2} s^{-1}.

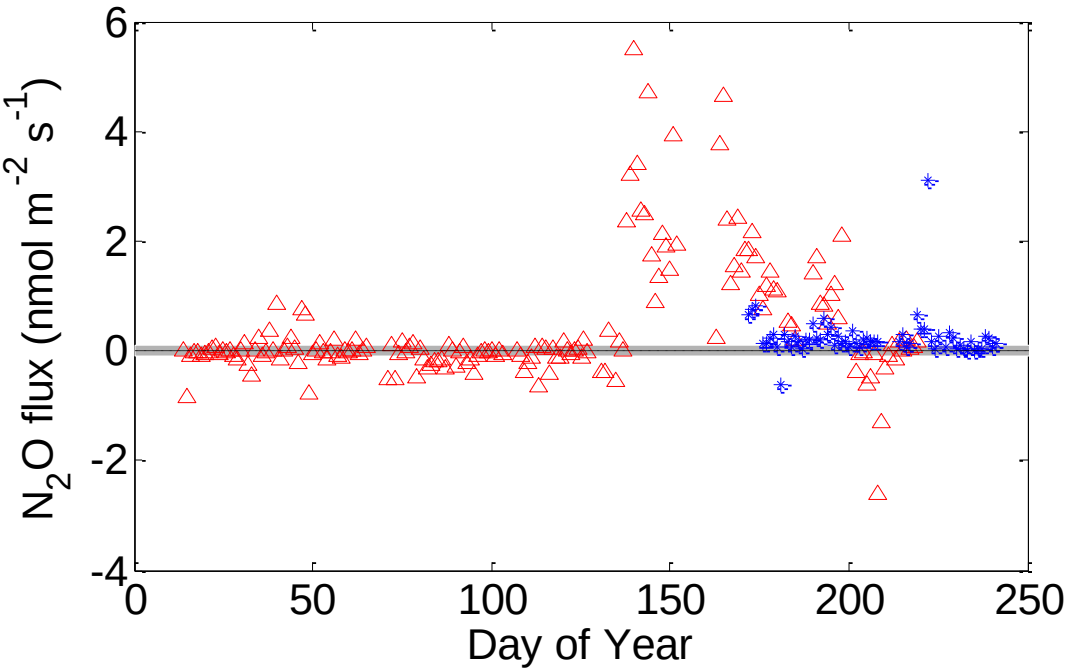

Figure 3.4. Daily median N_2O flux from soil-soybean (blue star) and soil-corn (red triangle). Grey area – background noise level.

3.3.4. Impact of fertilization

Fertilization significantly increased N_2O emission from soil, and led to greater N_2O emission from the corn plants during the early growing season. From DOY 163 to 180, fertilized corn emitted N_2O at the rate of 0.16 nmol m^{-2} s^{-1}, accounting for 9.0 % of the soil-corn emission, while unfertilized corn emitted only 0.06 nmol m^{-2} s^{-1}. However, the N_2O emission from corn plants was only sustained for about 20 days, when N_2O flux from soil was very strong, and was compensated by the uptake in the later growing season. As a result, no significant difference was noted between N_2O flux from fertilized and unfertilized corn plants (Figure 3.5).

Fertilizer is not usually applied during the soybean phase at the soybean-corn rotation field in upper Midwest, since the fertilization at sowing was ineffective in most cases (Beard and Hoover, 1971; Bharati *et al.*, 1986; Gutierrez-Boem *et al.*, 2004; Mendes *et al.*, 2003). As an alternative for increasing soybean yield, fertilizer application during the reproductive stages has been proposed, and its impact on the soybean productivity has been examined (Freeborn *et al.*, 2001; Salvagiotti *et al.*, 2008; Wesley *et al.*, 1998). However, the impact of this fertilization approach on yield is very inconsistent, and few studies have examined its impact on N_2O emission. We provided a preliminary test of the plant response to late season fertilization by applying fertilizer (24-8-16, NPK; ScottsMiracle-Gro, Marysville, OH) at the rate of 500 kg N ha^{-1} to three randomly selected soybean plants in the middle of the growing season (July 10 DOY 192). We chose a fertilization rate that was the upper limit of the N fertilization in growing season based on literature values, in order to maximize the N_2O signal. The Total soil N and Nitrate-N increased from 0.078% and 8 mg kg^{-1} to 0.094% and 38 mg kg^{-1}, respectively.

The preliminary test of the impact of late season fertilization on N_2O plant flux suggested that fertilization increased the plant N_2O flux to 2.01 nmol m^{-2} s^{-1}, nearly two magnitudes higher than the unfertilized soybean plant flux. All plants emitted N_2O during nighttime (3.08 nmol m^{-2} s^{-1}), but showed both positive and negative flux during the daytime, and the averaged flux during the observation period was slightly negative (-0.34 nmol m^{-2} s^{-1}). Further investigation of the impact of nitrogen fertilizer on N_2O emission from soybean plants should be pursued.

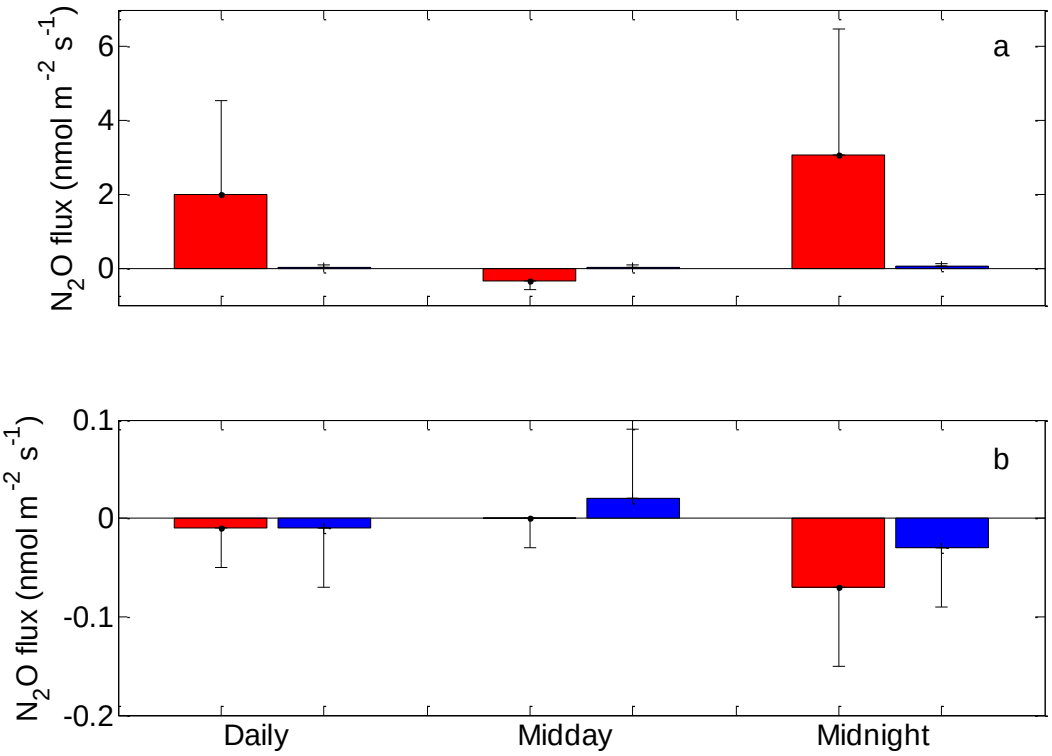

Figure 3.5. Daily, midday (10:00-16:00 LST), and midnight (20:00-04:00 LST) fluxes averaged over the soybean (a) and corn (b) growing seasons. Error bars are standard deviations of the replicate plants. Blue bar – unfertilized plant flux; red bar – fertilized plant flux.

3.3.5. Tall tower N_2O concentration and regional flux

During the observation period (DOY 243 - 269, 2009), N_2O concentration at 3 m showed a weak diurnal pattern. The diurnal composite of N_2O concentration on 3 m (Figure 3.6b) shows that N_2O concentration was generally high at night, and low during the day, but with a day-to-day variation. The hourly mean N_2O concentration increased after sunset and reached a peak (332.2±25.1 ppb) around 1:00; after sunrise, it dropped steadily until 16:00 (322.9±4.5 ppb). This diurnal pattern was similar to the pattern seen for CO_2 (Figure 3.6a), and it suggested that N_2O emission from the land surface was accumulated near the ground at night. In contrast, N_2O concentration at 200 m was slightly elevated during the day because of the well mixing with the N_2O enriched air near the land surface. Throughout the observation period, the N_2O concentration on 200 m was 324.8 ppb, about 2.1 ppb higher than the N_2O concentration above the boundary layer. This background N_2O concentration was determined by the observation at the NWR site in Colorado, the closest background site operated by NOAA. Both the gradient between 3 m and 200 m level at the tall tower and the higher concentration at the tall tower site than the background site indicate the landscape around the tall tower was a source of N_2O.

According to the equilibrium boundary-layer method, the N_2O flux during the observation period was 0.19±0.04 nmol m^{-2} s^{-1} (Chapter 4). The extrapolated annual fluxes according to the WBI and SGP both suggested a small emission period triggered by spring thaw and stronger emissions in May and June after fertilization (Figure 3.7). The annual N_2O flux from the landscape around the tall tower was 0.37±0.12 nmol m^{-2} s^{-1}, equivalent to 3.24±1.05 kg N_2O-N ha^{-1} yr^{-1}. This result was consistent with the annual flux reported by Griffis *et al.* (in review)

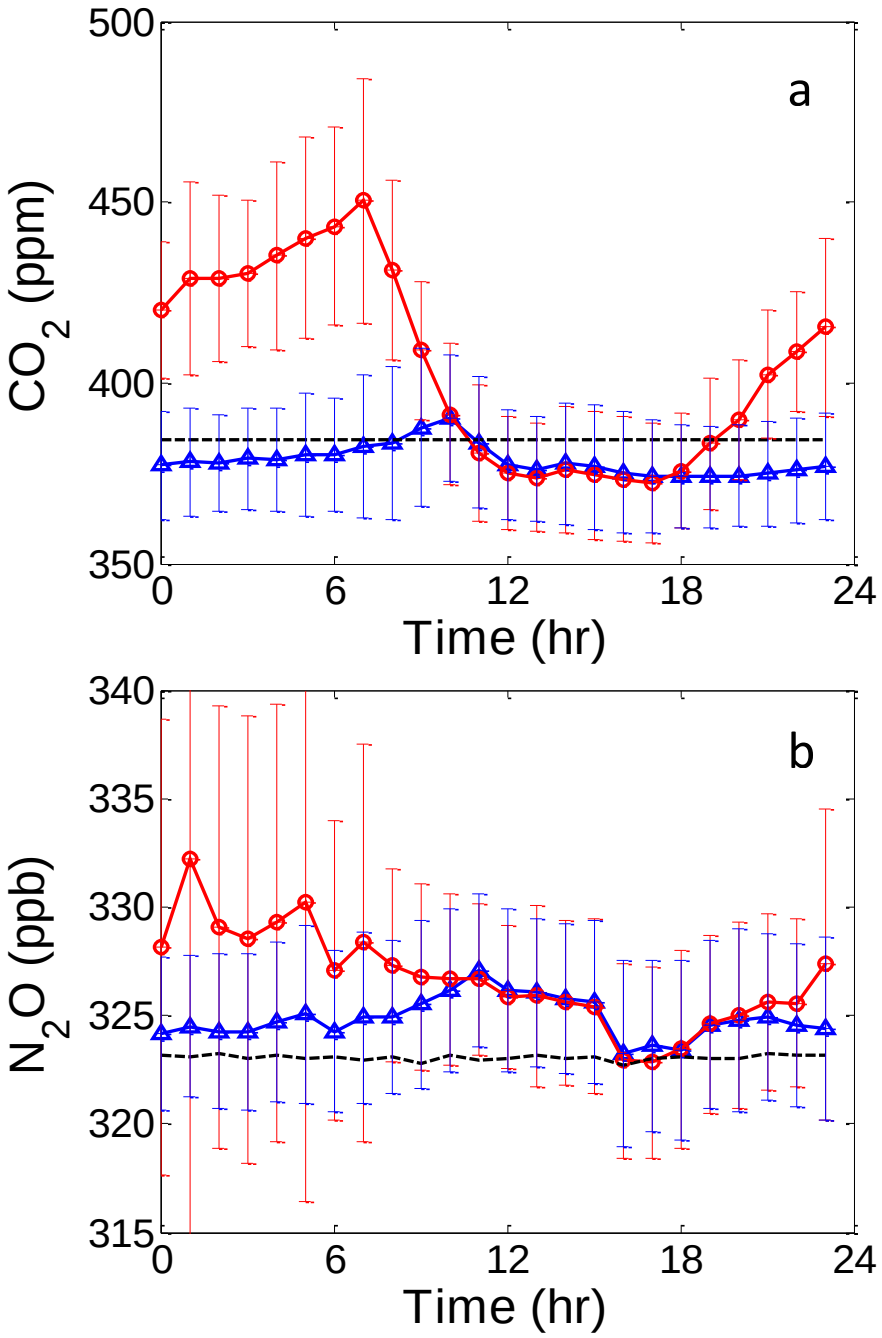

Figure 3.6. Diurnal composite of CO_2 (a) and N_2O (b) concentration at the heights of 3 m and 200 m above the ground during DOY 243-269, 2009. Red circles and blue triangles are the hourly mean values of the concentration at 3 m and 200 m, respectively, and error bars are the standard deviations of 30-min observations.

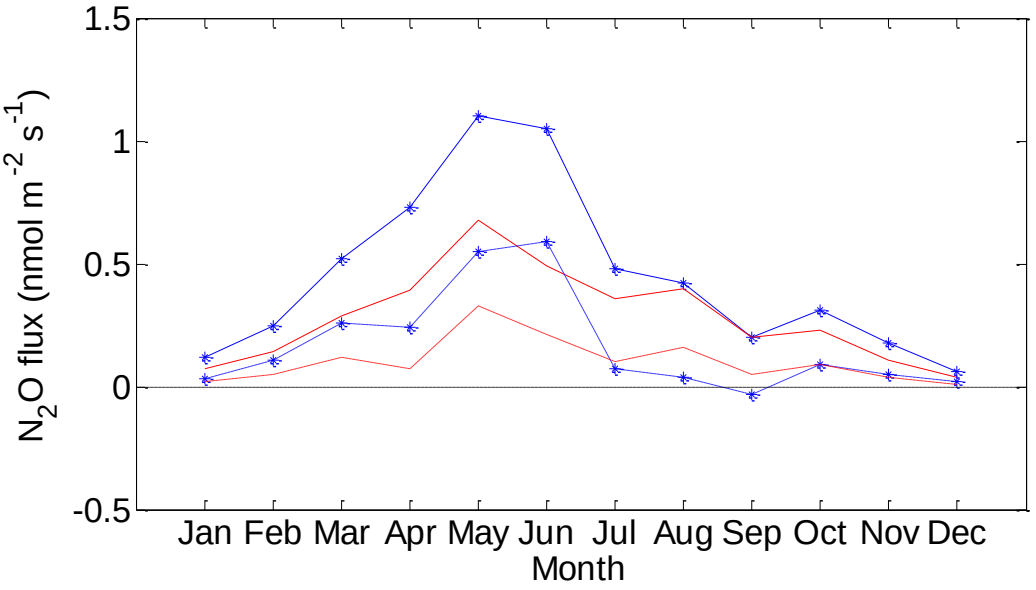

Figure 3.7. A summary of estimated regional N_2O fluxes. Solid line with star–tall tower N_2O flux estimated based on WBI site seasonal pattern; solid line–tall tower N_2O flux estimated based on SGP site seasonal pattern; dashed line with star–N_2O flux at WBI site; dashed line–N_2O flux at SGP site.

3.4. Discussion

3.4.1. Plant flux and soil-plant flux

The N_2O fluxes from soybean and corn plants were relatively small compared to the fluxes from the soil-plant ecosystem (Figures 3.8a and 3.9a, Table 3.3).

The daily averaged N_2O flux from soybean plants throughout the growing season accounted for about 12% of the emission from the soil-soybean ecosystem. The nighttime N_2O emission from soybean plants was relatively higher than the daytime emission, while the nighttime emission from the soil-soybean ecosystem was relatively lower than the daytime. Therefore, soybean plants accounted for about 30% of the nighttime emission from the soybean-plant ecosystem.

Throughout the observation period, the averaged N_2O flux from fertilized corn plants was slightly negative (-0.01 ± 0.04 nmol m^{-2} s^{-1}), more than one magnitude lower than the N_2O flux from the soil-corn ecosystem. This confirms that, after fertilization, soil is the major source of N_2O emission, and it dominates the N_2O flux from the soil-corn ecosystem.

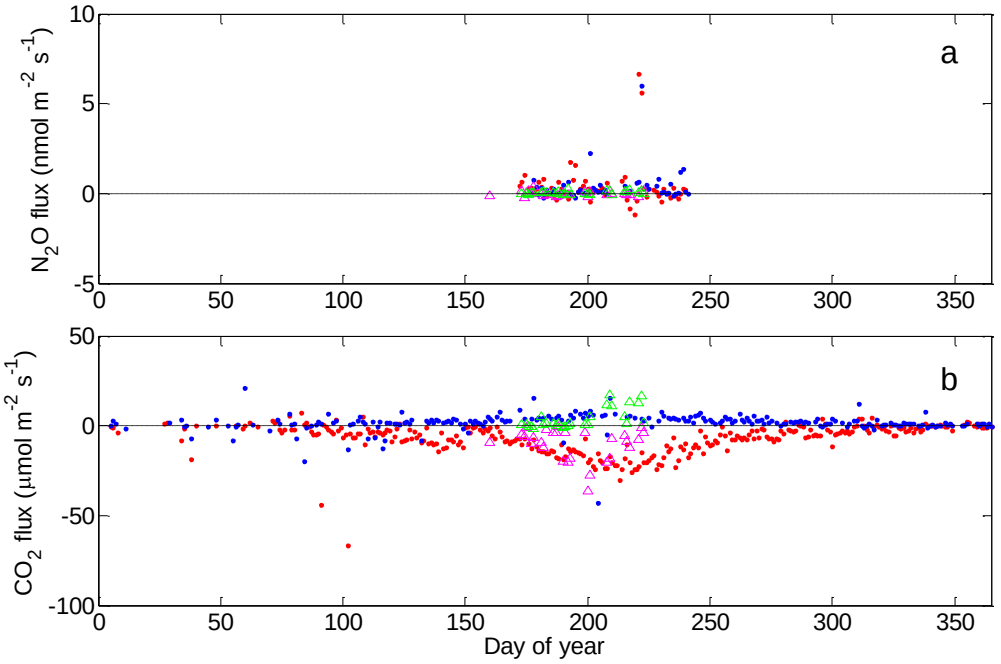

Figure 3.8. Comparison of N_2O fluxes (a) and CO_2 fluxes (b) from unfertilized soybean plant and soil-soybean ecosystem, 2008: magenta triangles – midday flux from soybean; green triangles – midnight flux from soybean; red dots – midday flux from the soil-soybean ecosystem; blue dots- midnight flux from the soil-soybean ecosystem.

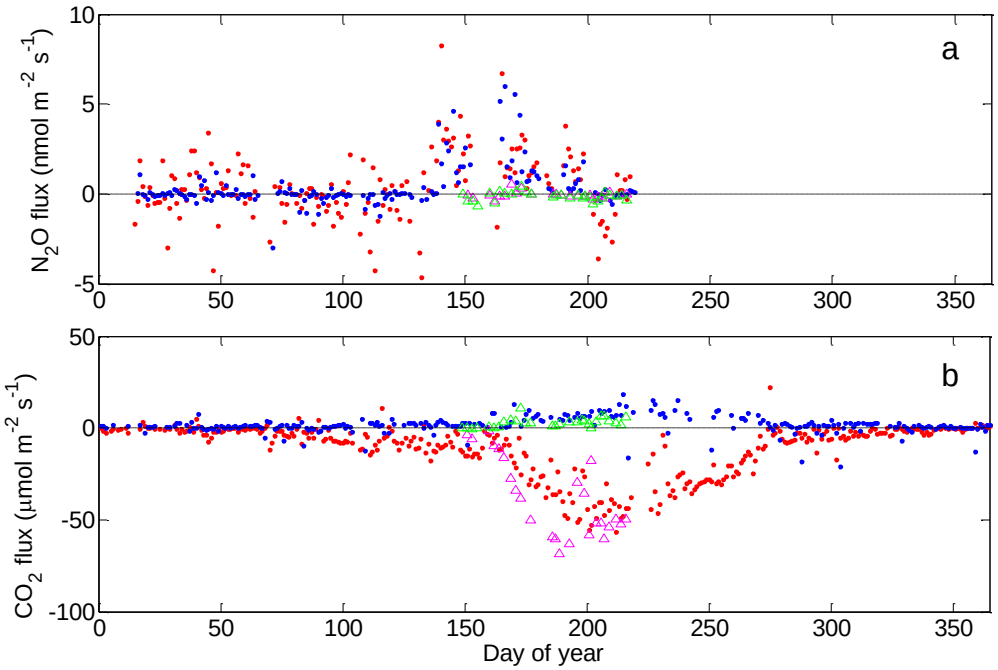

Figure 3.9. Comparison of N_2O fluxes (a) and CO_2 fluxes (b) from fertilized corn plant N_2O and soil-corn ecosystem, 2009: magenta triangles – midday flux from corn; green triangles – midnight flux from corn; red dots – midday flux from the soil-corn ecosystem; blue dots- midnight flux from the soil-corn ecosystem.

Table 3.3. Midnight, midday, and daily N_2O fluxes from plants and soil-plant ecosystems during the growing season (chamber measurement period).

	Midnight N_2O flux (nmol m^{-2} s^{-1})	**Midday N_2O flux (nmol m^{-2} s^{-1})**	**Daily N_2O flux (nmol m^{-2} s^{-1})**
Fertilized corn	-0.07	-0.00	-0.01
Soil-corn	1.30	0.89	0.95
Unfertilized soybean	0.06	0.02	0.03
Soil-soybean	0.20	0.52	0.26

3.4.2. The origin of the plant N_2O flux

Two mechanisms have been proposed for plant N_2O flux. One considers plants as a conduit that mediates N_2O exchange between the soil and the atmosphere (Chang *et al*., 1998), the other considers plants as a producer that generates N_2O in the process of photoassimilation (Smart and Bloom, 2001).

Several lines of evidence from our observations suggest that corn plants mediated soil-atmosphere exchange of N_2O. First, throughout the growing season, the N_2O flux from the fertilized corn plant was noticeably correlated with the soil-corn flux ($p<0.05$, student's t-test, Figure 3.10). Considering the corn plant flux was mostly one magnitude smaller than the soil-corn flux, the latter could be considered as the soil flux. As a result, the corn plant flux and soil flux were well correlated. Second, the small period of N_2O emission from the corn plants in the middle of the growing season (DOY 163-180) corresponded to the peak soil emission. Third, soil water content at night, which is critical for N_2O emission from cropland (Desjardins *et al.,* 2010; Grant and Pattey, 2003), was also positively correlated with the corn plant N_2O fluxes ($p<0.005$, student's t-test).

The corn N_2O flux was mostly negative during the later growing season even when the soil-corn N_2O flux was positive, indicating an uptake mechanism within the corn plant. This observation is consistent with the N_2O uptake reported by Grundmann *et al.* (1993). Using a ^{15}N labeling technique, Grundmann *et al.* found that corn leaves absorbed N_2O, and that part of the absorbed N_2O was metabolized to plant tissue, while the rest may be stored .

According to the correlation between the corn flux and soil-corn flux (Figure 3.10), the mean uptake rate by the corn plants throughout the growing season was 0.03 nmol m^{-2} s^{-1}, and the corn plant mediated about 5% of the soil N_2O flux.

N_2O flux from soybean plants was correlated with the CO_2 flux at night ($p<0.01$, student's t-test), but it is not clear yet whether soybean plants mediate soil N_2O flux through respiration or if soybean plants can produce N_2O during respiration. Since the N_2O flux from soybean plants was higher at night and lower during the day, opposite to the pattern of the N_2O flux from soil-soybean ecosystem, it is possible that soybean plants can produce N_2O. Further investigation is needed to determine the mechanism of N_2O production and emission from soybean plants.

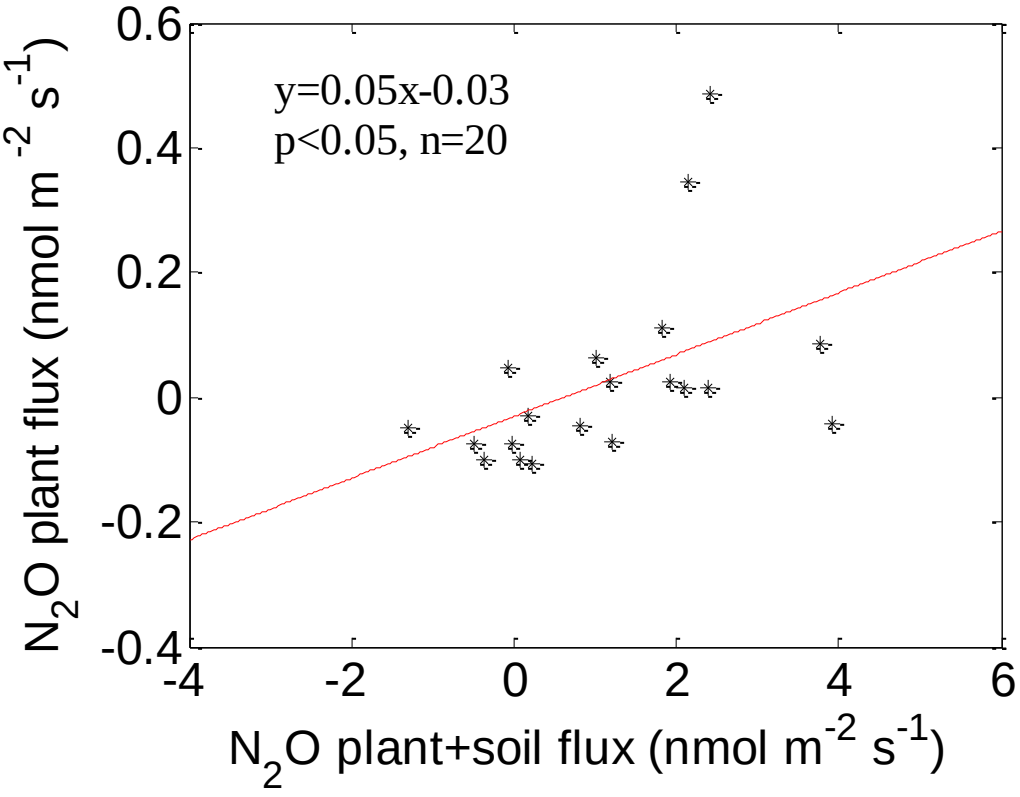

Figure 3.10. The linear correlation between N_2O flux from fertilized corn plant and the corn-soil ecosystem throughout the growing season.

3.4.3. Uncertainties in the flux-gradient measurement

The flux-gradient method assumes similarity in the eddy diffusivities for a trace gas and that of the momentum flux (i.e. *Sc*=1, where *Sc* is the turbulent Schmidt number), which may lead to an underestimate of the trace gas by about 40% (Flesch *et al.*, 2002). In order to evaluate this potential bias in the flux-gradient method, we compared the measured plant CO_2 flux and soil-plant CO_2 flux during the observation period (Figure 3.8b, 3.9b). CO_2 flux was chosen because it was measured during the same time by similar method and CO_2 fluxes from plants and the soil-plant ecosystem are better understood. The CO_2 plant flux was significantly correlated with soil-plant flux during the daytime (p <0.001, student's t-test), when the plant flux dominated the soil-plant flux. Throughout the growing season (DOY 149 –DOY 216), the mean CO_2 plant flux for the daytime and nighttime was -39 ± 3 μmol m^{-2} s^{-1} and 3 ± 1 μmol m^{-2} s^{-1}, respectively. The soil-plant CO_2 flux was -30 ± 2 μmol m^{-2} s^{-1} during the day, and 6 ± 2 μmol m^{-2} s^{-1} at night. The difference between soil-plant CO_2 fluxes and CO_2 fluxes for both daytime and nighttime were similar to CO_2 emission from the soil, suggesting that no significant bias was caused by assuming the turbulent Schmidt number as 1 in our study.

In addition, we compared the soil-plant N_2O flux measured by flux-gradient method with the soil N_2O flux measured by the chambers. The soil chamber flux was chosen for comparison because it provides a direct measurement for soil N_2O flux, which dominates the N_2O flux from the soil-plant ecosystem. To make the comparison, all the N_2O fluxes measured by the flux-gradient method in 2008 and 2009 are summarized in Figure 3.11. In addition, the results of soil chamber measurements for 2010 in the soybean and corn fields were added for comparison, unfortunately we do not have simultaneous

measurements using both approaches due to limited resources. The comparison shows 1) the soil-corn flux in May and June was about 5 times higher than the soil flux, but it is within the N_2O spatial variation range observed in Fassbinder *et al.* (2012); 2) the soil-corn flux in July and August and soil-soybean flux for the entire growing season was not significantly different from the soil flux. As a result, it is unlikely that the flux-gradient method underestimated the N_2O flux from soil-plant ecosystem.

Finally, it is inevitable to have data gaps in the measurements during periods when the approach breaks down due to inadequate turbulent mixing, or instrument problems. Therefore, a gap-filling strategy is needed in order todevelop a net annual N_2O budget. Five strategies have been proposed for for gap-filling the N_2O flux. These include: linear extrapolation, moving average, look-up table, multivariate model, and neural network analysis (Kroon *et al.*, 2010; Mishurov and Kiely, 2011; Ryan *et al.*, 2004). Monthly linear extrapolation generates reasonable annual N_2O flux similar to the more sophisticated methods, such as look-up table (Mishurov and Kiely, 2011), but it does not require the input of some environment parameters that were not measured frequently in our observation (Kroon *et al.*, 2010; Ryan *et al.*, 2004).In this study, in order to examine the seasonal pattern and estimate the annual N_2O flux, we first applied the monthly linear extrapolation to both soil-plant flux and soil flux (i.e. we used the average of all available data within each month as the monthly mean). According to Kroon *et al.* (2010) and Mishurov and Kiely (2011), the annual N_2O flux calculated from linear extrapolation was within ±10% of the flux calculated from the look-up table or multivariate model, so we assumed ±10% as the uncertainties range of the monthly flux of our observation. Then we filled the gap of the monthly mean soil-plant flux with available soil flux, and at the

end, assign the rest missing data in winter month as half of the October value with the variation from 0 to October value. Assuming a normal distribution of the flux estimates for each month, we used a Monte Carlo simulation to determine the uncertainties in the annual N_2O fluxes, and found that the annual N_2O fluxes from soybean and corn field were 1.08±0.11 and 2.53±0.18 kg N_2O-N ha^{-1} yr^{-1}

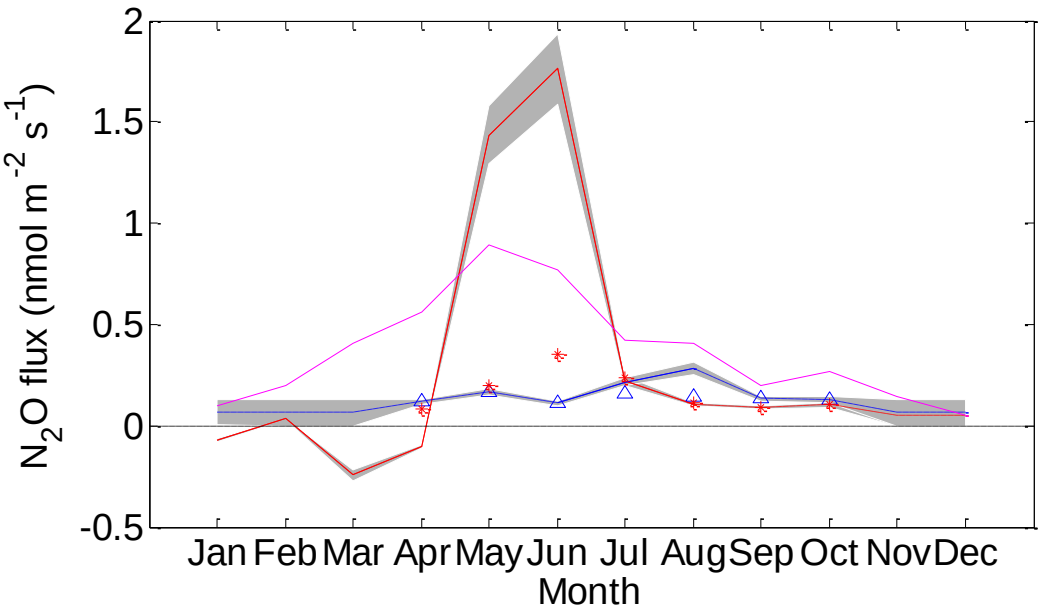

Figure 3.11. A summary of N_2O fluxes from corn and soybean soil and plant-soil ecosystems. Blue line– N_2O flux from the soil-soybean ecosystem; red line– N_2O flux from the soil-corn ecosystem; blue triangles– N_2O flux from a soil chamber in the soybean field; red stars– N_2O flux from a soil chamber in the corn field; magenta line– regional N_2O flux; black dashed line– zero flux; grey area–the uncertainty caused by gap-filling.

3.4.4. Cumulative cropland emission and emission factors

The cumulative N_2O flux from the soil-plant ecosystem in our study is comparable with that reported in previous studies. In soybean season (2008), cumulative N_2O emission from the soybean-soil ecosystem was 1.08±0.11 kg N_2O-N ha^{-1}, within the emission range reported by Gregorich *et al.* (2005) in Eastern Canada (1.73 ±1.32 kg N_2O-N ha^{-1}). With similar soil conditions (silt loam), Wagner-Riddle *et al.* (1997) reported that cumulative N_2O emission was 0.91 kg N_2O-N ha^{-1} in May and June, and 0.50 kg N_2O-N $ha^{-1}$from July to September in southern Ontario, Canada. The emission in May and June was two times higher than our observations. We hypothesize that this was related to their treatment of two years of manure application during fallow conditions prior to tillage and soybean planting in the spring. Their July to September emission was similar to our emission estimates.

During the corn season (2009), the accumulative annual N_2O emission was 2.53±0.18 kg N_2O-N ha^{-1}, and the emission factor was 1.24%, within1.3%–1.5%, which was the range of N_2O emitted per unit of N input as summarized in a review by Liebig *et al.* (2005). The N input in corn field in 2009 included synthetic fertilizer (112 kg N ha^{-1}), N input from crop residue (72 kg N ha^{-1}, estimated based on IPCC guideline), and N input from the loss of soil organic matters (20 kg N ha^{-1}, ranged from 0 to 40 kg N ha^{-1}, reported by Baker and Griffis (2005).The accumulated N_2O flux from our observations suggests the IPCC emission factor approach provides a good estimation of the direct N_2O emission from corn field, but underestimated the emission from the soybean field by a factor of 2 (Figure 3.12). The details of the IPCC calculation is provided in the supplementary materials (Section 3.7.2.). Biological Nitrogen Fixation (BNF) plants, such as soybean

and alfafa, fix Nitrogen at the rate of 84 and 152 kg N ha^{-1} yr^{-1}, comparable to the synthetic fertilizer application rate, usually about150 kg N ha^{-1} yr^{-1} for corn. If including the nitrogen fixed by soybean as part of the nitrogen addition in our IPCC estimation, the annual N_2O emission was 1.18 kg N_2O-N ha^{-1}, close to our measurement and literature report. Consequently, it is necessary to consider including the nitrogen fixed by BNF crops as part of the nitrogen input to the soil.

However, accounting only for N_2O emitted directly from the cropland is not a comprehensive approach for evaluating the impact of croplands on the regional and global N_2O budget. The indirect N_2O emissions need to be considered at these larger scales. Mainly two indirect emission pathways have been included in the IPCC guideline: nitrogen volatilization and leaching/runoff. According to the cropland management data in the soybean-corn rotation field, we calculated the indirect emissions from the two pathways and they were 0.06 and 0.27 kg N_2O-N ha^{-1} yr^{-1} respectively, or about 3% and 15% of the direct emission.

The total emission estimated from the IPCC method during the corn year was similar to the emission calculated by Davidson's method (2009), which is based on a global scale analysis (Figure 3.12). In contrast, considering only the N_2O emission from the newly fixed nitrogen throughout the nitrogen cycle, Crutzen *et al.* (2008) reported the emission factor as 3-5% globally (Figure 3.12). With this emission factor, we found that all the N_2O emission (including direct and indirect emission) caused by nitrogen addition in the corn and soybean field was 4.53 kg N_2O-N ha^{-1} yr^{-1}, about 2.5 time of the observed direct emission. The major difference between the IPCC approach and the Crutzen approach is that the former considers the N_2O emission from manure as part of the indirect emission

since the manure nitrogen originated from the crops. However, even after assuming that all the harvested crop nitrogen in our soybean-corn rotation field was transformed to manure nitrogen, the N_2O emission was still only about 1 kg N_2O-N ha^{-1} yr^{-1}, less than half of the difference between the indirect emissions estimated by IPCC approach and the Crutzen approach. This discrepancy suggess that the IPCC approach might largely underestimate the indirect emission from the cropland, by underestimating the emission factor for the activities currently included in the guideline and neglecting the elevated emission from natural sources due to the recycling of the "new" nitrogen in the ecosystem.

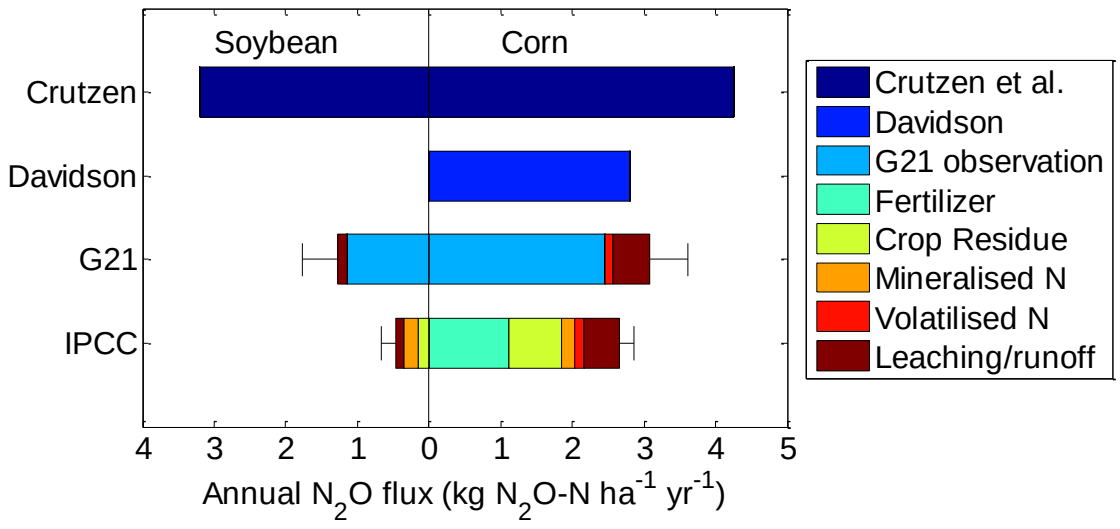

Figure 3.12. A summary of annual N_2O fluxes from corn and soybean field using different methods. From the top to the bottom, the bars shows the annual N_2O flux from soybean and corn field estimated with Crutzen et al.'s method (2008), Davidson's method (2009), flux gradient measurement at G21 site in 2008 and 2009, and IPCC guidelines (2006). The indirect emission in the G21 bar was borrowed from the result estimated based on IPCC guidelines. The error bar for G21 denotes the uncertainty from gap-filling. The error bar for IPCC reflects the uncertainty in estimating nitrogen input from different sources.

3.4.5. The role of croplands in the regional N_2O budget

The regional N_2O flux developed from the tall tower measurement and the equilibrium boundary layer method represents the emission from an area 10^5-10^6 km^2 around the tall tower, and the land cover composition within the tall tower footprint was analyzed based on USDA Crop Data Layer data in 2009 (Chapter 4). Therefore, cropland accounted for about 40% of the land cover in the tall tower's footprint, and the direct N_2O emission from cropland contributed about 30% to the regional flux (3.24±1.05 kg N_2O-N ha^{-1} yr^{-1}) within the vicinity of the tall tower.

However, comparing to other sources, the direct N_2O emission from cropland was about 2.6 times the N_2O emission from natural ecosystems (including water, forest, and grassland) and urban area (Figure 3.13), and 2.3 times the emission from manure production. In this comparison, we used the emission intensity reported in the literature, and the land cover information within the tall tower footprint. The N_2O emission from manure was estimated from the averaged manure production in corn belt (Griffis *et al.*, in review),

Based on the composition of the land cover and reported emission rate for each land cover type, I can assemble the regional flux as 1.72 ± 0.26 kg N_2O-N ha^{-1} yr^{-1}, only 53% of the observed regional flux. The uncertainty range was determined by a Monte Carlo simulation by assuming the N_2O flux density from each source follows the normal distribution. If the Crutzen emission factor is applied, the indirect emission from cropland will be largely increased and the regional flux will reach 2.08± 0.42 kg N_2O-N ha^{-1} yr^{-1}, in the range of the observed regional at the tall tower. Therefore, it is very likely that the

large discrepancy between the assembled and the observed regional flux was from the underestimation of indirect cropland emission in the assembled flux.

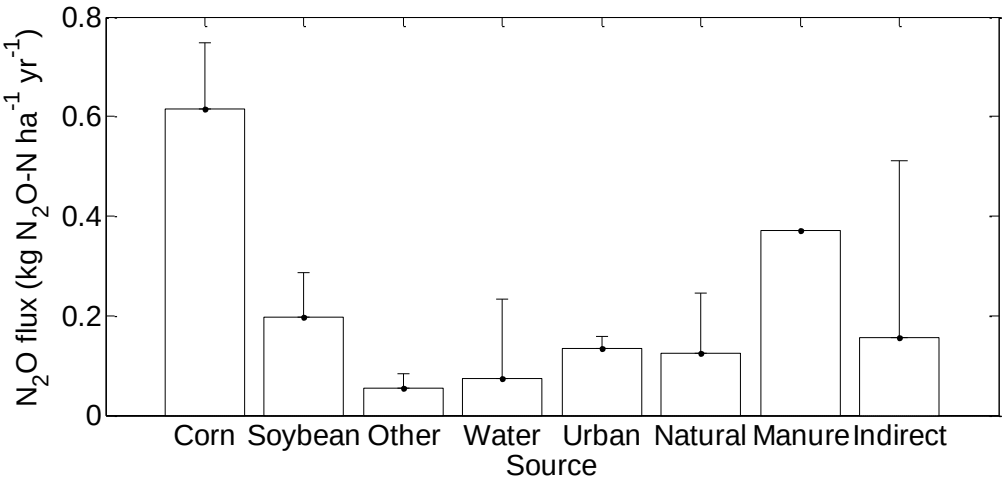

Figure 3.13. N_2O fluxes from different sources (weighted by land cover types) within the tall tower footprint. The error bar on the indirect emission from cropland denotes the range of indirect emissions estimated from IPCC guidelines and Crutzen *et al.* (2008). "Other" means the direct N_2O flux from all crop types, except corn and soybean. The "Natural" source mainly includes forest and grassland.

3.4.6. The uncertainties in landscape-scale flux estimation

In addition to equilibrium boundary layer method, we applied two other boundary layer methods, modified Bowen ratio (MBR) method and modified nocturnal boundary layer (MNBL) method, to determine the regional flux. These methods were used to provide an independent check on the regional N_2O flux estimated from the equilibrium method. All three methods indicate that the landscape around the tower was a strong source of N_2O.

During the nighttime, N_2O fluxes calculated with the MBR method were 1.09 ± 0.56 nmol m^{-2} s^{-1}, in agreement with the nighttime emission pattern suggested by concentration and gradients at the tall tower. The N_2O gradient between 3 m and 200 m was mostly positive at night and close to zero during the day. During the observation period, 23 out of 25 midnight N_2O gradients (22:00-4:00) were negative; similarly, all 25 midnight CO_2 gradients were negative (10:00-16:00). Only 25 midnight data sets were available because the data at the night of DOY 255 were missing. The midnight N_2O gradients and CO_2 gradients were well correlated: $G_{NO2}= 2.8\times10^{-4} G_{CO2}+4.4\times10^{-5}$ (linear correlation r= 0.65; number of observations n=25) (Figure 3.14a). During the daytime, due to the well mixed boundary layer, the difference in midday N_2O concentration between 3 m and 200 m was very small (-0.1 ± 0.6 ppb), and the correlation with CO_2 gradient was very weak (r=0.23; n=25). Since about 64% of the midday N_2O gradients were positive and 36% were negative, it is difficult to determine whether the landscape uptake or emit N_2O during the daytime.

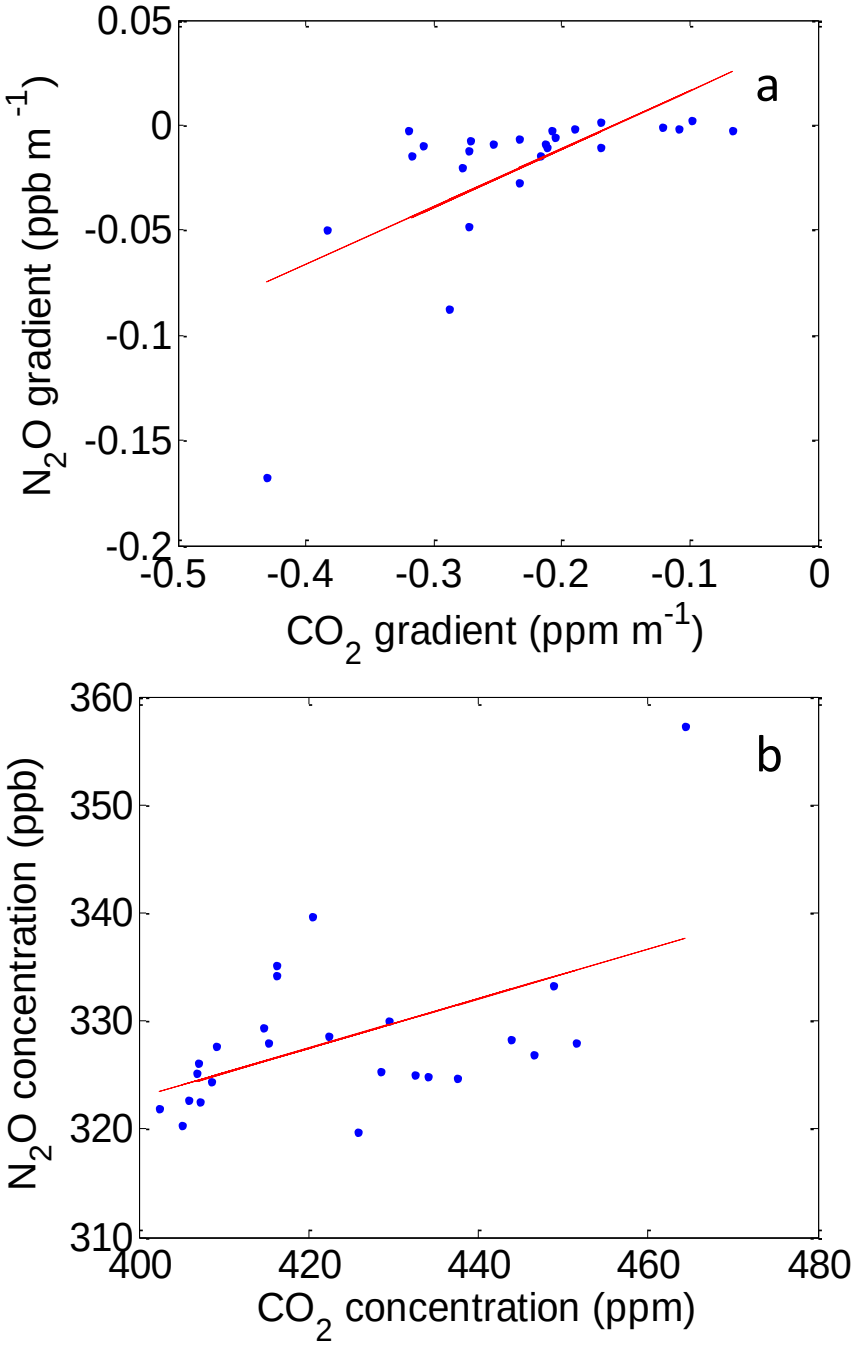

Figure 3.14. Linear relationship between the N_2O and CO_2 gradients (a) and concentration (b), DOY 243 – 269, 2009. The results of the linear regression are shown as red lines. Each data point represents a block average between 22:00-04:00 LST.

The use of the MBR method has received considerably scrutiny. The method is built on the assumption of similarity -- that scalars are transported indiscriminately. In other words, the *K* value in Equation 3.1 is the same for any trace gas. Even though this assumption does not usually hold at night, several lines of evidence were found during the observation period to support the flux estimates: 1) The diffusivities for CO_2 and H_2O, calculated from their concentration gradients measured from the tall tower and the fluxes measured in the soybean and corn fields, were linearly correlated ($p<0.001$, student's t-test). The slope of the regression close to unity suggests that the assumption that scalars are transported indiscriminately was a good approximation; 2) The midnight block average of the N_2O concentration was positively and linearly correlated with the midnight block average of the CO_2 concentration (Figure 3.14b). This correlation suggests that N_2O and CO_2 accumulated similarly near the ground.

The modified nocturnal boundary layer method determines the nighttime N_2O flux from the concentration build-up near the land surface using CO_2 as a tracer (Kelliher *et al.*, 2002). This independent method also gave a similar regional N_2O flux at night—providing further support for the other two methods. During the tall tower observation period, the midnight concentrations of N_2O and CO_2 at 3 m were correlated ($p<0.005$, student's t-test) (Figure 3.14b), and the N_2O flux was estimated at 0.90 ± 0.65nmol m^{-2} s^{-1}.

3.5. Conclusions

Unfertilized soybean plants emitted N_2O at the rate of 0.03 nmol m^{-2} s^{-1}, about 10% of the N_2O emission from soil-soybean ecosystem, while corn plants were a negligible sink of N_2O during the growing season. Both soybean and corn may mediate part of N_2O

emission from soil, but soybean plant may produce N_2O while corn plant may consume N_2O. The impact of fertilization on corn plant flux throughout the growing season was not significant, but the late-season fertilization increased soybean plant flux by nearly two orders of magnitude.

The annual N_2O emissions from soil-soybean and soil-corn ecosystems were 1.08±0.11 and 2.53±0.18 kg N_2O-N ha^{-1}, comparable to reported literature values. IPCC provided good estimation for direct emission from soil-corn ecosystem, but underestimated direct emission from soil-soybean ecosystem by a factor of 2 due to neglecting the nitrogen input through BNF. In addition, IPCC largely underestimated the indirect N_2O emission caused by nitrogen enhancement in cropland, which led to underestimating regional N_2O flux by about 50%. As a result, the BNF should be included as part of nitrogen input to the ecosystem in the IPCC guideline, and the emission factor for indirect N_2O emission from cropland should be further investigated.

3.6. References

Baker, J.M. and Griffis, T.J., 2005. Examining strategies to improve the carbon balance of corn/soybean agriculture using eddy covariance and mass balance techniques. Agricultural and Forest Meteorology, 128(3-4): 163-177.

Bavin, T.K., Griffis, T.J., Baker, J.M. and Venterea, R.T., 2009. Impact of reduced tillage and cover cropping on the greenhouse gas budget of a maize/soybean rotation ecosystem. Agriculture Ecosystems & Environment, 134(3-4): 234-242.

Beard, B.H. and Hoover, R.M., 1971. Effects of nitrogen on nodulation and yield of irrigated soybeans. Agronomy Journal, 63(5): 815-816.

Betts, A.K., Helliker, B. and Berry, J., 2004. Coupling between CO_2, water vapor, temperature, and radon and their fluxes in an idealized equilibrium boundary layer over land. Journal of Geophysical Research-Atmospheres, 109(D18).

Bharati, M.P., Whigham, D.K. and Voss, R.D., 1986. Soybean response to tillage and nitrogen, phosphorus, and potassium fertilization. Agronomy Journal, 78(6): 947-950.

Chang, C., Janzen, H.H., Cho, C.M. and Nakonechny, E.M., 1998. Nitrous oxide emission through plants. Soil Science Society of America Journal, 62(1): 35-38.

Chen, X., Boeckx, P., Shen, S. and Van Cleemput, O., 1999. Emission of N_2O from rye grass (*Lolium perenne* L.). Biology and Fertility of Soils, 28(4): 393-396.

Crutzen, P.J., Mosier, A.R., Smith, K.A. and Winiwarter, W., 2008. N_2O release from agro-biofuel production negates global warming reduction by replacing fossil fuels. Atmospheric Chemistry and Physics, 8(2): 389-395.

Davidson, E.A., 2009. The contribution of manure and fertilizer nitrogen to atmospheric nitrous oxide since 1860. Nature Geoscience, 2(9): 659-662.

De Klein, C.A.M., Smith, L.C. and Monaghan, R.M., 2006. Restricted autumn grazing to reduce nitrous oxide emissions from dairy pastures in Southland, New Zealand. Agriculture Ecosystems & Environment, 112(2-3): 192-199.

Denmead, O.T., 2008. Approaches to measuring fluxes of methane and nitrous oxide between landscapes and the atmosphere. Plant and Soil, 309(1-2): 5-24.

Desjardins, R.L., Pattey, E., Smith, W.N., Worth, D., Grant, B., Srinivasan, R., MacPherson, J.I. and Mauder, M., 2010. Multiscale estimates of N_2O emissions from agricultural lands. Agricultural and Forest Meteorology, 150(6): 817-824.Fassbinder, J.J., Schultz, N.M., Baker, J.M. and Griffis T.J., 2012. Automatic, low-power chamber system for measuring N_2O emissions. Journal of Environmental Quality, accepted with revisions.

Fassbinder, J.J., Schultz, N.M., Baker, J.M. and Griffis T.J., 2012. Automatic, low-power chamber system for measuring N_2O emissions. Journal of Environmental Quality, accepted with revisions.

Flesch, T.K., Prueger, J.H. and Hatfield, J.L., 2002. Turbulent Schmidt number from a tracer experiment. Agricultural and Forest Meteorology, 111(4): 299-307.

Forster, P. et al., 2007. Changes in atmospheric constituents and in radiative forcing. In: Climate Change 2007: The physical science basis. Contribution of Working Group I to the Fourth Assessment Report of the Intergovernmental Panel on Climate Change (Solomon, D. Qin, M. Manning, Z. Chen, M. Marquis, K. Averyt, M. Tignor and H. Miller, Editors). Cambridge, UK: Cambridge University Press.

Freeborn, J.R., Holshouser, D.L., Alley, M.M., Powell, N.L. and Orcutt, D.M., 2001. Soybean yield response to reproductive stage soil-applied nitrogen and foliar-applied boron. Agronomy Journal, 93(6): 1200-1209.

Grant, R.F. and Pattey, E., 2003. Modelling variability in N_2O emissions from fertilized agricultural fields. Soil Biology & Biochemistry, 35(2): 225-243.

Gregorich, E.G., Rochette, P., VandenBygaart, A.J. and Angers, D.A., 2005. Greenhouse gas contributions of agricultural soils and potential mitigation practices in Eastern Canada. Soil & Tillage Research, 83(1): 53-72.

Griffis, T.J., Lee, X., Baker, J.M., Sargent, S.D. and King, J.Y., 2005. Feasibility of quantifying ecosystem-atmosphere $C^{18}O^{16}O$ exchange using laser spectroscopy and the flux-gradient method. Agricultural and Forest Meteorology, 135(1-4): 44-60.

Griffis, T.J., Lee, X., Baker, J.M., Russelle, M., Zhang, X., Venterea, R. and Millet D., 2012. Large nitrous oxide emission factors for the United States Corn Belt revealed by atmospheric concentration measurements. Submitted to Nature October 1, 2012, currently in review.

Grundmann, G.L., Lensi, R. and Chalamet, A., 1993. Delayed NH_3 and N_2O uptake by maize leaves. New Phytologist, 124(2): 259-263.

Gutierrez-Boem, F.H., Scheiner, J.D., Rimski-Korsakov, H. and Lavado, R.S., 2004. Late season nitrogen fertilization of soybeans: effects on leaf senescence, yield and environment. Nutrient Cycling in Agroecosystems, 68(2): 109-115.

Helliker, B.R., Berry, J.A., Betts, A.K., Bakwin, P.S., Davis, K.J., Denning, A.S., Ehleringer, J.R., Miller, J.B., Butler, M.P. and Ricciuto, D.M., 2004. Estimates of net CO_2 flux by application of equilibrium boundary layer concepts to CO_2 and water vapor measurements from a tall tower. Journal of Geophysical Research-Atmospheres, 109(D20).

IPCC,1997. Guidelines for national greenhouse gas inventories. Intergovernmental Panel on Climate Change/Organization for Economic Cooperation and Development, OECD, Paris.

IPCC, 2006. IPCC Guidelines for National Greenhouse Gas Inventories, 5 volumes, Institute for Global Environmental Strategies, Hayama, Kanagawa, Japan.

Kaimal, J.C. and Finnigan, J.J., 1994. Atmospheric Boundary Layer Flows. Their Structure and Measurement. Oxford University Press, 288 pp.

Kelliher, F.M., Reisinger, A.R., Martin, R.J., Harvey, M.J., Price, S.J. and Sherlock, R.R., 2002. Measuring nitrous oxide emission rate from grazed pasture using Fourier-transform infrared spectroscopy in the nocturnal boundary layer. Agricultural and Forest Meteorology, 111(1): 29-38.

Kort, E.A., Eluszkiewicz, J., Stephens, B.B., Miller, J.B., Gerbig, C., Nehrkorn, T., Daube, B.C., Kaplan, J.O., Houweling, S. and Wofsy, S.C., 2008. Emissions of CH_4 and N_2O over the United States and Canada based on a receptor-oriented modeling framework and COBRA-NA atmospheric observations. Geophysical Research Letters, 35(18).

Kroon, P.S., Hensen, A., Jonker, H.J.J., Ouwersloot, H.G., Vermeulen, A.T. and Bosveld, F.C., 2010. Uncertainties in eddy covariance flux measurements assessed from CH_4 and N_2O observations. Agricultural and Forest Meteorology, 150(6): 806-816.

Lensi, R. and Chalamet, A., 1981. Absorption of nitrous oxide by shoots of maize. Plant and Soil, 59(1): 91-98.

Liebig, M.A. et al., 2005. Greenhouse gas contributions and mitigation potential of agricultural practices in northwestern USA and western Canada. Soil & Tillage Research, 83(1): 25-52.

Marinho, E.V.A., DeLaune, R.D. and Lindau, C.W., 2004. Nitrous oxide flux from soybeans grown on Mississippi alluvial soil. Communications in Soil Science and Plant Analysis, 35(1-2): 1-8.

Mendes, I.C., Hungria, M. and Vargas, M.A.T., 2003. Soybean response to starter nitrogen and *Bradyrhizobium* inoculation on a Cerrado oxisol under no-tillage and conventional tillage systems. Revista Brasileira De Ciencia Do Solo, 27(1): 81-87.

Miller, S.M., Kort, E.A., Hirsch, A.I., Dlugokencky, E.J., Andrews, A.E., Xu, X., Tian, H., Nehrkorn, T., Eluszkiewicz, J., Michalak, A.M. and Wofsy, S.C., 2012. Regional sources of nitrous oxide over the United States: Seasonal variation and spatial distribution. Journal of Geophysical Research-Atmospheres, 117.

Mishurov, M. and Kiely, G., 2011. Gap-filling techniques for the annual sums of nitrous oxide fluxes. Agricultural and Forest Meteorology, 151(12): 1763-1767.

Misselbrook, T.H., Cape, J.N., Cardenas, L.M., Chadwick, D.R., Dragosits, U., Hobbs, P.J., Nemitz, E., Reis, S., Skiba, U. and Sutton, M.A., 2011. Key unknowns in estimating atmospheric emissions from UK land management. Atmospheric Environment, 45(5): 1067-1074.

Molodovskaya, M., Warland, J., Richards, B.K., Oeberg, G. and Steenhuis, T.S., 2011. Nitrous Oxide from Heterogeneous Agricultural Landscapes: Source Contribution Analysis by Eddy Covariance and Chambers. Soil Science Society of America Journal, 75(5): 1829-1838.

Mosier, A. et al., 1998. Closing the global N_2O budget: nitrous oxide emissions through the agricultural nitrogen cycle: OECD/IPCC/IEA phase II development of IPCC guidelines for national greenhouse gas inventory methodology. Nutrient Cycling in Agroecosystems, 52(2-3): 225-248.

Muller, C., 2003. Plants affect the in situ N_2O emissions of a temperate grassland ecosystem. Journal of Plant Nutrition and Soil Science-Zeitschrift Fur Pflanzenernahrung Und Bodenkunde, 166(6): 771-773.

Phillips, F.A., Leuning, R., Baigenta, R., Kelly, K.B. and Denmead, O.T., 2007. Nitrous oxide flux measurements from an intensively managed irrigated pasture using micrometeorological techniques. Agricultural and Forest Meteorology, 143(1-2): 92-105.

Pihlatie, M., Ambus, P., Rinne, J., Pilegaard, K. and Vesala, T., 2005. Plant-mediated nitrous oxide emissions from beech (*Fagus sylvatica*) leaves. New Phytologist, 168(1): 93-98.

Ravishankara, A.R., Daniel, J.S. and Portmann, R.W., 2009. Nitrous Oxide (N_2O): The dominant ozone-depleting substance emitted in the 21st century. Science, 326(5949): 123-125.

Ryan, M., Muller, C., Di, H.J. and Cameron, K.C., 2004. The use of artificial neural networks (ANNs) to simulate N2O emissions from a temperate grassland ecosystem. Ecological Modelling, 175(2): 189-194.

Salvagiotti, F., Cassman, K.G., Specht, J.E., Walters, D.T., Weiss, A. and Dobermann, A., 2008. Nitrogen uptake, fixation and response to fertilizer N in soybeans: A review. Field Crops Research, 108(1): 1-13.

Smart, D.R. and Bloom, A.J., 2001. Wheat leaves emit nitrous oxide during nitrate assimilation. Proceedings of the National Academy of Sciences of the United States of America, 98(14): 7875-7878.

Wagner-Riddle,C.,Thurtell,G.W.,Kidd,G.K.,Beauchamp,E.G.,Sweetman,R.,1997. Estimates of nitrous oxide emission from agricultural fields over 28 months. Canadian Journal of Soil Science 77, 135–144

Wesley, T.L., Lamond, R.E., Martin, V.L. and Duncan, S.R., 1998. Effects of late-season nitrogen fertilizer on irrigated soybean yield and composition. Journal of Production Agriculture, 11(3): 331-336.

Zheng, X.H., Mei, B.L., Wang, Y.H., Xie, B.H., Wang, Y.S., Dong, H.B., Xu, H., Chen, G.X., Cai, Z.C., Yue, J., Gu, J.X., Su, F., Zou, J.W. and Zhu, J.G., 2008. Quantification of N_2O fluxes from soil-plant systems may be biased by the applied gas chromatograph methodology. Plant and Soil, 311(1-2): 211-234.

Zou, J.W., Huang, Y., Sun, W.J., Zheng, X.H. and Wang, Y.S., 2005. Contribution of plants to N_2O emissions in soil-winter wheat ecosystem: pot and field experiments. Plant and Soil, 269(1-2): 205-211.

3.7. Supplementary materials

3.7.1. A summary of measurement information

Table 3.4. A summary of the observation periods for the three scales measured.

	Start date	End date
Plant flux soybean 2008 (Chamber)	160	225
Soil-plant flux 2008 (flux tower)	172	242
Plant flux corn 2009 (Chamber)	147	218
Soil-plant flux 2009 (flux tower)	14	220
Regional flux 2009 (tall tower)	243	269

Table 3.5. A summary of concentration differences between the inlet and outlet during blank tests.

	Blank test	Site number	Mean (ppb)	Standard deviation (ppb)
Soybean season	0610 small chamber	2	-0.04	0.40
(2008)	0614 medium chamber	2	-0.08	0.64
	0702 medium chamber	2	-0.01	0.60
Corn season	0630 medium chamber	2	-0.06	0.82
(2009)	0701 medium chamber	4	-0.21	1.30
	0703 large chamber	4	-0.05	1.20
	0730 large chamber	4	-0.44	1.10
	0806 large chamber	4	-0.19	1.30

Note: The mean value shown in the table was the 24-hour average of the difference between the outlet –and inlet concentrations.

Table 3.6. A summary of inlet height on the 10 m tower for the 2009 corn season.

Date	z1 (m)	z2 (m)
0 -189	1.0	2.0
190	1.5	2.2
191-197	1.9	2.85
198-320	2.25	3.25
321-365	1.0	2.0

Table 3.7. LAI and dry weight of fertilized and unfertilized plants over the growing season.

DOY	LAI (m^2 m^{-2}) Fertilized	LAI (m^2 m^{-2}) Unfertilized	Dry weight (gdw $plant^{-1}$) Fertilized	Dry Weight (gdw $plant^{-1}$) Unfertilized
		Soybean 2008		
174	N/A	0.2	N/A	0.4
181	N/A	0.4	N/A	0.7
190	N/A	0.7	N/A	1.2
196	N/A	1.2	N/A	3.0
203	N/A	2.4	N/A	5.7
210	N/A	2.8	N/A	7.3
217	N/A	3.1	N/A	11.1
224	N/A	3.3	N/A	12.2
231	N/A	2.5	N/A	14.5
238	N/A	2.0	N/A	12.6
242	1.7	1.8	22.6	16.5
		Corn 2009		
149	0.1	0.1	0.26	0.32
158	0.4	0.4	1.9	2.8
166	0.6	0.5	5.0	5.2
173	1.8	1.3	17	13
180	3.1	1.9	54	37
187	4.0	3.5	126	105
193	5.6	2.9	168	97
201	5.1	3.5	202	171
208	5.1	3.2	231	181
216	5.0	3.0	181	110

3.7.2. Calculation of N_2O emission based on IPCC guidelines

According to IPCC guideline (2006), the direct N_2O emission from the soybean-corn rotation field was calculated with

$$N_2O_{Direct} - N = (F_{SN} + F_{CR} + F_{SOM}) \cdot EF_1$$

In this equation, F_{SN} is the amount of synthetic nitrogen fertilizer applied in the field; F_{CR} is the nitrogen input from the crop residue, it was calculated with the equation in the guideline, and no residue was removed from the field; F_{SOM} is the nitrogen input through the mineralization of the soil nitrogen, it was calculated by the loss of organic carbon in soil; EF_1 is the emission factor for the nitrogen input in cropland, and the default value is 0.01 (0.003-0.03) kg N_2O-N (kg N)$^{-1}$. Here, the numbers in parenthesis was the range of possible value.

The indirect emission includes volatilization and leaching/runoff, calculated by the following equation.

$$N_2O_{Indirect} - N = (F_{SN} \cdot Frac_{GASF}) \cdot EF_4 + (F_{SN} + F_{CR} + F_{SOM}) \cdot Frac_{LEACH} \cdot EF_5$$

EF_4 and EF_5 are the emission factors for volatilization and leaching/runoff respectively, and their default values are 0.01 (0.002-0.05) kg N_2O-N (kg N)$^{-1}$ and 0.0075 (0.0005-0.025) kg N_2O-N (kg N)$^{-1}$ respectively. The fraction of volatilized nitrogen from synthetic fertilizer ($Frac_{GASF}$) is 0.1 (0.03-0.3), while the fraction of lost nitrogen through leaching/runoff ($Frac_{LEACH}$) is 0.3(0.1-0.8). In our calculation, we used default values.

Chapter 4: Estimating greenhouse gas fluxes from an agriculture-dominated landscape using multiple planetary boundary layer methods

Abstract

Quantification of regional greenhouse gas (GHG) fluxes is essential for establishing mitigation strategies and evaluating their effectiveness. To date, regional (10^2-10^6 km^2) GHG investigations remain relatively rare, especially for nitrous oxide (N_2O) and methane (CH_4). The uncertainties in these emissions estimates remain large. Sectorial and spatial aggregation is used to calculate GHG fluxes on a regional level; however, few studies have been carried out to assess these estimates. To address this knowledge gap, this study, , used multiple top-down approaches based on trace gas observations from a very tall tower to estimate GHG regional fluxes and to evaluate the GHG fluxes derived from bottom-up approaches. We first applied and evaluated the eddy covariance, equilibrium, inverse modeling (Carbon Tracker), and flux aggregation methods based on three-years of carbon dioxide (CO_2) measurements at the tall tower. We then applied the equilibrium method for estimating CH_4 and N_2O fluxes with one-month high-frequency CH_4 and N_2O gradient measurements, and evaluated the uncertainties in this methodology. Finally, we evaluated the current GHG inventory and the importance of CH_4 and N_2O fluxes compared to the CO_2 flux from an agriculture-dominated landscape. The results indicate that: 1) flux aggregation method, eddy covariance method, equilibrium method, and Carbon Tracker all produced the same seasonal pattern of the regional CO_2 flux (10^4-10^6 km^2), but the equilibrium method significantly underestimated the growing season CO_2 flux by about 60%. 2) Bottom-up inventories (Emission Database for Global Atmospheric Research) significantly underestimated the regional CH_4 and N_2O emissions by factors of six and two. 3) CH_4 and N_2O emissions offset more than 60% of the annual CO_2 uptake. Hence, CH_4 and N_2O are critical for regional GHG

budgeting in this agriculture-dominated landscape, and multiple top-down approaches provide robust information for evaluating and constraining the current GHG inventory.

4.1. Introduction

Greenhouse gas (GHG) mitigation strategies and evaluation require information about GHG fluxes on the regional scale (10^2-10^6 km^2) (Chen *et al.*, 2008; Nisbet and Weiss, 2010). To fill this scale gap, some researchers build ecosystem models and aggregate the modeled flux based on land information (e.g., Desai *et al.*, 2008; Tang *et al.*, 2012; Xiao *et al.*, 2008), while others use GHG concentration observations in combination with atmospheric transport models to derive land surface flux (Lauvaux *et al.*, 2012; Peters *et al.*, 2007). The aggregation method is a bottom-up approach. Another bottom-up method is the IPCC national GHG inventory system (IPCC, 2006) based on emission factors and statistical data concerning anthropogenic activities. The bottom-up applications are relatively easy to implement; however, they need independent verification, because uncertainties in land cover, anthropogenic activity, vegetation flux, and emission factors can lead to large biases (Chen *et al.*, 2008; Levy *et al.*, 1999). Hence, there is a strong motivation for using top-down methods to constrain the regional fluxes.

There are several top-down methods for estimating regional GHG fluxes, including tall-tower eddy covariance (Davis *et al.*, 2003), the equilibrium boundary layer approach (Bakwin *et al.*, 2004; Betts *et al*., 2004; Desai *et al.*, 2010; Helliker *et al.*, 2004), and inverse modeling (Peters *et al.*, 2007). Each method uses different assumptions, has inherent advantages and disadvantages, and is sensitive to different parameters (Table 4.1). Eddy covariance (EC) provides a direct measurement of the flux using measurement of the wind fluctuations and the scalar of interest. EC is used occasionally for CO_2 flux measurement on tall towers (Davis *et al*., 2003*;* Haszpra *et al.*, 2005*).* There have been few tall-tower flux observations of CH_4 and N_2O due to instrument limitations (Desai *et*

al., 2012), and the uncertainty for these measurement is relatively large (20–300% for CH_4, 30–1800% for N_2O) (Kroon *et al.*, 2010). Based on the mass balance in the boundary layer, the equilibrium method assumes that the exchange at the top of the boundary layer and the exchange at the land surface are equilibrium over periods longer than a month (Helliker *et al.*, 2004). The largest source of uncertainty of this method lies in determining the background concentration above the boundary layer and the subsidence rate at the top of the boundary layer. Inverse modeling determines the land surface flux using atmospheric transport models that are constrained by observed trace gas concentrations. The prior land surface flux, abundance and accuracy of land surface observations, the meteorological inputs, and atmospheric transportation schemes are all important for determining the accuracy of the modeled flux (Peters *et al.*, 2007).

In this study, we used several top-down approaches to evaluate the bottom-up fluxes of CO_2, CH_4, and N_2O for a region dominated by agriculture. The inter-comparison of multiple techniques was used to identify systematic biases of each method and to constrain the overall uncertainties. We first used CO_2 to evaluate the equilibrium boundary layer method against tall-tower eddy covariance, flux aggregation, and the flux produced by an inverse model. We then applied this method to estimate the CH_4 and N_2O fluxes. The final task was to compare the CH_4 and N_2O fluxes with EDGAR42 (European Commission, Joint Research Centre [JRC]/Netherlands Environmental Assessment Agency [PBL], Emission Database for Global Atmospheric Research [EDGAR], release version 4.2, http://edgar.jrc.ec.europa.eu, 2011), an inventory dataset used widely in atmospheric models (Jeong *et al.*, 2012).

Table 4.1. A summary of top-down methods applied in quantifying regional CO_2 fluxes in this study

Method	**Applied gas species**	**Frequency**	**Function**	**Critical parameters for estimation**	**Footprint/resolution**
Eddy Covariance (closed-path)	CO_2	Hourly	$F_{EC} = \overline{w'c'} + F_{Storage}$	wind and trace gas concentration fluctuation (High frequency-high accuracy)	100h in neutral and unstable conditions; 200h and 350h in stable condition; here, h is the measurement height (Denmead, 2008; Leclerc and Thurtell, 1990; Schuepp *et al*., 1990) 10^5 km^2 (Gloor *et al*., 2001)
Equilibrium boundary layer method	CO_2, CH_4, N_2O	Monthly	$F_{Eq} = \rho W(c_+ - c_m)$	Absolute value of trace gas concentration, background concentration	10^6 km^2 (Bakwin *et al*., 2004)
Inversion (Carbon Tracker)	CO_2	Daily 2000-2010		Atmospheric transport scheme, prior inventory	Resolution: 1° by 1°

4.2. Data and Methods

4.2.1. Research site

The boundary layer observations were made on a 244 m communication tower (KCMP) located at the Rosemount Research and Outreach Center, University of Minnesota, about 25 km south of Minneapolis/Saint Paul (44°41'19"N, 93°4'22"W). According to the USDA Crop Data Layer (CDL) data in 2009, the landscape around the KCMP tall tower was dominated by cropland, which accounted for about 40% of the land cover within 10 km radius of the tower and 37% within the 600 km radius. Corn and soybean were the dominant crop species, accounting for 55% and 38% of the cropland, respectively. About 40% of the land (within 600 km radius around the tall tower) was covered by forest and grassland and pasture. The rest was composed of developed land, wetland, and open water. The land cover pattern described here for 2009 had a smaller corn to soybean ratio as that reported by Griffis *et al*. (2010) for 2007. The small difference was attributed to greater corn production in 2007, stimulated by ethanol biofuel demand.

4.2.2. Mixing ratio data

CO_2 mixing ratios at the 32 m, 56 m, 100 m, and 200 m height above the ground were measured by a tunable diode laser analyzer (TDL) (model TGA 100A, Campbell Scientific Inc., Logan, UT, USA) (Griffis *et al*., 2010). The air on the four levels was drawn down by a large vacuum pump (model DOA-V502A-FB, Gast Group Inc., Benton Harbor, MI, USA) through four Synflex tubes (6.25 mm ID) at a line pressure of 60 kPa and at a flow rate of 16 L min^{-1}. The air from different heights was sampled sequentially, each for 30 s. The sample air was dried prior to analysis using a Nafion drier and brought to a common temperature. The CO_2 mixing ratio profile measurement was calibrated

against National Oceanic and Atmospheric Administration-Earth System Research Laboratory (NOAA-ESRL) standards. The hourly precision of the CO_2 measurement was approximately 0.03 ppm.

In addition, an intensive campaign was carried out from August 30 to September 25 (DOY 243 - 269), 2009. During this campaign, we measured CO_2, H_2O, CH_4, and N_2O mixing ratios at the 200 m and 3 m height on the KCMP tower. Air was drawn from the 200 m and 3 m height at a flow rate of 1.3 L min^{-1} and 0.9 L min^{-1}, respectively, through two Synflex tubes (9.55 and 4.32 mm ID). A portion (0.6 L min^{-1}) of this flow was delivered to an infrared gas analyzer (IRGA; LI-6262, LI-COR, Lincoln, NE, USA) for CO_2 and H_2O mixing ratio measurements, and a small amount (180 mL min^{-1}) was delivered to another TDL for CH_4 and N_2O measurements. Measurement precisions for CO_2, CH_4, and N_2O were 0.2 ppm, 1.2 ppb, and 0.5 ppb, respectively. The IRGA was manually calibrated with a standard CO_2 gas (391.03 ± 0.03 ppm) and a dew point generator (LI-610, LI-COR) at the beginning of the experiment. The accuracy of its measurement was improved in post-field analysis by adding offsets so that its 200-m reading matched that registered by the TDL CO_2 analyzer for the same height. The TDL was plumbed to a four-port manifold that used a switching sequence in the order of 200 m, 3 m, calibration zero and calibration span, with 30 s spent on each port and the first 15 s after each switching omitted from the analysis. The N_2O concentration of calibration span was calibrated with NOAA-ESRL gold standard (Cylinder #CA07980). The CH_4 concentration of the calibration span was calibrated against a known standard provided by a local supplier (Scott-Marrin, Inc.), and was traceable to the NOAA-ESRL standard scale.

4.2.3. Eddy covariance data

A closed-path EC system installed at the height of 100 m on the KCMP tower was used to measure the CO_2 flux from 2007 to 2009 (Griffis *et al*., 2010). This system consisted of a 3-D sonic anemometer-thermometer (model CSAT3, Campbell Scientific) and the TDL analyzer (model TGA 100A, Campbell Scientific) for CO_2 concentration. The sample tube was 125 m long (6.25 mm ID, Synflex), which resulted in a typical lag time of 11 s, with Reynolds numbers exceeding 3500. Fluctuations in w and c were recorded at 10 Hz, and a block averaging time of 60-min was used in order to capture the dominant flux-containing frequencies.

In addition, in 2009 two closed-path eddy covariance systems were used at two 10 m towers in the middle of corn (G21) and soybean fields (G19) (Baker and Griffis, 2005) about 3 km away from the KCMP tower. They provided half-hourly fluxes of CO_2 and H_2O of these fields.

4.2.4. Top-down flux estimation methods

4.2.4.1. Tall tower eddy covariance

Briefly, the tall tower CO_2 flux was estimated as the sum of eddy covariance term measured at the 100 m ($\overline{w'c'}$) and the storage term between land surface and 100 m ($F_{Storage}$).

$$\mathrm{F_{EC}} = \overline{\mathrm{w'c'}} + \mathrm{F_{Storage}} \quad (1)$$

Here, we assume that horizontal and vertical advection were negligible (Davis *et al*., 2003; Griffis *et al*., 2010). Wind velocities and fluxes were transformed into the planar fit

coordinate system (Lee *et al*., 2004). Eddy fluxes were computed using the maximum covariance method with strict limits on window size based on manifold pressure and flow rates. Flux losses attributed to a combination of sensor separation, sonic path averaging, tube attenuation, and block averaging were estimated using the analytical model of Massman (2000). These losses typically ranged between 5% and 20%. A detailed description of the eddy covariance system and flux calculations can be found in Griffis *et al*. (2010).

It is well established that the eddy flux measurement does not perform well in stable conditions, and friction velocity (u_*) has been used frequently to screen out the flux measurements of poor quality (Davis *et al*., 2003; Goulden *et al*., 1996). In this study, we discard all the flux data when u_* was less than 0.10 m s^{-1} (Griffis *et al*., 2010).

Large negative fluxes in the early morning has been observed in many EC studies, and it may lead to an overestimation of CO_2 uptake during the growing season by about 20% (Anthoni *et al*., 1999; Davis *et al*., 2003; C Yi *et al*., 2000). Davis *et al*. (2003) suggested that the bias is caused by horizontal and vertical advections, and it could be corrected by excluding the negative CO_2 flux that exceeds a defined level, or by replacing it with observation at a lower level. In this study, we excluded the morning data (between 6 a.m. and 10 a.m. LST) when the storage term was lower than -4 μmol m^{-2} s^{-1}.This storage term correction reduced the estimated CO_2 uptake during growing season (May to September) by 18%, consistent with that reported in the literature.

The monthly CO_2 flux was determined by the mean of the composite diurnal variation of CO_2 flux. This averaging strategy was applied in this study for all the monthly values in

order to avoid biases caused by outliers and the asymmetry associated with more missing data from nighttime versus daytime. In 2009, excluding the missing data period caused by the malfunctioning of the EC vacuum pump, DOY 140 (May 19th) to 197 (July 15th), the available data was 78%. The u_* and storage term screening eliminated an additional 12% and 2% of the data, respectively (Davis *et al*., 2003). Instead of filling the data gaps, we have estimated the monthly means based on the diurnal composite of the scalar quantities.

4.2.4.2. Equilibrium method

The equilibrium method (Eq) provides a way to quantify regional trace gas fluxes from mixing ratio measurements in the boundary layer (Bakwin *et al*., 2004; Betts *et al*., 2004; Denmead *et al*., 1996; Desai, 2010; Helliker *et al*., 2004; Williams *et al*., 2011). So far, this method has been applied to CO_2 but not to CH_4 and N_2O. On the assumption that horizontal advection and storage are negligible in the boundary layer budget when averaged over enough time (weeks), the land surface flux (F_{Eq}) is in balance with the exchange at the top of boundary layer, as

$$F_{Eq} = \rho W(c_+ - c_m) \quad (2)$$

where c_+ and c_m are the mixing ratio of CO_2, CH_4 or N_2O above and within the boundary layer, respectively; ρ and W are air density and the vertical velocity, respectively, at the top of boundary layer. c_+ was assumed as the concentration measured at Niwot Ridge site (NWR, 40°3'11"N, 105°35'10"W) CO, US, the closest background site operated by NOAA (Conway *et al*., 1994). c_m was the CO_2 concentration measured by TDL and calibrated by NOAA-ESRL standard. The concentration used in the equation (c_+ and c_m)

was the mean of the composite diurnal variation of CO_2 concentration for a month. The equilibrium method was applied for 2009.

We used the following two methods to determine ρW (Helliker *et al*., 2004) for the three GHGs:

$$\rho W = \frac{F_w}{c_{w,+} - c_{w,m}} \quad (3)$$

$$\rho W = -\Omega/g \quad (4)$$

where F_w is the water vapor flux measured at the KCMP tower (derived from latent heat flux), $c_{w,m}$ is the water vapor mixing ratio measured at the KCMP tower $c_{w,+}$, and Ω is the water vapor mixing ratio and pressure vertical velocity (in units of Pa s^{-1}) at the 700 hPa level in the NCEP/NCAR Reanalysis-2 data (provided by the NOAA/OAR/ESRL PSD, Boulder, Colorado, USA, from <http://www.esrl.noaa.gov/psd/>). In addition, for CH_4 and N_2O, we also used CO_2 as a tracer to determine ρW:

$$\rho W = \frac{F_C}{c_{C,+} - c_{C,m}} \quad (5)$$

where F_C is the CO_2 flux measured by the eddy covariance system at 100 m at the KCMP tower; $c_{C,+}$ and $c_{C,m}$are the CO_2 mixing ratio measured at NWR background site and on 200 m level of the KCMP tower, respectively.

4.2.4.3. Inverse modeling

We used the CO_2 flux product from the global inversion model Carbon Tracker (http://www.esrl.noaa.gov/gmd/ccgg/carbontracker/) (Peters *et al*., 2007) as a reference to compare with the flux determined with the other methods. This product provides a daily

CO_2 flux from 2000-2010 at a spatial resolution of 1° by 1°, so the number of grid points within the 100 km, 200 km, 300 km, 600 km radius of the tower is 2, 10, 25, and 90, respectively. The inversion CO_2 flux consists of fossil fuel burning, fire, land, and ocean flux. The fossil fuel burning and fire components are prescribed according to the EDGAR v4.0 inventory (Olivier *et al*., 2005).

4.2.5. Flux aggregation

The regional trace gas budget can be estimated by aggregating the sectorial and spatial fluxes based on sectorial statistics and land cover information (Chen *et al*., 2008; Desai *et al*., 2008; Nisbet and Weiss, 2010; Tang *et al*., 2012). The total CO_2 flux from the landscape was estimated as the sum of the biological and anthropogenic fluxes. In this study, the anthropogenic flux was the prescribed fossil fuel flux in the Carbon Tracker product, consistent with EDGAR inventory. The biological flux was calculated by aggregating the CO_2 flux from six major land cover types within the tall tower footprint. The six land cover types are cropland (corn and soybean), forest, grassland/pasture, wetland, open water, and developed land. The cropland CO_2 flux was the weighted average of the flux measured with EC in a soybean field and a corn field near the KCMP tower as described above. The forest CO_2 flux was obtained from the AmeriFlux data archive (Level 2 data) for the deciduous forest in the University of Michigan Biological Station, about 662 km northeast of the KCMP tower (Curtis *et al*., 2005; Schmid *et al*., 2003). The grassland CO_2 flux was also from AmeriFlux for, Fermi Prairie, Illinois (US-IB2), about 503 km southeast of the KCMP tower (Matamala *et al*., 2008). Each of the three land cover types was measured by EC flux towers in 2009 (Table 4.2, Figure 4.1). The biological CO_2 flux from wetland, open water, and developed land was considered as

negligible in this study based on their small area contribution. The aggregation radius was tested from 100 km to 600 km, and the results are summarized in Section 4.3.2.

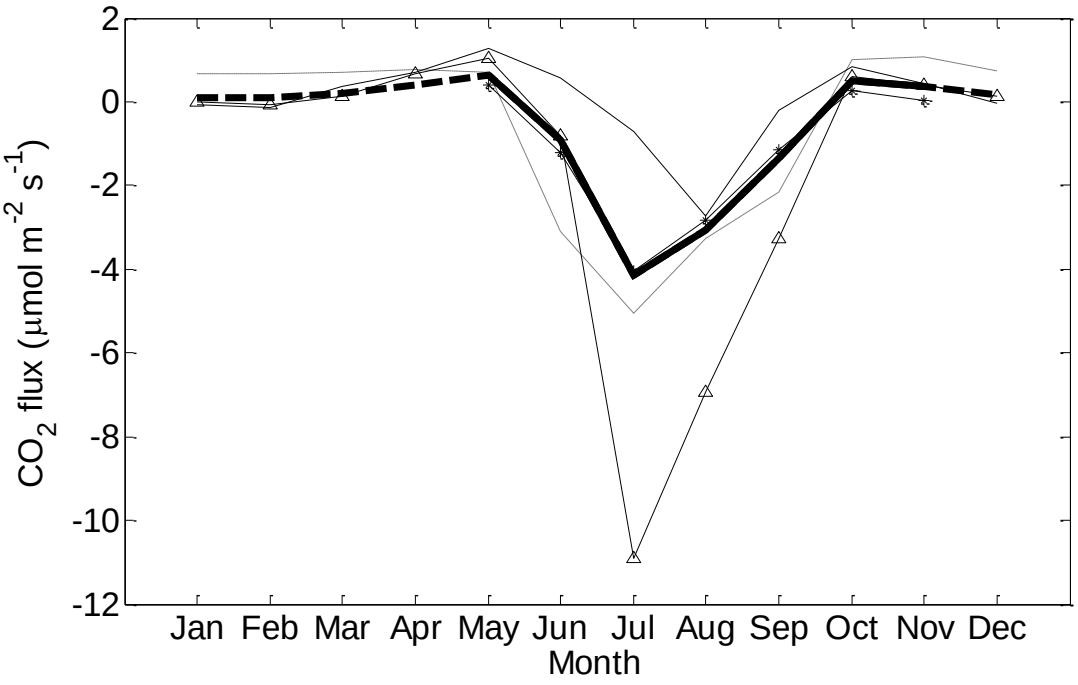

Figure 4.1. The Biological CO_2 flux (thick solid line) from the landscape around the tall tower, calculated from monthly averages of CO_2 flux from major land cover types. The fluxes from Corn (solid line with triangle) and Soybean (thin solid line) field were measured by eddy covariance tower at G21 and G19 site in Minnesota. The fluxes from forest (dashed line) and grassland (solid line with star) were from AmeriFlux sites in North America (Table 4.2).

Table 4.2. Data source of biological flux and anthropogenic flux used in flux aggregation method

	Data source	Observation year	Citation
Biological flux			
Cropland (corn)	Rosemount G21	2009	(Baker and Griffis, 2005)
Cropland (soybean)	Rosemount G19	2009	(Baker and Griffis, 2005)
Deciduous forest	UMBS	2009	(Curtis *et al*., 2005; Schmid *et al*., 2003)
Grassland	USIB2	2009	(Matamala *et al*., 2008)
Anthropogenic flux	Prescribed fossil fuel emission from Carbon Tracker	2009	(Peters *et al*., 2007)

4.3. Results

4.3.1. Climate

The year 2009 was dryer than the climate normal (1980–2010). The annual precipitation was 537 mm, 31% less than the climate normal. During the intensive campaign (DOY 243–269), the wind speed was generally low, with an average value of 0.43 m s^{-1} at about 2 m above the canopy in the EC corn field 3 km from the KCMP tower. The total precipitation during this period was only 13 mm and was recorded on the morning of DOY 268.

4.3.2. Constraints on the regional CO_2 flux

The EC CO_2 flux measured on the KCMP tower exhibits a strong seasonal pattern (Figure 4.2). From October to April, the landscape was a net source of CO_2, and the averaged emissions rate was 0.59±0.08 μmol m^{-2} s^{-1} (the mean and standard deviation of the three annual values from 2007 to 2009). From May to September, the landscape was a sink of CO_2, reaching the peak uptake in July at the rate of -4.13±1.05 μmol m^{-2} s^{-1}. There was no monthly mean data for June 2007 and June 2009 due to measurement problems. Since June is the only month that is missing CO_2 flux for 2009, we gap-filled it according to the pattern observed in 2008, and the CO_2 flux observed in two adjacent months in 2009. As a result, the annual cumulative C fluxes in 2008 and 2009 were -120 and -179 g C-CO_2 m^{-2} yr^{-1}, respectively.

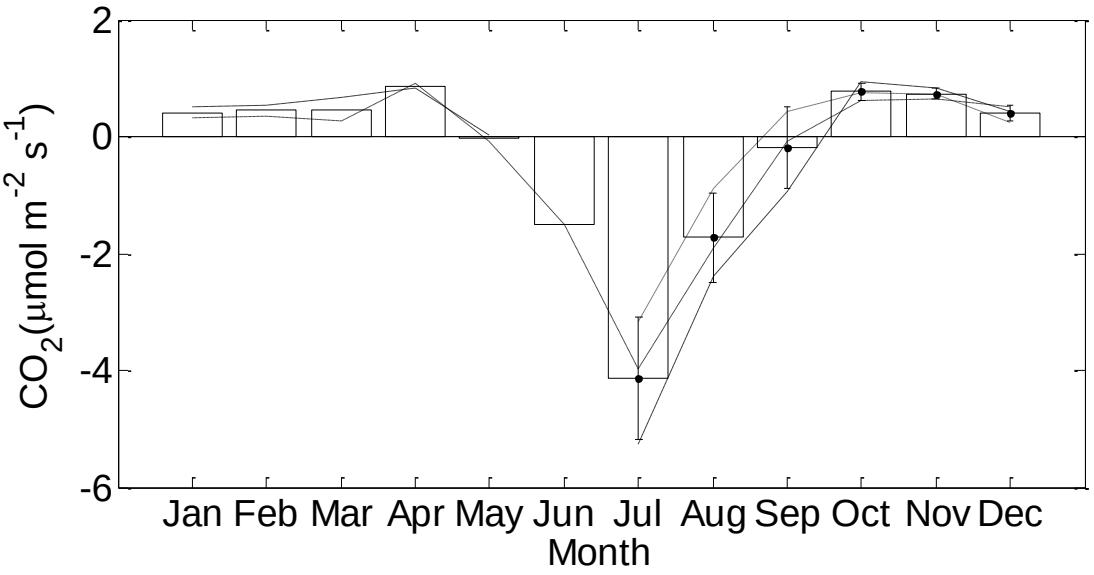

Figure 4.2. Monthly averages of CO_2 flux in 2007 (dotted line), 2008 (chain dotted line), and 2009 (dashed line) measured with EC on the tall tower. White bars are the mean monthly value from the available data during the three-year observation period. Error bars on the top of white bars are the standard deviation of the three years, and they are only available for July to December due to the data availability.

The challenge of using the tall tower EC flux to constrain the regional CO_2 flux is to determine the footprint of the EC flux. We first used a simple circular footprint method by assuming the landscape within a circle centered at the tall tower contributed equally to the measured flux. We used the Carbon Tracker (CT) and the flux aggregation (FA) methods to estimate the CO_2 flux for a radius up to 600 km. The monthly flux from these methods in all the radius ranges correlated well with the EC flux ($r > 0.9$, $p < 0.001$) (Table 4.3), suggesting the land surface flux was relatively homogeneous and was dominated by the seasonal pattern of the biological flux. Further, to test the accuracy of the estimation, the Nash-Sutcliffe efficiency (NSE) was calculated (Nash and Sutcliffe, 1970), given EC flux as the observation value (o_i) and flux from CT and FA in different ranges as the modeled value (m_i).

$$\mathrm{NSE} = 1 - \frac{\sum(o_i - m_i)^2}{\sum(o_i - \bar{o})^2} \tag{6}$$

It is considered as a very good fit when *NSE*>0.75, and as a good fit when 0.65<*NSE*≤0.75 (Moriasi *et al*., 2007). The results show that EC monthly flux fits very well with the averaged flux from both CT and FA methods within a radius of 200 km or bigger (*NSE* >0.80), and as the radius increased from 200 km to 600 km, the CT and FA fluxes did not change significantly. CT and FA fluxes within a 100 km radius were more positive than EC flux, mainly due to strong local impact of anthropogenic emission from the Minneapolis/Saint Paul urban area. Consequently, we consider the EC flux as representing the averaged flux from 600 km radius around the KCMP tower, and it agreed well with both CT and FA on a 10^5 to 10^6 km^2 scale. This footprint scale is larger

than Leclerc and Thurtell (1990) and Schuepp *et al*. (1990)'s estimations; however, it agrees with that of Gloor *et al*. (2001).

To determine the KCMP tower footprint and examine whether the KCMP tower flux was sensitive to a different footprint shape and weighting, we also used Stochastic Time-Inverted Lagrangian Transport (STILT) model (Lin *et al*., 2003). During September, when the intensive observation was carried out, we released 100 air parcels per hour from the 200 m level at the KCMP tower, and transported these parcels backwards for two days. The distribution of these air parcels determined the tall tower footprint. By overlaying the weighted footprint map with the land cover map, we were able to determine the composition of land cover types in the KCMP tower footprint: 65% for cropland, 11% for forest, 11% for grassland, 2% for wetland, 4% for open water, and 6% for developed land. The aggregated flux based on this new footprint was -1.01μmol m^{-2} s^{-1} for September, 2009; in comparison, the EC flux during the same period was -0.93 μmol m^{-2} s^{-1}, and the flux aggregated within a 300 km or 600 km circle was -1.04 μmol m^{-2} s^{-1} and -0.94 μmol m^{-2} s^{-1}, respectively. As a result, the landscape heterogeneity around the KCMP tower is relatively similar/consistent, extending from a 300 km to 600 km circle, and the regional CO_2 flux estimated at the KCMP tower was not sensitive to a different footprint shape and weighting, The EC measurement at the KCMP tower could reflect the regional CO_2 flux from a 300km to 600 km circle around the tall tower.

Table 4.3. Correlation coefficient and NSE between EC flux and the other two methods. CT is Carbon Tracker, FA is flux aggregation method.

Methods\Distance		5 km	10 km	20 km	50 km	100 km	200 km	300 km	600 km
CT	***NSE***	NA	NA	NA	NA	0.41	0.82	0.92	0.94
	r	NA	NA	NA	NA	0.96	0.97	0.98	0.99
FA	***NSE***	0.48	0.49	0.37	0.23	0.58	0.90	0.95	0.94
	r	0.98	0.98	0.98	0.98	0.98	0.98	0.98	0.98

Considering the EC flux measured at the KCMP tower as the best estimate of the regional CO_2 flux, we evaluated the performance of the equilibrium method. The equilibrium method successfully produced the seasonal pattern but underestimated the annual uptake of CO_2 by the landscape (Figure 4.3). We examined the CO_2 flux from equilibrium methods using ρW estimated from two approaches (Equation 3 for F_{EH} and Equation 4 for F_{EO}). The methods were applied when rainy days (precipitation<1 mm) were excluded and when rainy days were not excluded. All CO_2 equilibrium flux estimates significantly correlated with the EC flux (r>0.84, p<0.01); however, their summer values (June–August) were smaller in magnitude than the EC flux and the FA flux. Removing rainy days caused both equilibrium fluxes to be more negative, but it remained substantially lower than the EC flux.

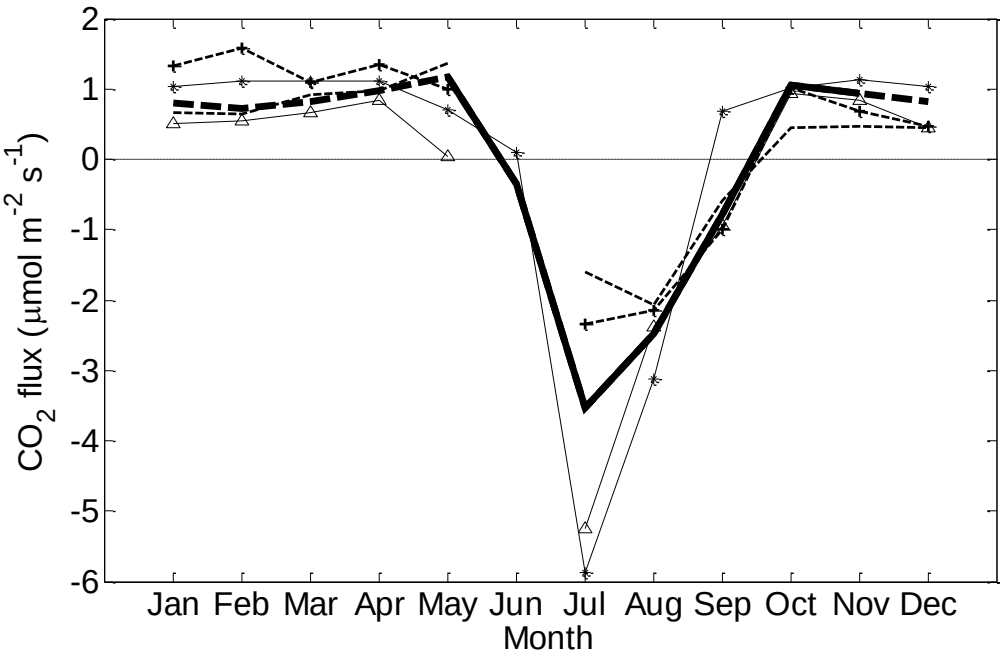

Figure 4.3. Monthly averages of CO_2 flux in 2009 estimated by flux aggregation (thick solid line), eddy covariance method (line with triangle), Carbon Tracker (line with star), Equilibrium method with H_2O as a tracer (thin dashed line), and Equilibrium method using NCEP data (thin dashed line with cross). The flux aggregation flux ended in October because the grassland data was missing in November and December.

4.3.3. GHG concentration pattern

During the intensive campaign, the CO_2 mixing ratio at the height of 200 m increased from 365.2 ppm during the first five days to 406.2 ppm during the last five days (Figure 4.4). The mixing ratio changed from below that at the NWR (384.4 ppm) to above that at the NWR site, indicating a transition of the landscape from a CO_2 sink to a source. This observation is consistent with the observed seasonal pattern in the CO_2 flux shown in Figure 4.3.

The mean CH_4 mixing ratios during the observation period were 2.096 ppm and 2.017 ppm at the heights of 3 m and 200 m, respectively. The CH_4 mixing ratio at both heights was consistently higher than the background mixing ratio at NWR (1.844ppm), suggesting the landscape around the KCMP tower was a CH_4 source.

The N_2O mixing ratio during the observation period was also higher than that at NWR. The averaged N_2O mixing ratios at the heights of 3 m and 200 m were 4.0 ppb and 2.1 ppb higher than the value at NWR site (322.7 ppb), respectively. Both the vertical gradient between the 3 m and 200 m height and the difference between the 200 m height and the background site indicate that the landscape was a N_2O source during the observation period.

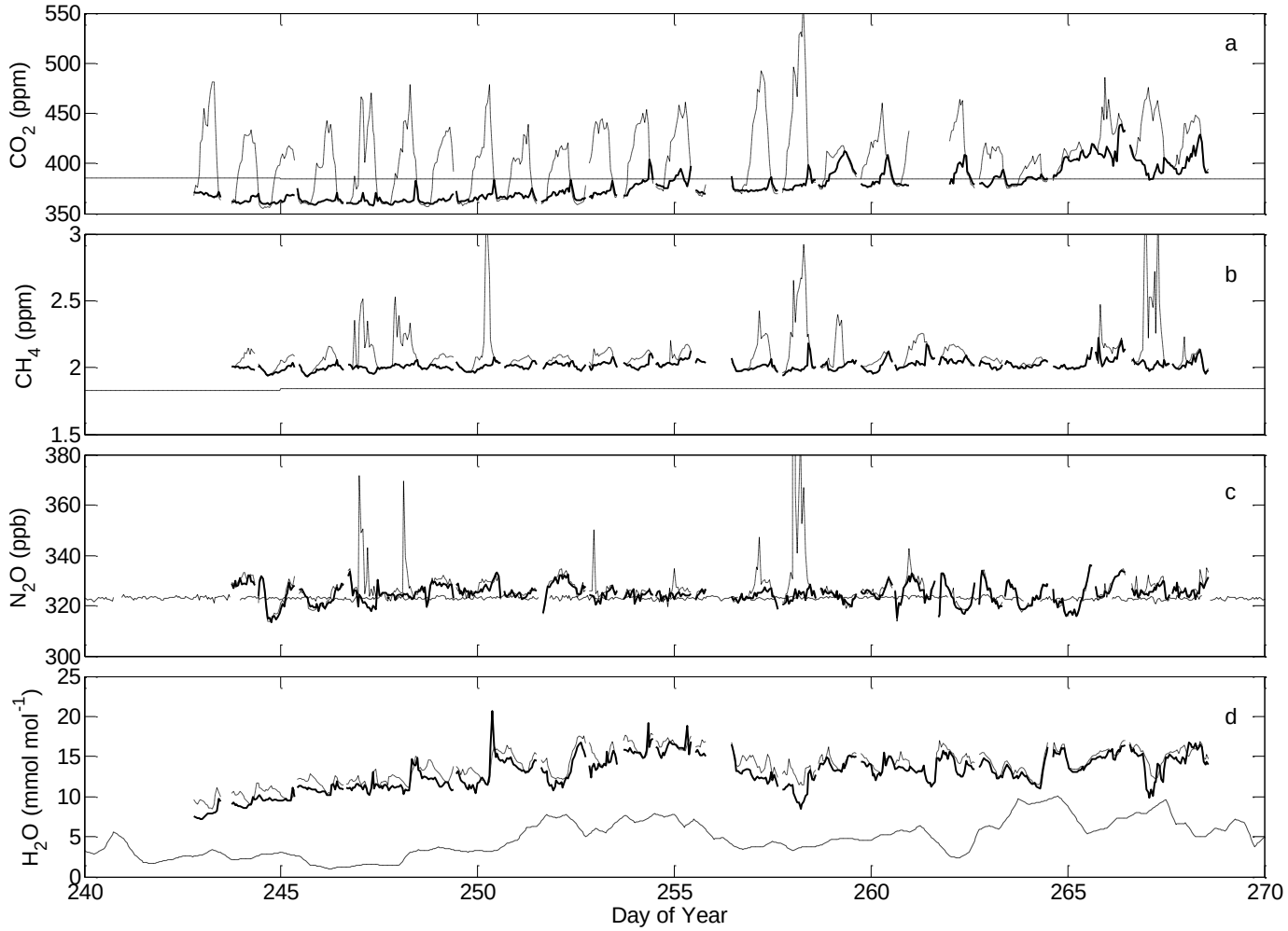

Figure 4.4. Hourly averages of CO_2 (a), CH_4 (b), N_2O (c), and H_2O (d) mixing ratio during the observation period from DOY 243 to DOY 269, 2009. Solid line— mixing ratio on 200 m. Dot-dash line— mixing ratio on 3 m. Dashed line— mixing ratio at Niwot Ridge site.

4.3.4. Regional CH_4 and N_2O fluxes

Since the equilibrium method produced a relatively good match with monthly EC flux in estimating regional CO_2 flux except July, we applied it in estimating regional CH_4 and N_2O fluxes during the intensive campaign in the later growing season in 2009. ρW determined by three methods (using CO_2 tracer and H_2O tracer, and using NCEP reanalysis data) converged at -0.09±0.02 mol m^{-2} s^{-1}. As a result, the CH_4 and N_2O fluxes were 16.0±3.1 nmol m^{-2} s^{-1} and 0.19±0.04 nmol m^{-2} s^{-1}, respectively during the intensive campaign.

4.4. Discussion

4.4.1. Regional CO_2 flux

Determining the annual CO_2 budget on a regional scale is challenging because CO_2 flux has both diurnal and seasonal cycles and the magnitude of annual average is typically substantially smaller than the seasonal and diurnal variations. For example, in 2009, the tall tower's annual average EC flux was -0.47 µmol m^{-2} s^{-1}**,** while the seasonal variation was about 6 µmol m^{-2} s^{-1} and the diurnal variation during summer time was about 40 µmol m^{-2} s^{-1}, about 10 and 100 times, respectively, higher than the annual average. A small systematic bias in daily and monthly flux estimation, such as that caused by the data-screening and gap-filling approaches, can be significant for the annual average CO_2 flux.

To quantify the regional CO_2 flux, intensive investigation has been conducted through observation at the LEF site, which is about 260 km northeast of our tall tower (Davis *et al*., 2003; Bakwin *et al*., 2004; Helliker *et al*., 2004; Ricciuto *et al*., 2008). Based on EC

measurements on the tall tower, Ricciuto *et al*. (2008) reported that the annual NEE was 120 g C m^{-2} yr^{-1} with a strong inter-annual variation (140 g C m^{-2} yr^{-1}). This result was consistent with Davis *et al*.'s (2003) result but higher than Hellliker *et al.*'s (2004) EC flux for 2000, which was -71 g C m^{-2} yr^{-1}. The major difference is that Hellliker *et al.* (2004) did not gapfill the data, and all the reported CO_2 fluxes exclude the period when water vapor flux was not available.

Following Davis *et al.*'s (2003) data processing procedure, the annual 2009 CO_2 flux at our tower was -179 g C m^{-2} yr^{-1} (Table 4.4), which is more negative than the annual fluxes at the LEF site reported by both Hellliker *et al.* (2004) and Ricciuto *et al*. (2008). We believe that our estimate is reasonable because the footprint of the LEF tower primarily includes forest and wetlands, both of which are less productive than the cropland surrounding our tall tower.

The annual NEE estimated by the FA method, a bottom-up approach, also supports that the landscape (up to10^6 km^2) around the KCMP tower was a strong carbon sink, but it was -54 g C m^{-2} yr^{-1}, only about 30% of the EC estimate. FA underestimated the July uptake by 48 g C m^{-2}. Three factors may lead to the bias in the estimation: 1) the accuracy of the land cover information. Even though the accuracy of land use classification by CDL has reached 71% (Griffis *et al*., 2010), it may not be sufficient for annual NEE estimation, especially for a land cover type with strong NEE contribution. For example, if the area of corn production were underestimated by 30% (only about 6% of the whole landscape), it would lead to an underestimation of 36 g C m^{-2} yr^{-1}, which is about 42% of the annual NEE estimated by FA. 2) NEE information of each land cover type. Even though the amount of flux information associated with different land cover

types has improved with the FLUXNET program (Baldocchi *et al*., 2001), NEE measurement are still lacking for many land cover types in the US upper-Midwest region. For the land cover types that are already being measured, the data usually require gap-filling, and it is rare to have replicates (Desai, 2010). NEE from major vegetation types in 2009 was summarized and compared with literature values in Table 4.4; however, it should be noted that the reference value might be different from our measurement due to significant interannual variability. 3) Anthropogenic emissions. The uncertainties in national anthropogenic emission of CO_2 have been improved to less than 10% (NRC, 2010); nevertheless, large uncertainties still exist on a regional scale.

In the current CO_2 inventory, cropland is usually considered as carbon neutral, and the transition from forest to cropland is expected to result in a significant source of carbon (IPCC, 2006). However, it is undeniable that some crops, such as corn, are more productive than forest, and they could serve as a carbon sink if the post-harvest emissions could be carefully managed. As a result, cropland's role in the carbon budget should be reconsidered, and a CO_2 mitigation strategy could be developed around cropland management.

Table 4.4. A summary of annual NEE estimated from different methods. NEE in "Reference" column is from the study in Midwest US in recent years.

	Annual NEE (g C m^{-2})	
	This study	Reference
Tall tower Eddy Covariance	-179	16±19 (Davis *et al*., 2003) -71 (Helliker *et al*., 2004) 16 (Bakwin *et al*., 2004)
Carbon Tracker	-59	-58 (Desai *et al*., 2010)
Equilibrium	49 to 74	-110±14 (Desai *et al*., 2010) -38 (Helliker *et al*., 2004) 79 (Bakwin *et al*., 2004)
Flux Aggregation	-54	
Corn	-599	-466±38 (Hernandez-Ramirez *et al*., 2011) -576±101 (Hollinger *et al*., 2005)
Soybean	10	-13±39 (Hernandez-Ramirez *et al*., 2011) -32±161 (Hollinger *et al*., 2005)
Grassland	-214	-268 (Suyker and Verma, 2001)
Forest	-227	-240±24 (Schmid *et al*., 2000) -137±49 (Schmid *et al*., 2003)
Fossil fuel	162	
Other methods		
Interannual Flux Tower Upscaling Experiment (IFUSE)		-321±13 (Desai *et al*., 2010)
Mesoscale inverse modeling		-183±35 (Lauvaux *et al*., 2012)

4.4.2. Uncertainties in the equilibrium CO_2 flux method

The equilibrium method effectively reproduced the seasonality of the CO_2 flux, but its estimate of annual NEE was 49 to 74 g C m^{-2} yr^{-1}, which was more positive compared to the estimates derived from the other three methods (EC, CT, FA). In this case, the lower and the higher limits were estimated by using H_2O as a tracer (F_{EH}) and the ρW in the NCEP reanalysis data (F_{EO}). The data gap in June was filled with the average of May and July.

Similarly, the LEF tower site reported more positive annual CO_2 flux derived from the equilibrium method than the eddy covariance approach (Table 4.4.). Using the equilibrium boundary method, the annual CO_2 flux was 79 and -38 g C m^{-2} yr^{-1}, respectively for 1997 and 2000 (Bakwin *et al*., 2004; Helliker *et al*., 2004), compared to 16 and -71 g C m^{-2} yr^{-1}, respectively, which, according to the same study, resulted from using the eddy covariance method. The difference between the annual flux estimates derived from the two methods may be due to the systematic bias in determining CO_2 concentration at the top of the boundary layer. Both Bakwin *et al*. (2004) and Helliker *et al*. (2004) used the CO_2 concentration measured on 396 m of the LEF tower as the concentration at the top of boundary layer, while Desai *et al*. (2010) used the aggregated concentration along the tall tower profile. From 1997 to 2006, Desai *et al*.' s (2010) flux estimates using the equilibrium boundary layer method was -110±14 g C m^{-2} yr^{-1}, which is much more negative than that cited by Bakwin *et al*. (2004) and Helliker *et al*. (2004). Consequently, the strategy for determining CO_2 concentration at the top of boundary layer, even though it has a negligible impact on monthly flux, may strongly influence the annual flux estimate.

Despite the systematic bias in CO_2 concentration, the equilibrium method also underestimated the CO_2 uptake during the growing season. For example, the EC flux was -5.26 μmol m^{-2} s^{-1} in July 2009 and the equilibrium method gave a flux of -1.96 μmol m^{-2} s^{-1} for the same month. To bring the equilibrium flux into agreement with the tall-tower EC flux, ρW would have to increase to -0.52 mol m^{-2} s^{-1} for July 2009, which is much larger in magnitude than -0.08 ±0.09, the average July value for 2007 to 2011 obtained with NCEP reanalysis data. Therefore uncertainties in ρW cannot fully explain the flux bias.

Instead, we hypothesize that the growing season flux bias was caused by horizontal advection. A large spatial gradient of CO_2 concentration was observed by a network of nine towers in upper Midwest U.S. during the Mid-Continent Intensive (MCI) in North American Carbon Program from 2007 to 2009 (Miles *et al*., 2012). Miles *et al*. (2012) reported that the CO_2 gradients between the KCMP tower and other sites range from 0.3 to 2.1 ppm / (100 km^{-1}) during growing season.

In order to examine whether advection can lead to the underestimation of equilibrium flux, we calculated the advection flux term (F_{adv}) with Equation 7 for July, when equilibrium flux was less than 50% of EC flux (Bakwin *et al*., 2004).

$$\mathrm{F_{adv}} = \frac{P}{RT}\int_{0}^{\mathrm{h}} \mathrm{U}\frac{\partial \mathrm{C}}{\partial \mathrm{x}}dz \qquad (7)$$

where P is the air pressure; R is the gas constant (8.31 Pa m^3 K^{-1} mol^{-1}); T is the air temperature (in K); h is the height of atmospheric boundary layer; U is the horizontal wind speed; C is the CO_2 mixing ratio; $\partial C/\partial x$ is the CO_2 concentration gradient on the

horizontal coordinate (x); and z is the vertical coordinate. To quantify the advective flux, we assume that averaged boundary layer height in July was 1000 m based on a long term observation at LEF tower site (Yi *et al*., 2001). The averaged wind speed at the KCMP tower in July was at 5.43 m s^{-1}. As a result, the absolute value of the advective flux term ranges from 0.63 to 4.38 μmol m^{-2} s^{-1}, corresponding to concentration gradients of 0.3 and 2.1 ppm / (100 km). In comparison, the EC flux in July was -5.26 μmol m^{-2} s^{-1}. Therefore, the advective flux is significant when the spatial CO_2 gradient is large and may explain the observed disparity between these approaches

The Carbon Tracker 3-D CO_2 concentration product also shows large CO_2 depletion in the upper Midwest Corn Belt during the growing season due to the strong CO_2 uptake by agricultural systems. According to this product, the mean concentration of the 34 m – 1274 m air layer had a gradient of 0.8 ppm / (100 km) along the prevailing wind (from northwest) in July 2009 (Figure 4.5). Using a mean wind speed of 5.4 m s^{-1} recorded on the tall tower and a boundary layer depth of 1000 m (Yi *et al.*, 2001), the resulting advective flux was -1.88 μmol m^{-2} s^{-1}, which is comparable to the bias of the equilibrium method. In comparison, with the same method, the advective flux at the 100 m level was estimated according to the accumulated concentration below 125 m level, and the results suggest that advection was negligible (only -0.02 μmol m^{-2} s^{-1}) on 100 m level at the tall tower site. Therefore, it is reasonable to assume a negligible advective term for the EC method at 100 m. The larger advection term for the equilibrium method can be expected since the concentration gradient is accumulated over a much larger column of air.

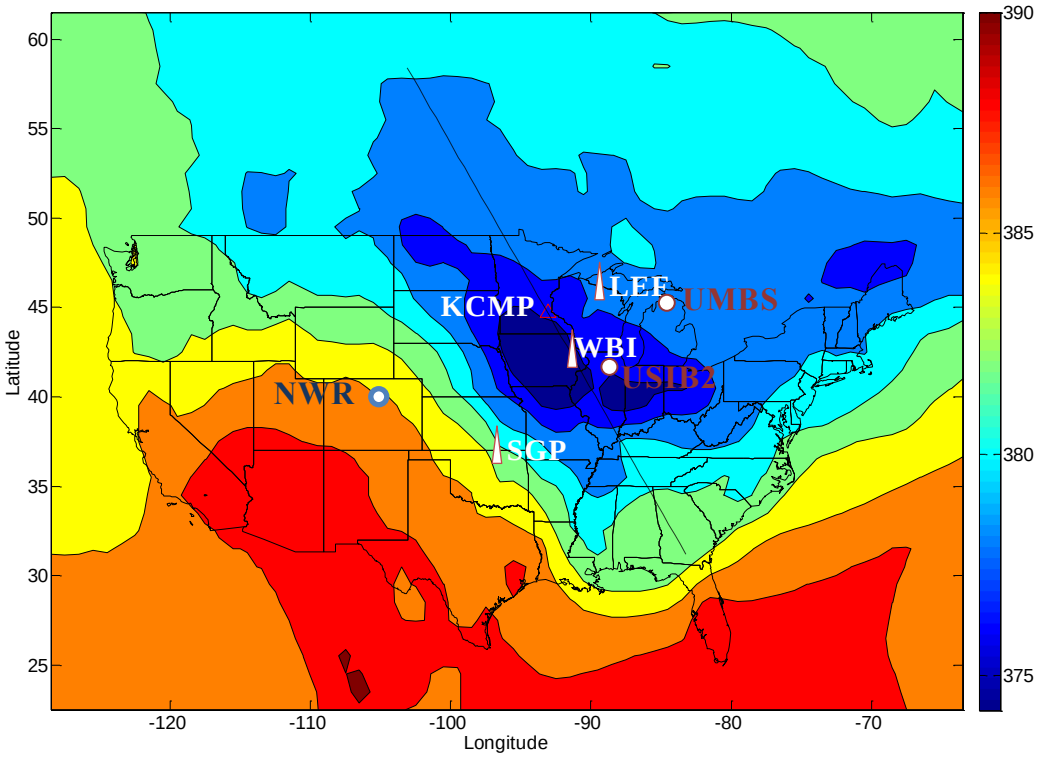

Figure 4.5. CO_2 concentration averaged from land surface to 1274.1 m (Level 6) according to Carbon Tracker 3D CO_2 concentration product in July. Dashed line — previling wind direction in July from northwest to southeast. Red triangle — KCMP tall tower site; orange triangle — tall tower obserservotory operated by NOAA; dark red circle— Ameriflux sites; blue circle — background observation site. The color scale is CO_2 concentration with ppm as the unit. The resolution of the concentration data is 1° by 1°.

4.4.3. Uncertainties in the equilibrium CH_4/N_2O flux method

4.4.3.1. Uncertainties in concentration measurement

The difference between mixing layer concentration and background concentration is critical to the equilibrium method. The bias in result could be caused by: 1) the difference between NWR site and the real-time concentration right above the boundary layer, or 2) systematic bias in measuring the concentration at 200 m.

The averaged CH_4 concentration during the intensive campaign in the nearby background sites were 1.883 ppm (Cold Bay, Alaska, US), 1.887ppm (Barrow, Alaska, US), and 1.842 ppm (NWR, Colorado, US). The CH_4 concentration data in the GLOBALVIEW product in September 2008 suggested that, at the same latitude, aircraft-measured CH_4 concentrations ranged between 1.809 and1.909 ppm (GLOBALVIEW-CH_4, 2009). Thus, using the NWR site might underestimate the CH_4 concentration above the boundary layer by about 0.05 ppm, and it will lead to an overestimation of 4.6 nmol m^{-2} s^{-1}, about 30% of the estimated flux. In addition, even though the TDL measurement precision for CH_4 was below 3 ppb, the calibration gas was measured as 2.234 ± 0.055 ppm; thus, we considered 0.055 ppm as the potential measurement bias of the absolute value of the CH_4 concentration. As a result, the range of CH_4 flux estimates could be revised to 6.2-21.1 nmol m^{-2} s^{-1}. This range could be refined by a direct measurement of CH_4 concentration at the top of the boundary layer, and a more accurate GC measurement of the calibration gas.

The uncertainties caused by the systematic bias between our KCMP tower and NOAA background sites could also be evaluated and constrained by quantifying the flux with the

other two independent boundary layer methods, which were only based on the relative concentration at 3 m and 200 m levels and the build-up of the CH4 concentration in the nocturnal boundary layer. We used a modified Bowen ratio method (Werner *et al*., 2003) and a modified nocturnal boundary layer method (Kelliher *et al*., 2002) to calculate the nighttime CH_4 flux. The former method assumes the vertical transport of a trace gas is driven by eddy diffusion and that the diffusivity was the same for all scalar quantities; the second method uses CO_2 as a tracer and assumes the build-up of CO_2 and CH_4 near the land surface was caused by land surface emissions. The CH_4 fluxes from these two methods were 14.8 ± 10.3 nmol m^{-2} s^{-1} and 17.1 ± 9.4 nmol m^{-2} s^{-1}, respectively, similar to equilibrium method estimation (Figure 4.6a). The results confirm that the CH_4 flux from the equilibrium method (16.0 nmol m^{-2} s^{-1}) gave a reasonable estimation of the regional flux. The detailed calculation was described in Zhang *et al*. (in review).

N_2O has a much more unified background concentration. The differences between the background sites in the northern hemisphere were less than 0.5 ppb. The N_2O measurement at the KCMP tower was calibrated by the NOAA gold standard; thus, it could be compared against the NOAA background site. As a result, the uncertainties in the background concentration and the measurement will lead to bias within 0.05 nmol m^{-2} s^{-1} for N_2O flux estimation, about 24% of the estimated N_2O flux. The modified Bowen ratio method and modified nocturnal boundary layer methods were applied to quantify the regional N_2O flux, and the results were 1.09 ± 0.56 nmol m^{-2} s^{-1} and 0.90 ± 0.65 nmol m^{-2} s^{-1}, both higher than the flux estimated from the equilibrium method (Figure 4.6b). The underestimation by the equilibrium method might be caused by neglecting advection, and it will be analyzed in Section 4.3.2.

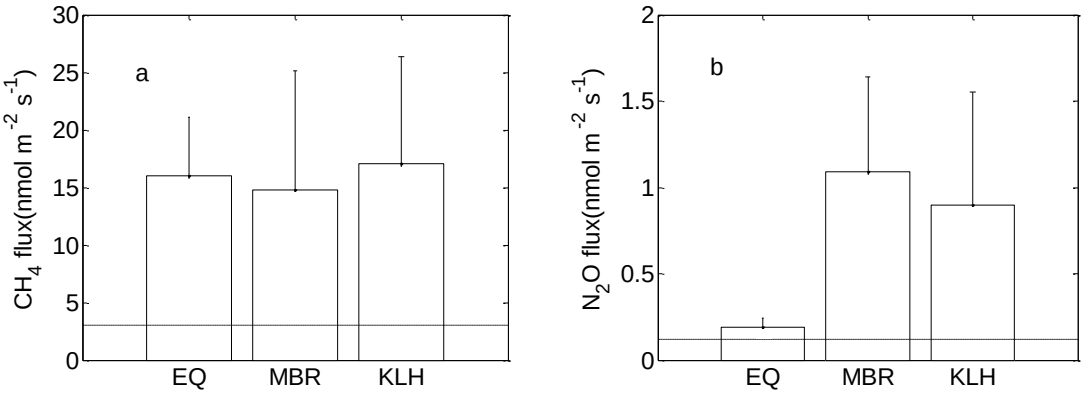

Figure 4.6. CH_4 (a) and N_2O (b) fluxes estimated from three different boundary layer budget methods: equilibrium method (EQ), modified Bowen ratio method (MBR), modified nocturnal boundary layer method (KLH).

4.4.3.2. Uncertainties in advection

Similar to CO_2, neglecting advection may also lead to a bias in the regional CH_4 and N_2O flux estimates. . The spatial gradient of the trace gases within the boundary layer is important for estimating advection ; unfortunately, few studies have been conducted to determine it due to scarce measurement availability.

CH_4 and N_2O concentration was only sampled at three towers in the Midwest US by NOAA Carbon Cycle Surface Network (Table 4.5) in 2009, and most samples were taken around noon time (Figure 4.7). Both the temporal and spatial resolutions of the measurement were insufficient to resolve the regional pattern of CH_4 and N_2O concentration. To make a preliminary evaluation of the advection term, we interpolated the concentration field in the Midwest based on the measurement at the three NOAA sites during the intensive campaign, and calculated the advection flux from the prevailing wind direction during the campaign (from the south to the north). At LEF site, we used the data from Pragrammable Flask Packages (PFP) sampling strategy, because such strategy had about five times more sampling points than Flask sampling strategy at LEF site, and the difference between PFP and Flask at LEF site was only about 10% and 0.5% of the difference between SGP and LEF with Flask sample for CH_4 and N_2O. The calculated advection terms were 6.3 and 0.17 nmol m^{-2} s^{-1} for CH_4 and N_2O respectively, about 40% and 88% of the fluxes calculated from equilibrium method. By including the N_2O concentration measurement at the KCMP tower, the advection term reached 0.85 nmol m^{-2} s^{-1}, similar to the difference between equilibrium methods and the boundary layer methods (0.82-0.90 nmol m^{-2} s^{-1}). CH_4 concentration was not included because the

measurement precision at KCMP was similar to the concentration difference between sites, as a result, large bias will be introduced in estimating the advection term if CH_4 concentration at KCMP site is included. These preliminary evaluations suggest that neglecting the advection term can lead to the underestimation of the regional CH_4 and N_2O flux, and more spatial information of CH_4 and N_2O concentration within the boundary layer is needed for determining the advection term at the KCMP tower.

4.4.4. Greenhouse gas budget

CH_4 and N_2O concentration measurements were not available throughout 2009; however, we can provide a preliminary annual flux by assuming that the seasonal pattern of the concentrations at the KCMP tower was similar to the pattern at the WBI and SGP tower sites (supplementary materials Figure 4.8). As a result, the annual regional CH_4 and N_2O fluxes were 20.6 nmol m^{-2} s^{-1} and 0.36 nmol m^{-2} s^{-1}, respectively, equivalent to 260 and 152 g CO_2 eq m^{-2} yr^{-1}, respectively, and offsetting 39% and 23% of the annual CO_2 uptake, respectively. The impact of advection was considered as negligible since there was no prevailing wind throughout the year of 2009. According to West *et al*. (2011), the harvested biomass in the KCMP tower footprint was around 140 g C m^{-2} yr^{-1}, accounting for 78% of the observed CO_2 uptake. Considering the carbon fixed by crops will be harvested and some will be transported and emitted outside the KCMP tower footprint, CH_4 and N_2O emissions may offset, and likely exceed, the CO_2 uptake by the agriculture-dominated landscape.

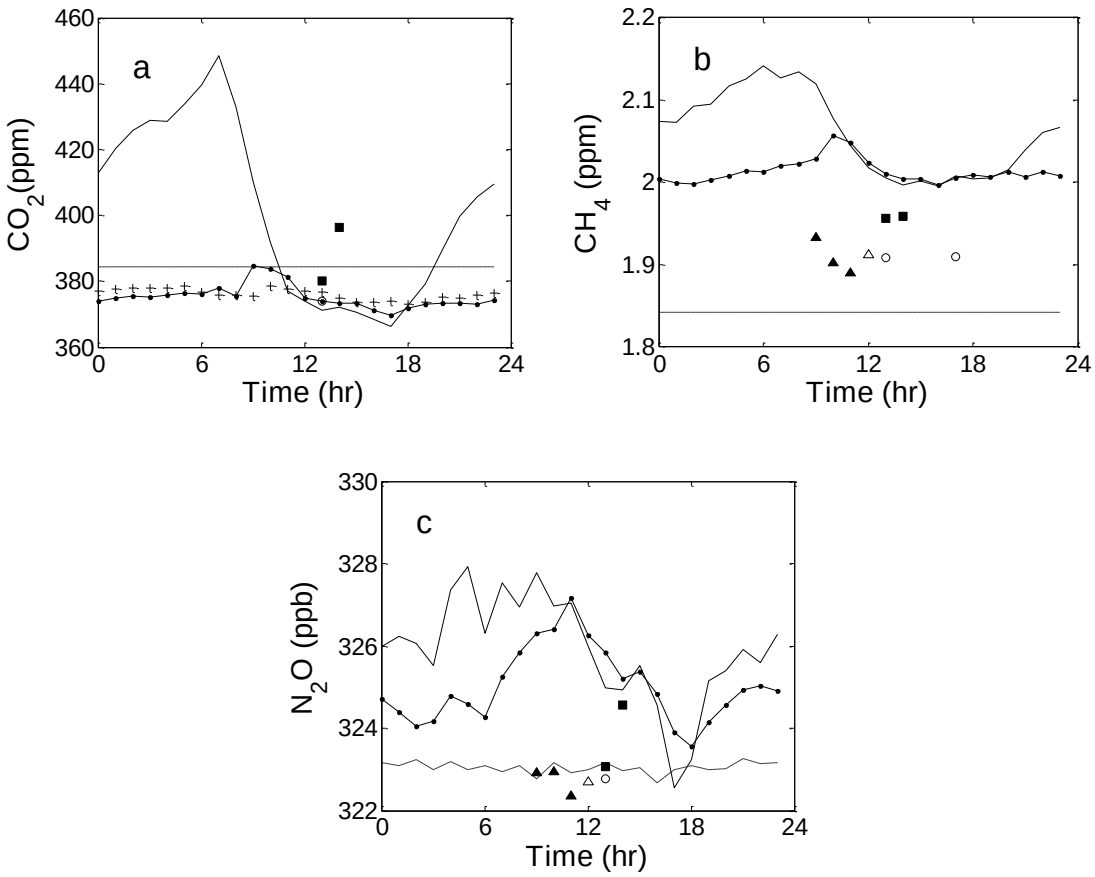

Figure 4.7. Diurnal composite of CO_2 (a), CH_4 (b), and N_2O (c) concentrations at the KCMP tall tower, NWR background site, and three other tall tower sites. Line with dot—concentration on 200 m of KCMP tower; solid line—concentration on 3 m of KCMP tower; dashed line—concentration at NWR background site; open and closed triangle — concentration at 396 m LEF tower by PFP and Flask sampling strategy, cross— CO_2 concentration at 396 m LEF tower, circle— concentration on 379 m of the WBI tower by PFP, closed square—concentration on 60 m of SGP tower by Flask sample strategy.

Table 4.5. A summary of the tall tower sample sites in Midwest United Sates

		Sampling strategy	Longitude	Latitude	Elevation	Intake height (above ground)	Citation
WBI	West Branch, Iowa	PFP	-91.353	41.725	242	379	(Andrews *et al*., 2008) (Andrews and Lang, 2010)
SGP	Southern Great Plains, Oklahoma,	Flask	-97.49	36.61	314	60	(Dlugokencky *et al*., 2011)
LEF	Park Falls, Wisconsin	PFP	-90.2723	45.9459	472	396	(Andrews *et al*., 2008)
		Flask	-90.2723	45.9459	472	396	(Dlugokencky *et al*., 2011)
KCMP	Rosemount, Minnesota	TDL	-93.0728	44.6886	290	200	

Note: PFP means the air were sampled with an automated Programmable Flask. The detailed sampling strategy could be found at http://www.esrl.noaa.gov/gmd/ccgg/aircraft/sampling.html

4.4.5. Comparison with the EDGAR42 Inventory

EDGAR42 has been widely used as an anthropogenic GHG inventory with fine spatial resolutions (0.1°x0.1°) (Jeong *et al*., 2012; Zhao *et al*., 2009); however, only a few studies have been conducted to evaluate it based on atmospheric observations. The limited studies so far in Europe and North America have indicated that EDGAR42 significantly underestimated N_2O and CH_4 emissions, with a regional bias of more than three times higher than EDGAR42 (Corazza *et al*., 2011; Kort *et al*., 2008; Miller *et al*., 2012; Thompson *et al*., 2011).

We first compared the CH_4 and N_2O fluxes at KCMP tower during the intensive campaign with EDGAR42 (within 300 km radius around the tower), and found the KCMP tower flux was at least four times and 50% higher than EDGAR42. In this comparison, the EDGAR42 estimate was scaled to the emissions in September using its seasonal factor (1.1 for September). Another comparison was between the preliminary estimates of annual CH_4 and N_2O flux based on KCMP tower measurement and EDGAR42 annual flux. The result also suggests that EDGAR42 underestimated the regional CH_4 and N_2O flux by factors of six and two, respectively.

The underestimation of the EDGAR42 inventory may be caused by: : 1) natural sources of CH_4 are not negligible, or 2) the bottom-up EDGAR42 inventory underestimated the anthropogenic emissions. Wetlands are considered as the major natural CH_4 source in this region. Even though wetlands accounted for less than 5% of the land around the KCMP tower, it might not be negligible in the regional CH_4 budget, since CH_4 emissions from wetlands may reach up to 350 mg m^{-2} day^{-1} (about 250 nmol m^{-2} s^{-1}) in September (Bridgham *et al*., 2006). EDGAR42 may underestimate CH_4 emission from the

anthropogenic sources as well, because it does not account for factors such as natural gas leakage, and may underestimate the CH_4 emissions from agricultural activities.

The underestimation of the N_2O flux in the EDGAR42 inventory should be mostly attributed to the underestimation of anthropogenic N_2O emission, since natural sources are not significant in the region around the KCMP tower. A recent study on global N_2O emission from natural ecosystems suggests soil emission in the upper-Midwest US is typically around 0.10 kg N ha^{-1} yr^{-1} (0.01 nmol m^{-2} s^{-1}) (Zhuang *et al*., 2012), only 10% of the EDGAR42 anthropogenic emission.

4.5. Conclusions

The regional budget of CO_2, CH_4, and N_2O was estimated with multiple top-down and bottom-up approaches. A framework for estimating and evaluating regional greenhouse gas budgets was developed based on tall tower observations, land cover type information, AmeriFlux data, and other available inventory data.

Regional CO_2 flux from the eddy covariance flux measurement at the KCMP tall tower, Carbon Tracker inverse modeling, and flux aggregation method had the same seasonality; however, there were some discrepancies in the annual carbon budget estimates. The annual CO_2 budget from the eddy covariance measurements was -179 g C-CO_2 m^{-2} yr^{-1} in 2009. The equilibrium method reproduced the seasonal pattern; however, it underestimated the July uptake by about 60%. The underestimation might be mainly caused by advection given the large spatial gradients in CO_2.

CH_4 and N_2O regional fluxes were estimated from the equilibrium method during the intensive campaign and were 16.0±3.1 and 0.19±0.04 nmol m^{-2} s^{-1}, respectively, four

times and 50% higher than in the EDGAR42 inventory. This suggests that EDGAR42 significantly underestimated CH_4 and N_2O emissions from the region.

Considering the global warming potential on a 100-year time scale, CH_4 and N_2O emissions from the landscape can offset more than 60% of the annual carbon uptake. If one includes the carbon leakage by crop harvest and transport, the regional CO_2 uptake might be less than the carbon equivalent of CH_4 and N_2O emissions. Consequently, it is critical to monitor and mitigate regional CH_4 and N_2O emissions from agriculture-dominated landscapes.

4.6. References

Anthoni, P.M., Law, B.E. and Unsworth, M.H., 1999. Carbon and water vapor exchange of an open-canopied ponderosa pine ecosystem. Agricultural and Forest Meteorology, 95(3): 151-168.

Andrews, A.E., Dlugokencky E., and Lang, P.M., 2008. Methane Dry Air Mole Fractions from the NOAA ESRL Surface Network using Programmable Flask Packages (PFP), 1992-2008, Version: 2012-09-19.

Andrews, A.E. and Lang, P.M., 2010. Carbon Dioxide Dry Air Mole Fractions from the NOAA ESRL Surface Network using Programmable Flask Packages (PFP), 1992-2010, Version: 2012-09-21.

Baker, J.M. and Griffis, T.J., 2005. Examining strategies to improve the carbon balance of corn/soybean agriculture using eddy covariance and mass balance techniques. Agricultural and Forest Meteorology, 128(3-4): 163-177.

Bakwin, P.S., Davis, K.J., Yi, C., Wofsy, S.C., Munger, J.W., Haszpra, L. and Barcza, Z., 2004. Regional carbon dioxide fluxes from mixing ratio data. Tellus Series B-Chemical and Physical Meteorology, 56(4): 301-311.

Baldocchi, D., Falge, E., Gu, L.H., Olson, R., Hollinger, D., Running, S., Anthoni, P., Bernhofer, C., Davis, K., Evans, R., Fuentes, J., Goldstein, A., Katul, G., Law, B., Lee, X.H., Malhi, Y., Meyers, T., Munger, W., Oechel, W., U, K.T.P., Pilegaard, K., Schmid, H.P., Valentini, R., Verma, S., Vesala, T., Wilson, K. and Wofsy, S., 2001. FLUXNET: A new tool to study the temporal and spatial variability of ecosystem-scale carbon dioxide, water vapor, and energy flux densities. Bulletin of the American Meteorological Society, 82(11): 2415-2434.

Betts, A.K., Helliker, B. and Berry, J., 2004. Coupling between CO_2, water vapor, temperature, and radon and their fluxes in an idealized equilibrium boundary layer over land. Journal of Geophysical Research-Atmospheres, 109(D18).

Bridgham, S.D., Megonigal, J.P., Keller, J.K., Bliss, N.B. and Trettin, C., 2006. The carbon balance of North American wetlands. Wetland, 26(4): 889-916.

Chen, B., Chen, J.M., Mo, G., Black, A. and Worthy, D.E.J., 2008. Comparison of regional carbon flux estimates from CO_2 concentration measurements and remote sensing based footprint integration. Global Biogeochemical Cycles, 22(2).

Conway, T.J., Tans, P.P., Waterman, L.S. and Thoning, K.W., 1994. Evidence for interannual variability of the carbon cycle from the National Oceanic and Atmospheric Administration/Climate Monitoring and Diagnostics Laboratory Global Air Samping Network. Journal of Geophysical Research-Atmospheres, 99(D11): 22831-22855.

Corazza, M., Bergamaschi, P., Vermeulen, A.T., Aalto, T., Haszpra, L., Meinhardt, F., O'Doherty, S., Thompson, R., Moncrieff, J., Popa, E., Steinbacher, M., Jordan, A., Dlugokencky, E., Bruehl, C., Krol, M. and Dentener, F., 2011. Inverse modelling of European N_2O emissions: assimilating observations from different networks. Atmospheric Chemistry and Physics, 11(5): 2381-2398.

Curtis, P.S., Vogel, C.S., Gough, C.M., Schmid, H.P., Su, H.B. and Bovard, B.D., 2005. Respiratory carbon losses and the carbon-use efficiency of a northern hardwood forest, 1999-2003. New Phytologist, 167(2): 437-455.

Davis, K.J., Bakwin, P.S., Yi, C.X., Berger, B.W., Zhao, C.L., Teclaw, R.M. and Isebrands, J.G., 2003. The annual cycles of CO_2 and H_2O exchange over a northern mixed forest as observed from a very tall tower. Global Change Biology, 9(9): 1278-1293.

Denmead, O.T., 2008. Approaches to measuring fluxes of methane and nitrous oxide between landscapes and the atmosphere. Plant and Soil, 309(1-2): 5-24.

Denmead, O.T., Raupach, M.R., Dunin, F.X., Cleugh, H.A. and Leuning, R., 1996. Boundary layer budgets for regional estimates of scalar fluxes. Global Change Biology, 2(3): 255-264.

Desai, A., Wang, W.G. and Cook, B.D., 2012. Uncovering mechanisms of episodic methane sources observed by a very tall eddy covariance tower, paper presented at 30th Conference on Agricultural and Forest Meteorology/1st Conference on Atmospheric Biogeosciences, Boston, MA, U.S.

Desai, A.R., 2010. Climatic and phenological controls on coherent regional interannual variability of carbon dioxide flux in a heterogeneous landscape. Journal of Geophysical Research-Biogeosciences, 115.

Desai, A.R., Helliker, B.R., Moorcroft, P.R., Andrews, A.E. and Berry, J.A., 2010. Climatic controls of interannual variability in regional carbon fluxes from top-down and bottom-up perspectives. Journal of Geophysical Research-Biogeosciences, 115.

Desai, A.R., Noormets, A., Bolstad, P.V., Chen, J., Cook, B.D., Davis, K.J., Euskirchen, E.S., Gough, C.M., Martin, J.G., Ricciuto, D.M., Schmid, H.P., Tang, J. and Wang, W., 2008. Influence of vegetation and seasonal forcing on carbon dioxide fluxes across the Upper Midwest, USA: Implications for regional scaling. Agricultural and Forest Meteorology, 148(2): 288-308.

Dlugokencky, E.J., Lang, P.M. and Masarie K.A., 2011. Atmospheric Methane Dry Air Mole Fractions from the NOAA ESRL Carbon Cycle Cooperative Global Air Sampling Network, 1983-2010, Version: 2012-09-21, Path: ftp://ftp.cmdl.noaa.gov/ccg/ch4/flask/event/.

GLOBALVIEW-CH4, 2009. Cooperative Atmospheric Data Integration Project – Methane. CD-ROM, NOAA ESRL, Boulder, Colorado (Also available on Internet via anonymous FTP to ftp.cmdl.noaa.gov, Path: ccg/ch4/GLOBALVIEW).

Gloor, M., Bakwin, P., Hurst, D., Lock, L., Draxler, R. and Tans, P., 2001. What is the concentration footprint of a tall tower? Journal of Geophysical Research-Atmospheres, 106(D16): 17831-17840.

Goulden, M.L., Munger, J.W., Fan, S.M., Daube, B.C. and Wofsy, S.C., 1996. Measurements of carbon sequestration by long-term eddy covariance: Methods and a critical evaluation of accuracy. Global Change Biology, 2(3): 169-182.

Griffis, T.J., Baker, J.M., Sargent, S.D., Erickson, M., Corcoran, J., Chen, M. and Billmark, K., 2010. Influence of C-4 vegetation on (CO_2)-C-13 discrimination and isoforcing in the upper Midwest, United States. Global Biogeochemical Cycles, 24: 16.

Haszpra, L., Barcza, Z., Davis, K.J. and Tarczay, K., 2005. Long-term tall tower carbon dioxide flux monitoring over an area of mixed vegetation. Agricultural and Forest Meteorology, 132(1-2): 58-77.

Helliker, B.R., Berry, J.A., Betts, A.K., Bakwin, P.S., Davis, K.J., Denning, A.S., Ehleringer, J.R., Miller, J.B., Butler, M.P. and Ricciuto, D.M., 2004. Estimates of net CO_2 flux by application of equilibrium boundary layer concepts to CO_2 and water vapor measurements from a tall tower. Journal of Geophysical Research-Atmospheres, 109(D20).

Hernandez-Ramirez, G., Hatfield, J.L., Parkin, T.B., Sauer, T.J. and Prueger, J.H., 2011. Carbon dioxide fluxes in corn-soybean rotation in the midwestern US: Inter- and intra-annual variations, and biophysical controls. Agricultural and Forest Meteorology, 151(12): 1831-1842.

Hollinger, S.E., Bernacchi, C.J. and Meyers, T.P., 2005. Carbon budget of mature no-till ecosystem in North Central Region of the United States. Agricultural and Forest Meteorology, 130(1-2): 59-69.

IPCC, 2006. IPCC Guidelines for National Greenhouse Gas Inventories, 5 volumes, Institute for Global Environmental Strategies, Hayama, Kanagawa, Japan.

Jeong, S., Zhao, C., Andrews, A.E., Bianco, L., Wilczak, J.M. and Fischer, M.L., 2012. Seasonal variation of CH_4 emissions from central California. Journal of Geophysical Research-Atmospheres, 117.

Kelliher, F.M., Reisinger, A.R., Martin, R.J., Harvey, M.J., Price, S.J. and Sherlock, R.R., 2002. Measuring nitrous oxide emission rate from grazed pasture using Fourier-transform infrared spectroscopy in the nocturnal boundary layer. Agricultural and Forest Meteorology, 111(1): 29-38.

Kort, E.A., Eluszkiewicz, J., Stephens, B.B., Miller, J.B., Gerbig, C., Nehrkorn, T., Daube, B.C., Kaplan, J.O., Houweling, S. and Wofsy, S.C., 2008. Emissions of CH_4 and N_2O over the United States and Canada based on a receptor-oriented modeling framework and COBRA-NA atmospheric observations. Geophysical Research Letters, 35(18).

Kroon, P.S., Hensen, A., Jonker, H.J.J., Ouwersloot, H.G., Vermeulen, A.T. and Bosveld, F.C., 2010. Uncertainties in eddy covariance flux measurements assessed from CH_4 and N_2O observations. Agricultural and Forest Meteorology, 150(6): 806-816.

Lauvaux, T., Schuh, A.E., Uliasz, M., Richardson, S., Miles, N., Andrews, A.E., Sweeney, C., Diaz, L.I., Martins, D., Shepson, P.B. and Davis, K.J., 2012. Constraining the CO_2 budget of the corn belt: exploring uncertainties from the assumptions in a mesoscale inverse system. Atmospheric Chemistry and Physics, 12(1): 337-354.

Leclerc, M.Y. and Thurtell, G.W., 1990. Footprint prediction of scalar fluxes using a Markovian analysis. Boundary-Layer Meteorology, 52(3): 247-258.

Lee, X.H., Massman, W., Law, B., 2004. Handbook of Micrometeorology: A Guide for Surface Flux Measurement and Analysis, Kluwer Academic Publishers, Dordrecht, 250pp.

Levy, P.E., Grelle, A., Lindroth, A., Molder, M., Jarvis, P.G., Kruijt, B. and Moncrieff, J.B., 1999. Regional-scale CO_2 fluxes over central Sweden by a boundary layer budget method. Agricultural and Forest Meteorology, 98-9: 169-180.

Lin, J.C., Gerbig, C., Wofsy, S.C., Andrews, A.E., Daube, B.C., Davis, K.J. and Grainger, C.A., 2003. A near-field tool for simulating the upstream influence of

atmospheric observations: The Stochastic Time-Inverted Lagrangian Transport (STILT) model. Journal of Geophysical Research-Atmospheres, 108(D16).
Massman, W. J., 2000. A simple method for estimating frequency response corrections for eddy covariance systems, Agricultural and Forest Meteorology, 104(3), 185-198.
Matamala, R., Jastrow, J.D., Miller, R.M. and Garten, C.T., 2008. Temporal changes in C and N stocks of restored prairie: Implications for C sequestration strategies. Ecological Applications, 18(6): 1470-1488.
Miles, N.L., Richardson, S.J., Davis, K.J., Lauvaux, T., Andrews, A.E., West, T.O., Bandaru, V. and Crosson, E.R., 2012. Large amplitude spatial and temporal gradients in atmospheric boundary layer CO_2 mole fractions detected with a tower-based network in the U.S. upper Midwest. Journal of Geophysical Research-Biogeosciences, 117.
Miller, S.M., Kort, E.A., Hirsch, A.I., Dlugokencky, E.J., Andrews, A.E., Xu, X., Tian, H., Nehrkorn, T., Eluszkiewicz, J., Michalak, A.M. and Wofsy, S.C., 2012. Regional sources of nitrous oxide over the United States: Seasonal variation and spatial distribution. Journal of Geophysical Research-Atmospheres, 117.
Moriasi, D.N., Arnold, J.G., Van Liew, M.W., Bingner, R.L., Harmel, R.D. and Veith, T.L., 2007. Model evaluation guidelines for systematic quantification of accuracy in watershed simulations. Transactions of the Asabe, 50(3): 885-900.
Nash, J.E. and Sutcliffe, J.V., 1970. River flow forecasting through conceptional models 1: discussion of principles. Journal of Hydrology 10: 282-290.
National Research Council, 2010. Verifying Greenhouse Gas Emissions: Methods to Support International Climate Agreements, The National Academies Press, Washington, D.C., 110 pp.
Nisbet, E. and Weiss, R., 2010. Top-Down Versus Bottom-Up. Science, 328(5983): 1241-1243.
Olivier, J.G.J., Aardenne, J.A.V., Dentener, F.J., Pagliari, V., Ganzeveld, L.N. and Peters, J.A.H.W., 2005. Recent trends in global greenhouse gas emissions:regional trends 1970–2000 and spatial distributionof key sources in 2000. Environmental Sciences, 2(2-3): 81-99.
Pacala, S.W., Hurtt, G.C., Baker, D., Peylin, P., Houghton, R.A., Birdsey, R.A., Heath, L., Sundquist, E.T., Stallard, R.F., Ciais, P., Moorcroft, P., Caspersen, J.P., Shevliakova, E., Moore, B., Kohlmaier, G., Holland, E., Gloor, M., Harmon, M.E., Fan, S.M., Sarmiento, J.L., Goodale, C.L., Schimel, D. and Field, C.B., 2001. Consistent land- and atmosphere-based US carbon sink estimates. Science, 292(5525): 2316-2320.
Peters, W., Jacobson, A.R., Sweeney, C., Andrews, A.E., Conway, T.J., Masarie, K., Miller, J.B., Bruhwiler, L.M.P., Petron, G., Hirsch, A.I., Worthy, D.E.J., van der Werf, G.R., Randerson, J.T., Wennberg, P.O., Krol, M.C. and Tans, P.P., 2007. An atmospheric perspective on North American carbon dioxide exchange: CarbonTracker. Proceedings of the National Academy of Sciences of the United States of America, 104(48): 18925-18930.
Ricciuto, D.M., Butler, M.P., Davis, K.J., Cook, B.D., Bakwin, P.S., Andrews, A. and Teclaw, R.M., 2008. Causes of interannual variability in ecosystem-atmosphere

CO_2 exchange in a northern Wisconsin forest using a Bayesian model calibration. Agricultural and Forest Meteorology, 148(2): 309-327.
Schmid, H.P., Grimmond, C.S.B., Cropley, F., Offerle, B. and Su, H.B., 2000. Measurements of CO_2 and energy fluxes over a mixed hardwood forest in the mid-western United States. Agricultural and Forest Meteorology, 103(4): 357-374.
Schmid, H.P., Su, H.B., Vogel, C.S. and Curtis, P.S., 2003. Ecosystem-atmosphere exchange of carbon dioxide over a mixed hardwood forest in northern lower Michigan. Journal of Geophysical Research-Atmospheres, 108(D14).
Schuepp, P.H., Leclerc, M.Y., Macpherson, J.I. and Desjardins, R.L., 1990. Footprint prediction of scalar fluxes from analytical solutions of the diffusion equation. Boundary-Layer Meteorology, 50(1-4): 353-373.
Suyker, A.E. and Verma, S.B., 2001. Year-round observations of the net ecosystem exchange of carbon dioxide in a native tallgrass prairie. Global Change Biology, 7(3): 279-289.
Tang, X.G., Wang, Z.M., Liu, D.W., Song, K.S., Jia, M.M., Dong, Z.Y., Munger, J.W., Hollinger, D.Y., Bolstad, P.V., Goldstein, A.H., Desai, A.R., Dragoni, D. and Liu, X.P., 2012. Estimating the net ecosystem exchange for the major forests in the northern United States by integrating MODIS and AmeriFlux data. Agricultural and Forest Meteorology, 156: 75-84.
Thompson, R.L., Gerbig, C. and Rodenbeck, C., 2011. A Bayesian inversion estimate of N_2O emissions for western and central Europe and the assessment of aggregation errors. Atmospheric Chemistry and Physics, 11(7): 3443-3458.
Werner, C., Davis, K., Bakwin, P., Yi, C.X., Hurst, D. and Lock, L., 2003. Regional-scale measurements of CH_4 exchange from a tall tower over a mixed temperate/boreal lowland and wetland forest. Global Change Biology, 9(9): 1251-1261.
West, T. O., Bandaru, V., Brandt, C. C., Schuh, A. E. and Ogle S. M., 2011. Regional uptake and release of crop carbon in the United States, Biogeosciences, 8(8), 2037-2046.
Williams, I.N., Riley, W.J., Torn, M.S., Berry, J.A. and Biraud, S.C., 2011. Using boundary layer equilibrium to reduce uncertainties in transport models and CO_2 flux inversions. Atmospheric Chemistry and Physics, 11(18): 9631-9641.
Xiao, J.F., Zhuang, Q.L., Baldocchi, D.D., Law, B.E., Richardson, A.D., Chen, J.Q., Oren, R., Starr, G., Noormets, A., Ma, S.Y., Verma, S.B., Wharton, S., Wofsy, S.C., Bolstad, P.V., Burns, S.P., Cook, D.R., Curtis, P.S., Drake, B.G., Falk, M., Fischer, M.L., Foster, D.R., Gu, L.H., Hadley, J.L., Hollinger, D.Y., Katul, G.G., Litvak, M., Martin, T.A., Matamala, R., McNulty, S., Meyers, T.P., Monson, R.K., Munger, J.W., Oechel, W.C., U, K.T.P., Schmid, H.P., Scott, R.L., Sun, G., Suyker, A.E. and Torn, M.S., 2008. Estimation of net ecosystem carbon exchange for the conterminous United States by combining MODIS and AmeriFlux data. Agricultural and Forest Meteorology, 148(11): 1827-1847.
Yi, C., Davis, K.J., Bakwin, P.S., Berger, B.W. and Marr, L.C., 2000. Influence of advection on measurements of the net ecosystem-atmosphere exchange of CO_2 from a very tall tower. Journal of Geophysical Research-Atmospheres, 105(D8): 9991-9999.

Yi, C., Davis, K.J., Berger, B.W. and Bakwin, P.S., 2001. Long-term observations of the dynamics of the continental planetary boundary layer. Journal of the Atmospheric Sciences, 58(10): 1288-1299.

Zhang, X., Lee, X.H., Griffis, T.J., Baker, J.M., Erickson, M.D., Hu, N., Xiao, W.(2012). The influence of plants on atmospheric methane in an agriculture-dominated landscape. In review.

Zhao, C.F., Andrews, A.E., Bianco, L., Eluszkiewicz, J., Hirsch, A., MacDonald, C., Nehrkorn, T. and Fischer, M.L., 2009. Atmospheric inverse estimates of methane emissions from Central California. Journal of Geophysical Research-Atmospheres, 114: D16302.

Zhuang, Q., Lu, Y. and Chen, M., 2012. An inventory of global N_2O emissions from the soils of natural terrestrial ecosystems. Atmospheric Environment, 47: 66-75.

4.7. Supplementary materials

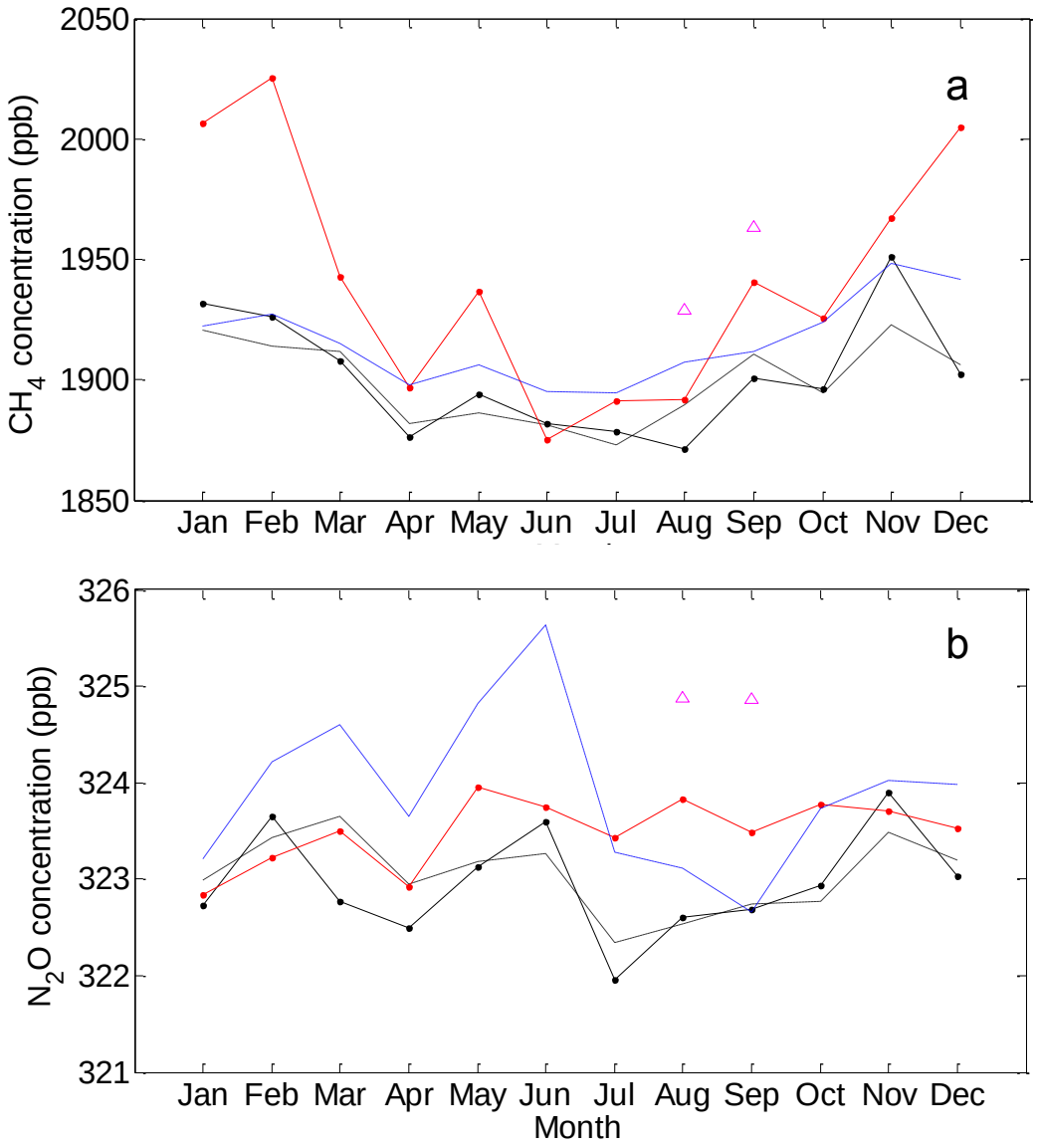

Figure 4.8. Monthly averaged CH_4 (a) and N_2O (b) concentrations in 2009 measured at KCMP (magenta), SGP (red), WBI (blue), and LEF (black). Dashed line denotes the concentration was from Flask program, solid line denotes PFP Flask program. Triangle denotes the concentration was measured by TDL.

Chapter 5: Summary and implications

5.1. Major results

5.1.1. Plant GHG fluxes

This dissertation research, for the first time, measured CH_4 and N_2O fluxes from the aboveground section of plant in a field with a newly designed plant chamber. The observation confirmed that terrestrial plants, such as corn and soybean, emit CH_4 in an aerobic environment (Keppler *et al.*, 2006). However, the emission rate during the daytime was 0.4 ± 0.1 nmol m^{-2} s^{-1}, about one magnitude smaller than Keppler *et al.*'s report, while at night soybean and corn plants both absorbed CH_4 at the rate of -0.8 ± 0.8 nmol m^{-2} s^{-1}.

As a nitrogen fixing plant, soybean was a net source of N_2O throughout the growing season, and the averaged emission rate was 0.03 nmol m^{-2} s^{-1}. N_2O flux from corn plant varied at different growth stages: it was found to mediate the N_2O emission from soil in the early growing season, when the soil emission was strong after fertilization, and the averaged emission rate during this period was 0.16 nmol m^{-2} s^{-1} for fertilized corn; the corn plant was switched to a small sink during the later growing season, and the uptake rate was -0.05 nmol m^{-2} s^{-1}.

Even though CH_4 and N_2O fluxes from corn and soybean plants were substantial, plant flux was mostly more than one magnitude lower than the soil-plant flux and the regional flux. This confirmed that neglecting plant flux in cropland flux estimation for CH_4 and N_2O would not lead to bias higher than 10%. This potential bias is much smaller than the uncertainties in quantifying CH_4 and N_2O soil fluxes due to the inherent heterogeneity of the soil flux. However, it is noticeable that N_2O emission from soybean plant may be

increased by nearly 100 times by intensive application of nitrogen fertilizer in the late growing season.

In contrast to CH_4 and N_2O fluxes, crop plants were critical for both soil-plant and regional CO_2 fluxes. The strong CO_2 uptake by cropland, primarily by corn plants, dominated the seasonal signal of CO_2 flux in a landscape almost half-covered by cropland. The carbon uptake by the cornfield was the strongest among other land cover types in the footprint of the tall tower, accounting for about 70% of the regional carbon uptake by the landscape in 2009.

5.1.2. Regional GHG fluxes

Top-down and bottom-up methods for quantifying regional CO_2 flux were examined for the landscape around the tall tower in 2009. The examined methods included eddy covariance, equilibrium, inverse modeling (Carbon Tracker), and flux aggregation methods. Regional CO_2 flux estimated from different methods exhibited the same seasonal variation pattern: CO_2 emission from the landscape was sustained from October to May, while the uptake reached the peak in July. However, we found that disparities still exist, to different extents, among the annual CO_2 budgets in this region. The equilibrium method underestimated the summer uptake by about 60%, mainly due to neglecting horizontal advection in the context of the large spatial gradient of CO_2.

Significantly higher CH_4 and N_2O concentrations on 200 m of the tall tower than the NWR background site in Colorado, United States were observed during the intensive campaign in 2009. Accordingly, the equilibrium method, supported by other boundary layer methods, determined the regional CH_4 and N_2O fluxes to be 16.0 ± 3.1 and 0.19 ±

0.04 nmol m^{-2} s^{-1}, respectively, during the intensive campaign. The regional emission rate of N_2O might be even higher if advection is taken into account.

Preliminary analysis of the annual CH_4 and N_2O fluxes from the tall tower region suggested that the EDGAR42 inventory underestimated regional CH_4 and N_2O emission by factors of six and two, respectively. The evaluation of N_2O was consistent with Griffis *et al.* (in review) and Kort *et al.* (2008), whereas the evaluation of CH_4 was higher than Kort *et al.* (2008). The underestimation by the current CH_4 and N_2O inventories indicated an underestimation of emissions from agriculture and industry sources and/or the absence of other important sources.

In the agriculture-dominated landscape surrounding the tall tower, the emission of CH_4 and N_2O offset more than 60% of the CO_2 uptake in 2009 (consider the global warming potential on a 100-year time scale). The CH_4 and N_2O emissions are more significant than the CO_2 uptake, if accounting for the CO_2 emitted outside the tall tower region, due to crop transport and consumption.

5.1.3. Nitrogen enrichment

Nitrogen enrichment through both biological nitrogen fixation and fertilization leads to a significant amount of N_2O emission from cropland. The accumulated N_2O emission during the growing season (April to September) from the soybean and fertilized corn plot was 0.74 and 2.58 kg N_2O-N ha^{-1}, respectively. Nitrogen loss through N_2O during the corn growing season accounted for 2.3% of the nitrogen input, indicating an emission factor higher than IPCC guidelines (IPCC, 2006) but smaller than the emission factor estimated from a global top-down approach (Crutzen *et al.*, 2008).

5.2. Implications and further research

Big disparities between the current bottom-up GHG inventory and the top-down observation highlighted the urgency of providing more constraints on the regional GHG fluxes from bottom-up methods. If the bottom-up inventory in the Midwest US, where information on both anthropogenic and natural sources and sinks of GHG is more readily available than in other parts of the world, underestimated the CH_4 and N_2O emission by factors of six and two, the uncertainties in the GHG inventory from other countries, especially developing countries, are potentially large. Therefore, monitoring, reporting, and verifying (MRV) of GHG are essential for a GHG mitigation strategy, and it is necessary to include regional GHG fluxes monitoring based on atmospheric observation.

GHG concentration measurement at the tall tower can provide invaluable information for the purpose of constraining regional GHG fluxes, and, compared to other atmospheric observation such as aircraft and remote sensing, it is long-term, continuous, precise, and relatively inexpensive. In addition to evaluating the bottom-up inventories, tall tower observation may also yield information about the existence of the emission hotspot in its footprint. For example, the disparity between the regional N_2O flux observed at the tall tower and the accumulated soil flux in the tall tower footprint indicated that a strong N_2O source might be missing from the inventory. Moreover, the increasing tall tower observation network in Canada enables the observation of new emission hotspots due to newly emerged human activities. For example, the elevated CH_4 at Lac Labiche site may be attributed to the hydraulic fracturing activities in northern Alberta (personal communication with D. Worthy and T. Griffis, 2012; data may be found at http://www.ec.gc.ca/mges-ghgm/). Even though the conclusions of both cases are still

highly speculative, they highlight the information that tall tower observation can provide on the regional scale and underline the necessity of improving capacity in using tall tower observation to constrain regional flux.

So far, utilizing tall tower observation to constrain regional flux is limited by: 1) the density of the tall tower observations; 2) calibration among tall tower observations; and 3) the accuracy and resolution of methods for quantifying the regional flux. Multiple methods have been examined for quantifying regional CO_2 flux according to tall tower observation, such as eddy covariance, the equilibrium boundary layer budget method, and inverse modeling. Inter-comparison among the methods and against the bottom-up inventory can help to evaluate and improve these methods. Further endeavors should extend the coverage of the tall tower network and collaboration within it, and enhance the capacity for interpreting tall tower observation.

However, it is not enough simply to monitor the regional GHG. As a follow-up, efforts should be made to quantify the underestimated or missing sources of GHG. As part of such an effort, we carried out field measurement to determine the CH_4 and N_2O fluxes from soybean and corn plants, which had been neglected in estimation of GHG fluxes. Further investigation is needed to examine potential emission hotspots, such as drainage ditches for N_2O and a refinery for CH_4, within the tower footprint.

The results from this dissertation also highlighted the importance of nitrogen management in the climate change mitigation and ozone layer protection strategies. Nitrogen enhancement leads not only to increasing carbon sequestration by crop plants but also to increased N_2O emission from both crop plant and soil. In addition, indirect

N_2O emission caused by nitrogen addition on cropland is comparable to the onsite emission, and it needs to be better quantified. Furthermore, holistic evaluation of the cropland management strategy targeting GHG mitigation should include the consideration of both direct and indirect N_2O emission.

5.3. Reference

Crutzen, P.J., Mosier, A.R., Smith, K.A. and Winiwarter, W., 2008. N_2O release from agro-biofuel production negates global warming reduction by replacing fossil fuels. Atmospheric Chemistry and Physics, 8(2): 389-395.

Griffis, T.J., Lee, X., Baker, J.M., Russelle, M., Zhang, X., Venterea, R. and Millet D., 2012. Large nitrous oxide emission factors for the United States Corn Belt revealed by atmospheric concentration measurements. Submitted to Nature October 1, 2012, currently in review.

IPCC, 2006. IPCC Guidelines for National Greenhouse Gas Inventories, 5 volumes, Institute for Global Environmental Strategies, Hayama, Kanagawa, Japan.

Keppler, F., G., H.J.T., M., B. and Rockmann, T., 2006. Methane emissions from terrestrial plants under aerobic conditions. Nature, 439: 187-191.

Kort, E.A., Eluszkiewicz, J., Stephens, B.B., Miller, J.B., Gerbig, C., Nehrkorn, T., Daube, B.C., Kaplan, J.O., Houweling, S. and Wofsy, S.C., 2008. Emissions of CH_4 and N_2O over the United States and Canada based on a receptor-oriented modeling framework and COBRA-NA atmospheric observations. Geophysical Research Letters, 35(18).

Appendix I Photos of field experiment set-up

Figure A1.1. Field set-up of plant flux sampling system for the corn year. An 8 m by 30 m unfertilized zone was preserved during the corn season in 2009. Two sets of sampling tube were extended into the corn field, and could be connected to the sampling sets of tube in three directions, where fertilized and unfertilized corn was randomly selected. All tube was insulated to reduce condensation inside. An overview of the sampling system is in Figure A 1.2. A soil chamber was installed to measure N_2O flux in the same plot by Joe Fassbinder.

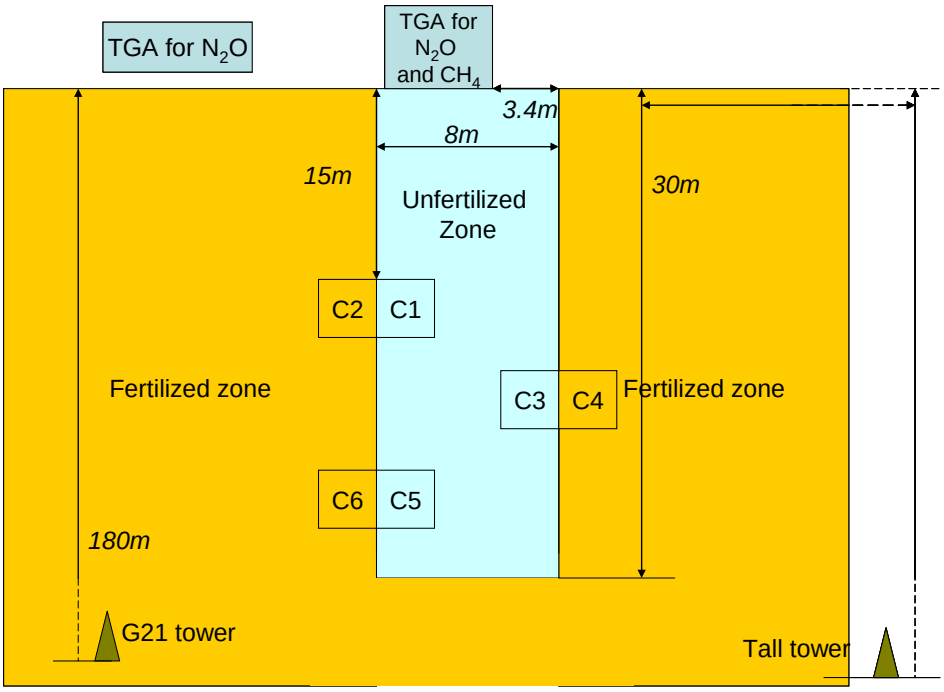

Figure A1.2. Sketch map of observation system set up for 2009.

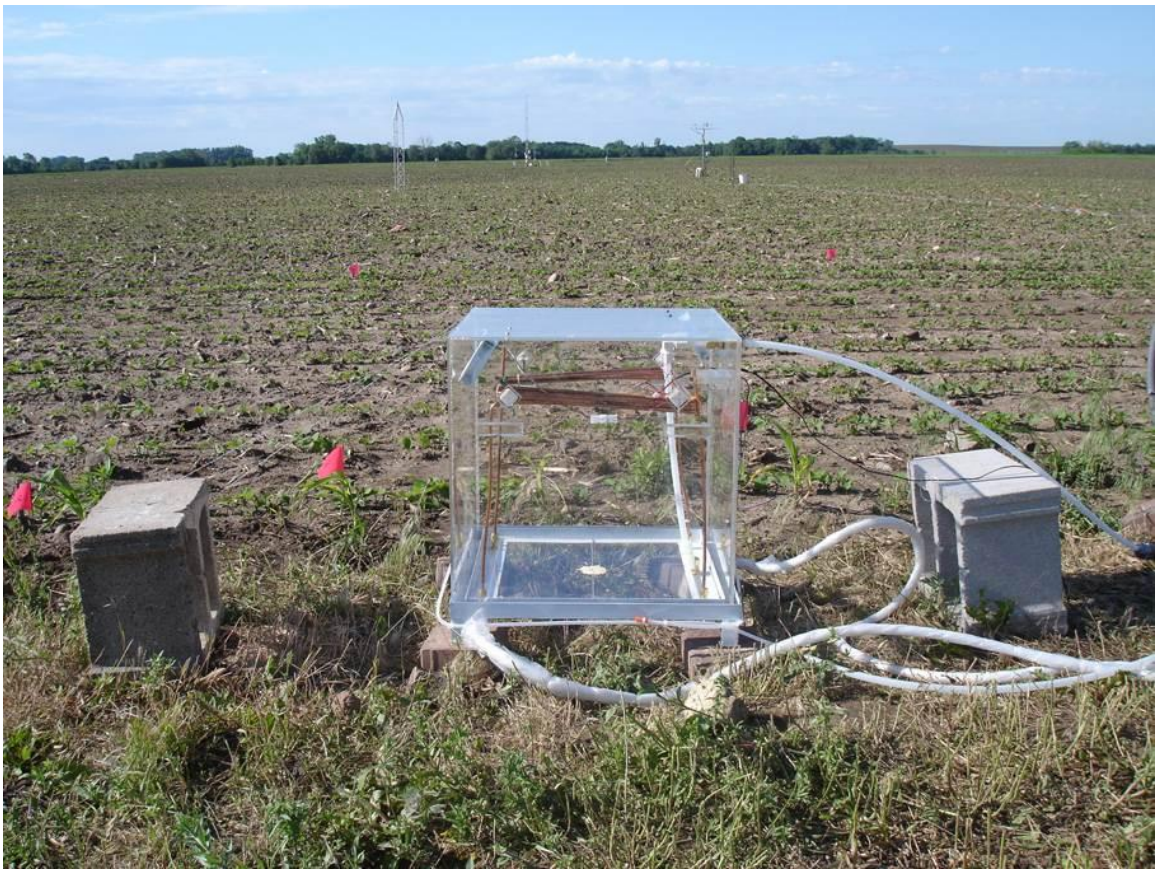

Figure A1.3. Chamber blank test set-up. A blank test was conducted for the medium chamber at the beginning of the growing season, by measuring the CH_4 and N_2O concentration from the inlet and outlet of the chamber without enclosing plants in it. The hole at the center of the bottom plates was designed to allow the plant stem to pass through, but it was sealed during the blank test. Three small towers were set up in the field for different measurements. The middle tower was equipped with a closed-path CO_2 eddy covariance system. Air was drawn at two levels of the towers at the edge of the field for continuous N_2O concentration analysis .As a result, N_2O flux from the soil-plant ecosystem was determined (Chapter 3). N_2O concentration was measured by TDL.

Figure A1.4. Soybean plant flux measured by the small chamber. Soybean plant flux was measured in the small chamber by enclosing the aboveground section of the plant inside the chamber. Ambient air was allowed to flow into the chamber from the bottom, and CO_2, H_2O, CH_4 and N_2O concentrations were measured.

Figure A1.5. Corn plant flux measured by the large chamber. Corn plant flux in the late growing season was measured by the large chamber, which consisted of the medium chamber with its bottom cover plates removed and a skirt made of transparent polyethylene sheets. The plexiglass part rested on a metal frame of adjustable height, ranging between 1 m and 1.7 m. The polyethylene skirt was attached to its side by a strong bonding tape. The contact of the skirt and the medium chamber cover was sealed by water kept in the base frame. The bottom of the skirt was loosely tied to the base of the plant allowing air to enter from the base of the plant.

Figure A1.6. Late-season fertilization experiment for soybean. Fertilizer (24-8-16, NPK; ScottsMiracle-Gro, Marysville, OH) was applied within 1 m radius around the sampled plant at the rate of 500 kg N ha^{-1} in July, 2008.

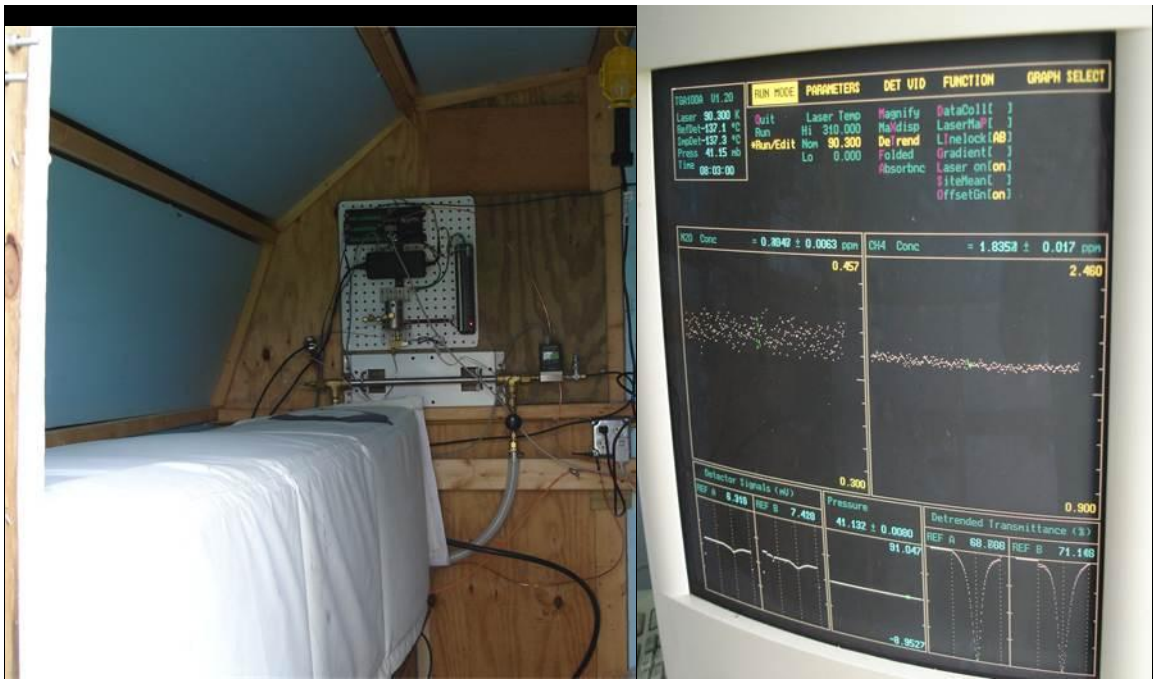

Figure A1.7. The setup of TDL sampling system and a screenshot of TDL measurement. The TDL (model TGA 100A, Campbell Scientific Inc., Logan, UT, USA) was settled on a steady bench inside a small hut close to the edge of the soybean-corn rotation field. The temperature inside the hut was maintained by an air conditioner. The two panels at the lower right corner are the absorption line for N_2O and CH_4.

Figure A1.8. A snapshot of the CO_2 and H_2O measurement by an infrared gas analyzer (IRGA; LI-6262, LI-COR Inc., Lincoln, NE, USA). CO_2 and H_2O concentration was measured at a frequency of 1 Hz, and the 10-minute average value for each sampling site were recorded by a data logger.

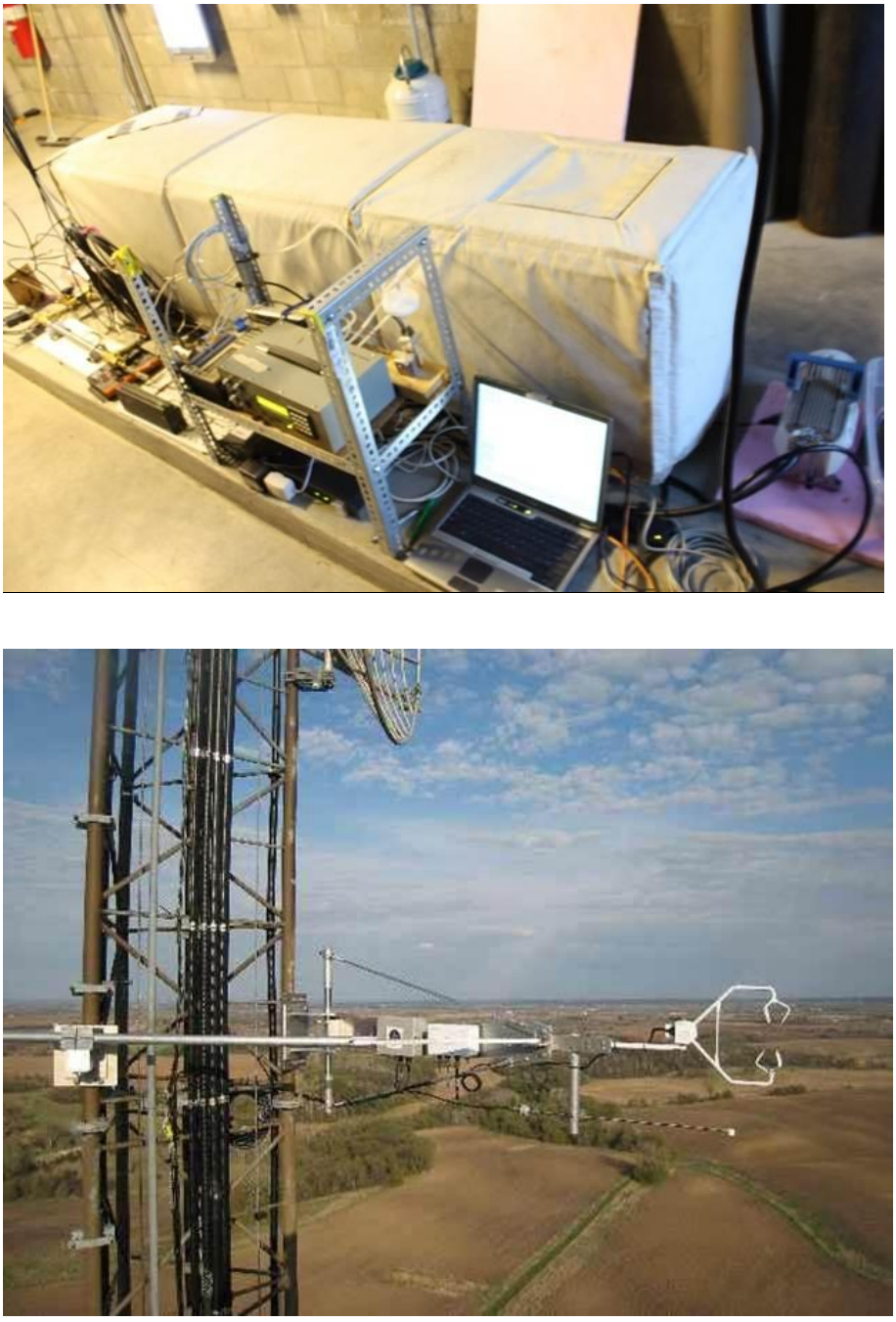

Figure A1.9. Tall tower observatory. The upper panel is the setup of LI-COR and TDL for measuring trace gas concentration from the air samples from 3 m and 200 m during the intensive campaign in 2009. The lower panel is a snapshot of the view from the 100 m level at the tall tower. The equipment attached to the tower is a 3-D sonic anemometer-thermometer (model CSAT3, Campbell Scientific) for eddy covariance measurement.

Figure A1.10. A group photo of the field work team at the University of Minnesota's Outreach, Research and Education Park, 2008